





IMMOBILIZATION OF HEAVY METALS IN HAZARDOUS FLY ASHES

Investigation on the feasibility of increasing immobilization efficiency by carbon mineralization

Master thesis Environmental Engineering

Maria Erica Biagini



Immobilization of heavy metals in hazardous fly ashes

Investigation on the feasibility of increasing immobilization efficiency by carbon mineralization

by

M. Erica Biagini

to obtain the degree of Master of Science

for the Master in Environmental Engineering at the Delft University of Technology.

Student number: 5156688

Project duration: February 12, 2024 – August 31, 2024

Thesis committee: Dr. ir. G. Ye, TU Delft, supervisor

Dr. habil. Julia Gebert, TU Delft

Dr. S. Zhang, Renewi

Cover: Picture taken on the site of Mineralz on the Maasvlakte.

Abstract

This study investigated the possibility of enhancing immobilization of heavy metals in hazardous fly ashes by mineral carbonation. The research initially investigated five different fly ashes for their chemical composition and carbonation potential. The highest lime content resulted in the highest carbonation potential, but mineral carbonation occurred also in other fly ashes with very limited free lime. One of the municipal solid waste incineration (MSWI) fly ash (FA) with a high heavy metal content and the highest carbonation potential was selected for further carbonation and immobilization investigations.

The selected MSWI FA was carbonized following the first three out of four possible different routes:

- 1. Pre-carbonation of fly ash and casting with binder
- 2. Pre-carbonation of fly ash-binder mixture and casting after carbonation
- 3. Curing of the sample in the carbonation chamber
- 4. Carbonation of fresh mixture during mixing

The materials were tested for their crystalline composition before and after curing as well as for effective carbonuptake. The second route resulted in the highest effective carbonation for the MSWI FA but also in the lowest compressive strength. The third route showed an increase in strength compared to the reference sample and effective reduction of final pH on the leachate and electrical conductivity. A fast shake leaching test was used to determine the leachability of relevant anions and cations from the mix designs. The results were compared with a reference sample prepared following a procedure used in industrial-scale applications and with the Dutch Soil Quality Decree and Regulation (Ministerie van Infrastructuur en Waterstaat, 2022).

The leaching tests resulted in an increased immobilization of lead, copper, and zinc for both a MSWI FA and a biomass (BM) FA also selected for its high carbonation potential. The highest total immobilization was reached for the MSWI FA through pre-carbonation of fly ash-binder mixture as the high reduction of pH of the sample cured in the carbonation chamber increased the solubility of other heavy metals. The immobilized BM FA through carbon-curing resulted in the optimal immobilization solution, followed by the pre-carbonation of the mixture of binder and fly ash. For both tested materials, the addition of carbonation outperforms the reference samples.

The comparison with the Dutch soil decree showed promising outcomes for future development of mineral carbonation for immobilization of hazardous materials. The carbonized specimens met most of the requirements for construction materials, which were expected to be more stringent than those for landfill use. The materials were evaluated under a worst-case scenario, showing the effective reduction of lead leachability. The carbonation of hazardous materials offered potential for application in highly lead-polluting waste streams to reduce carbon emissions and contribute to a cleaner environment.

Acknowledgements

This thesis not only represents the end of my student career as MSc in Environmental Engineering, but it marks the end of what have been five full years at TU Delft. These last years of my life have been the most remarkable and life-teaching moments of my life, that would have not been possible without the support of my family. The passion and devotion they dedicate to their jobs and family, as well as the compassion that they grow for people around them is tremendously inspiring. This journey has changed me as a person and has changed me into a better version of myself. This research is the final phase of my journey as a Master student and was made possible by the support of several people. Therefore, I would like to convey my deepest gratitude to them.

Firstly, I would like to thank Renewi and Mineralz for providing me with all the help and resources to conduct this study. I would like to start by expressing my sincere gratitude to my manager Pascal Van der Ploeg for welcoming me from the very beginning and inundating me with the love for the company.

To continue, I would like to thank my committee for their guidance and constant support throughout the duration of this research. I would like to thank Shizhe Zhang for constantly reassuring me about my work and for pushing me in the right direction. The boost of ideas that irradiates from you really inspired me on wanting to know more and explore topics that I thought I could never even dare to look at. Really, thank you Shizhe.

I would also like to deeply thank the chair of my thesis committee Dr. Guang Ye for his lessons and in-depth feedback during the different phases of this research. Professor, from the very beginning not only you pushed me in the world of geopolymers, but you also introduced me to a whole community of fantastic people that is your CMMB group. I will miss our monthly meetings, they have been not only inspiring, but a real eyes-opening of a whole new part of research that I have never even considered. Thank you professor.

My deepest gratitude goes also to my second supervisor Dr. habil. Julia Gebert. Dear professor, besides your infinite knowledge in what seemed for me obscure chemistry, I will carry with me two things. The first is the memory of our small fieldwork day measuring soil gas emissions, where not only everyone enjoyed working in the field, but the joy, calm and fun that you created around that day full on learning is astonishing. The second is your capacity of always expressing yourself, your point and all your knowledge in just a few, selected but at the same time extremely valuable words. I find it really inspiring as something I wish to also achieve in the future.

Sifra, Robert, thank you so much for welcoming me at Renewi and for spending together, even if only a few, wonderful days in the sun and in the cold together. I hope we will get to work together again because it was not only motivating and inspiring, but also precious and stimulating.

The next thanks go to the Microlab-group. Thank you to Maiko, that from the beginning you guided me through the world of concrete and cement with fun and excitement, while being a second father in the Netherlands. Thank you to John, Arjan and Ton for the help in the laboratories and for introducing me through all the testing equipment.

My sincere thanks go also to Karel, Auke, Michiel and Sian. Karel, thank you for guiding me through the carbonation experiments and spending so much time building the experimental equipment together. Auke, thank you for allowing me to work in your laboratory and still help me through my Bachelor and my Master. Michiel and Sian, it was lovely to work together again.

Yu Zeng and Patrick, thank you for kindly explaining me all you knew regarding XRD and QXRD, your help and your private lessons throughout all the months of my research made a difference in the quality of my results as well as my understanding of the topic. I would have not been able to without you.

Thank you also to all CMMB group. Thanks to Boyu, Farnaz, Guilherme, Luiz, Chen, Abdellah and Mayank, always all available to answer my questions and enlighten me by answering all the doubts I had in the most desperate days.

Sakshi, Gabriel, Ali, Shan, Eyüph, Jinbao, Borcu, Wen, Frank, Yanchen, Wouter, Sep and Ameya, thank you not only for being amazing colleagues but also for the moral support and fun we had together. With all the others from the department the last months were so joyful and great to overcome the long winter, spring and part of the summer together as a big family.

Thank you to all my master's friends. In particular to my fellow board members, to the waste and resource engineering fellow students and the American girls, for both the wonderful moments we shared together as well as the stresses that still made these last two years the most remarkable of probably all our lives.

Juliette and Yasha, thank you for being always by my side, for being such inspirational guides through all these years in the Netherlands and truly helping me rationalising the reality by sharing your lives with me.

I am so lucky that for the past two years, from my bachelor throughout all my master, Sil, you were by my side. Besides the dinners, lunches and rescuing after the >10h at the faculty, your time-efficiency and making everything look so down to heart, were important teachings that made me grow in the last years. I will forever cherish them also in my upcoming life.

Finally, I would also like to thank my family and friends who supported me through the entire Master by keeping me motivated and helping me to focus on achieving my goals. Mum, stefanus, dad, rossi, gemmina, marcolino, nonna, zio, maria and the rest of my family, thank you for sharing the struggles and still being my stable foundations. Stefanus, thank you, really, for implanting in me, so long ago, this desire of discovering and being curious and thank you for making possible to start this university that totally changed my life.

I will leave my last words to my grandfather, that I am sure is watching over me from wherever he is.

Contents

Abstract	3
Acknowledgements	4
Contents	1
Nomenclature	4
Abbreviations	4
Symbols	5
List of figures	6
List of tables	11
I. Introduction and overview	13
1. Introduction 1. Introduction	13
1.1 Background	13
1.2 Problem statement	13
1.3 Mineralz	15
	16
2. Objective and scope2.1 Research questions	17
2.1 Research questions 2.2 Research outline	18
3. Literature review	20
3.1 Hazardous fly ashes 3.1.1 Origin of fly ashes	20 22
3.2.2 Composition	22
3.3 Immobilization of heavy metals	23
3.3.1 Immobilization mechanisms	24
3.3.2 Immobilization techniques	25
3.3.2.a Solidification/stabilization and safe storage	25
3.3.2.b Thermal Treatment	26
3.3.2.c New technologies	27
3.4 Carbonation	29
3.4.1 Carbonation reactions	29
3.4.1 Water content	31
3.4.2 Dependence on temperature and pressure	31
3.4.3 Time dependency	33
3.4.5 Dependence on pH	35
3.4 Dutch regulations on hazardous waste disposal and landfilling	36
3.4.1 Regulations	36
3.4.2 Standardized tests	37
II. Experimental Investigation	38
4. Materials and methods	38
4.1 Material characterization	38
4.1.1 Chemical composition	39
4.1.2 Carbonation potential	40
4.1.3 Selection process	42
4.2 Carbonation and immobilization	43
4.2.1 Preliminary carbonation	43
4.2.1.a Selection carbonation conditions	44
4.2.1.b Carbonation conditions and carbon-uptake	45

Influence of water-content on carbon-uptake	45
Influence of pressure on reaction rate and carbon-uptake	46
4.2.2 Mix designs	46
4.2.2.a Pre-carbonated fly ash	47
4.2.2.b Pre-carbonated fly ash-binder mixture	48
4.2.2.c Curing in carbonation chamber	49
4.2.3 Physical stability	50
4.2.4.a Physical strength	50
4.2.3.b Slake test	51
4.3 Leaching experiments	52
4.3.1 Leaching material	53
4.3.2 Leaching procedure and extraction of leachate	54
4.3.3 Analysis of the leachate	55
4.4 Extra experiments	56
5. Material characterization	58
5.1 Chemical composition	58
5.1.1 Elemental analysis	59
5.1.2 Crystalline phases	61
5.2 Carbonation potential	65
5.2.1 Crystalline phases	66
5.2.2 Carbon-uptake	69
5.2 Selection of fly ashes	72
6. Carbonation and immobilization	73
6.1 Preliminary carbonation	73
6.1.1 Selection carbonation conditions (FA1_C1_1)	73
6.1.2 Influence of water-content on carbon-uptake (FA4_C1_WC)	74
6.1.3 Influence of pressure on reaction rate and carbon-uptake (FA1-B_C1_P)	75
6.2 Mixture designs	78
6.2.1 Pre-carbonated FA (FA1_C2)	78
6.2.2 Carbonated mixture (FA1-B_C2)	80
6.2.3 Carbonation after casting (FA1-B_C3)	83
6.3 Physical stability	86
6.3.1 Physical strength	87
6.3.2 Slake test	88
7. Leachability of heavy metals	89
7.1 Leaching material	89
7.1.1 Moisture content samples	90
7.1.2 Amount of leachate	90
7.2 Leaching procedure and extraction of leachate	91
7.3 Analysis on the Leachate	92
7.3.1 Electrical conductivity, pH and temperature	92
7.3.2 Heavy metals content and leaching species	93
7.4 Discussion	96
8. Extra experiments	97
8.1 Mixture designs	97
8.1.1 Pre-carbonated FA (FA2_C2)	97
8.1.2 Carbonated mixture (FA2-B_C2)	98
8.1.3 Carbonation after casting (FA2-B_C3)	98
8.2 Physical strength	99

8.3 Leachability of heavy metals	101
8.4 Discussion	104
III. Closure	105
9. Discussion	105
9.1 Limitations	106
9.2 Recommendations	107
10. Conclusion	108
10.1 Future research	108
Bibliography	109
Appendices	116
A. Literature review	116
B. Experimental investigation	117
B.1 Methodology	117
B.2 Characterization experiments	118
B.2 Carbonation Experiments	119
B.3 Leachability of Heavy Metals	121

Nomenclature

Abbreviations

Abbreviation	Definition
В	Binder
BM	Biomass
C2S	Dicalcium silicate
C3S	Tricalcium silicate
CBPS	Chemically bonded phosphate ceramics
CCA	Decarbonation of calcite
C-S-H	Calcium silicate hydrates
Dcr	Decarbonation
Dhy	Dehydration
DM	Dry matter
DTG	Differential thermogravimetric analysis
DR	Dry matter content ratio
DSC	Differential scanning calorimetry
FA	Fly ash
HMG	Decarbonation of hydromagnesite
K-A-S-H	Potassium aluminosilicate
	hydrate
L	Leachant
L/S	Liquid to solid ratio
LOI	Loss of ignition
MC	Moisture content
MGC	Decarbonation of magnesite
MSWI	Municipal solid waste incineration
N-A-S-H	Sodium aluminosilicate hydrate
S/L	Solid to liquid ratio
SSA	Specific surface area
TGA	Thermogravimetric analysis
XRD	X-ray Diffraction
XRF	X-ray Fluorescence
WtE	Waste to energy

Symbols

Symbol	Definition	Unit
% _{OM}	Organic Matter content	[-]
$\Delta m_{x\text{-}y^{\circ}C}$	Mass difference between TG at x°C and y°C	[-]
A_{I}	Assigned value for immobilization method	[-]
I_{m}	Immobilization efficiency	[-]
L	Leachate	[ml]
m	Mass	[g]
m_d	Dry mass	[g]
$m_{\rm i}$	Initial mass	[g]
$m_{\rm w}$	Wet mass	[g]
P	Pressure	[bar]
t_x	Exposure time	[days]

List of figures

Figure 1.1: Schematic representation of the storage procedure of hazardous fly ashes used by Mineral (¹ Tomic & Ducman, 2023; ² Singh & Budarayavalasa, 2021; ³ Mineralz, n.d. b)
FIGURE 2.1: POSSIBLE CARBONATION ROUTES DURING IMMOBILIZATION PROCESS OF FLY ASHES. (1) PRE-CARBONATION OF FLY ASH, (2) CARBONATION OF THE MIXTURE FLY ASH AND BINDER, (3) CARBONATION DURING CURING, (4) CARBONATION WHILE MIXING
FIGURE 2.2: DETAILED RESEARCH FLOW DIAGRAM ADDRESSING ALL THE QUESTIONS AND SUB-QUESTIONS IDENTIFIED IN TH METHODOLOGY AND IN THE RESEARCH QUESTION CHAPTER
Figure 3.1: Location and names of the 12 incineration plants in the Netherlands (De Leeuw & Koelemeijer 2022)
FIGURE 3.2: SCHEMATIC DRAWING OF WTE PLANT WITH GENERATION OF ENERGY, HEAT AND RESIDUAL FLY ASH AND BOTTOM ASH (CHESTER, 2016)
FIGURE 3.3: SCHEMATIC REPRESENTATION OF THE C-S-H STRUCTURE AND THE POTENTIAL LOCATIONS OF HEAVY METALS. (1 SUBSTITUTION ON THE EDGES OF THE CHEMICAL STRUCTURE, (2) PHYSICAL ENCAPSULATION BETWEEN INTERLAYED SPACE, (3) SUBSTITUTION OF CA IONS INTO STRUCTURE (VESPA ET AL., 2014)
Figure 3.4: Cross-sectional drawing representing a secured landfill and safe storage site (Liu et al., 2018). In the case of the Netherlands, the hazardous waste in the image referred as drummed waste is instead a stabilized monolithic waste
FIGURE 3.5: (A) SCHEMATIC REPRESENTATION OF SINTERING (GAO ET AL., 2022) AND (B) CROSS-SECTIONAL DRAWING OF A VITRIFICATION CHAMBER (BERNARDO ET AL., 2017)
FIGURE 3.6: SCHEMATIC REPRESENTATION OF GEOPOLYMERISATION MECHANISM (Vu & GOWRIPALAN, 2018)2
FIGURE 3.7: MECAHNISMS OF HEAVY METAL IMMOBILIZATION BY CARBONATION OF FLY ASHES (YUAN ET AL., 2023)2
Figure 3.8: Thermodynamic modelling of the stable hydrate assemblage in MgO-hydromagnesite blend hydrated at 20°C using a water/solid ratio of 1.20 (Winnefeld, 2019)
FIGURE 3.9: REPRESENTATION OF CARBONATION DISSOLUTION AND MINERALISATION IN LOW-WATER ENVIRONMENT (WANGET AL., 2021).
FIGURE 3.10: CARBON UPTAKE AS A FUNCTION OF S/L (A) AND TEMPERATURE (B) (BACIOCCHI ET AL., 2009)3
Figure 3.11: Carbonation efficiency of fly ash under supercritical conditions (80 bar) and low-pressure (4 bar) conditions (Yuan et al., 2022a).
FIGURE 3.12: KINETICS OF REACTION FOR CARBONATION OF ANHYDRITE AT 80°C (READAPTED FROM ALTREE-WILLIAMS E AL., 2017)
FIGURE 3.13: LEACHABILITY OF LEAD, ZINC AND COPPER FOR FA CARBONIZED FOR TIMES IN BETWEEN 0.125 AND 128 H (QUII ET AL., 2022).
FIGURE 3.14: MECHANISMS OF REACTIONS OF H_2SO_4 and HNO_3 with lead, copper and zinc to form insoluble salts (N et al., 2017).
FIGURE 3-15: GENERAL LEACHING BEHAVIOUR OF TWO SETS OF HEAVY METALS AS FUNCTION OF PH (KRÓLET AL., 2020). 30

$Figure\ 4.1: From\ Left\ to\ Right\ pictures\ of\ FA1, FA2, FA3, FA4, FA5\ and\ FA6\ used\ in\ this\ Research.\3$
FIGURE 4.2: (A) SAMPLE PREPARATION FOR QXRD ANALYSIS BY GRINDING THE FA AND MIXING IT WITH SI-POWDER. (E) SAMPLE IN THE SAMPLE HOLDER THAT WAS ANALYSED BY THE (C) D8 ADVANCED DIFFRACTOMETER
FIGURE 4.3: (A) CARBONATION CHAMBER AT FIXED TEMPERATURE OF 20°C, PRESSURE OF 1 BAR, RH OF 65% AND 1% CO (B) SAMPLE HOLDER FOR THE FLY ASHES TO ENSURE MAXIMUM CONTACT SURFACE TO THE ENVIRONMENT
FIGURE 4.4: (A) ALUMINA CRUCIBLE WITH ON AVERAGE 30 MG OF GRINDED AND DRIED SAMPLE. (B) CLOSED PICTURE OF THE CRUCIBLE WITH THE SAMPLE PLACED NEXT TO THE REFERENCE THERMOCOUPLE. (C) NETZSCH STA 449 F3 JUPITE SIMULTANEOUS THERMAL ANALYSER
FIGURE 4.5: (A) SMALL CARBONATION CHAMBER FROM THE GEOSCIENCE AND ENGINEERING LABORATORY AT TU DELFT. P, AND CO_2 concentration were controlled in the reaction chamber. (B) Larger carbonation chamber is Stevin I Laboratory at TU Delft where carbonation happened at fixed T, P, RH, and CO_2 concentration A .
FIGURE 4.6: EXPERIMENTAL SETUP OF CARBONATION CHAMBER FROM THE GEOSCIENCE AND ENGINEERING LABORATORY A TU Delft. A cylinder containing pressurized CO_2 is connected through capillary plastic tubes to a insulated stainless-steel vessel placed inside an oven. Temperature and pressure inside the vessel ar monitored, and the gas is released through a valve outside the oven.
FIGURE 4.7: (A) MEASURING SCALE FOR PREPARATION OF FLY ASH-BINDER-WATER MIXTURE. (B) HOBART INDUSTRIAL MIXIN DEVICE USED FOR MIXING THE MATERIALS BEFORE CASTING. (C) IDEAL EARTH-MOIST TEXTURE OF REFERENCE SAMPL AFTER MIXING
FIGURE 4.8: (A) FA AND WATER MIXTURE IN LARGE PLASTIC TRAY BEFORE PLACING IN THE CARBONATION CHAMBER. (EMIXTURE OF FA, BINDER AND WATER BEFORE CARBONATION
FIGURE 4.9: SCHEMATIC DRAWING OF CUTTING PLANE (RED) ON FA-B_C3 FOR CARBONATION DEPTH TEST. AFTER 28 DAYS THE SAMPLE IS REMOVED FROM THE POLYSTYRENE MOULD AND CUT PERPENDICULARLY TO THE PLANE EXPOSED TO CARBONATION. THE NEW SURFACE IS SPRAYED WITH PHENOLPHTHALEIN TO DETERMINE THE CARBONATION DEPTH5
FIGURE 4.10: (A) DUAL FLEXURAL AND COMPRESSIONAL MASET STRENGTH TEST. (B) MATERIAL UNDER FLEXURAL STRENGT TEST. (C) SPECIMEN TESTED FOR COMPRESSION STRENGTH TEST
FIGURE 4.11: (A) SCHEMATIC REPRESENTATION OF EXPERIMENTAL SETUP USED FOR THE SLAKE TEST. (B) REAL EQUIPMEN USED FOR THE TESTS
Figure 4.12: (A) Sartorius weighing scale with precision of ±0.1 g used to measure the material for the leachin tests. (B) Sieve used to separate the material with particle size larger than 10 mm. (C) Immobilize material after hammer crushing.
FIGURE 4.13: (A) MEASURING CYLINDER TO MEASURE THE CORRECT AMOUNT OF LEACHANT. (B) 1 LITRE GLASS BOTTLES USE FOR THE LEACHING EXPERIMENTS AS DENOTED FROM THE STANDARD NEN-EN 12457-4:2002.
FIGURE 4.14: (A) SCHEMATIC REPRESENTATION OF END-OVER-END TUMBLER AND (B) REAL DEVICE USED FOR THE SHAKE TEST
FIGURE 4.15: FILTERING EQUIPMENT USED TO SEPARATE THE LEACHATE FROM THE SUSPENDED MATERIAL
FIGURE 5.1: CUMULATIVE PARTICLE SIZE DISTRIBUTION (LEFT) AND PARTICLE SIZE DISTRIBUTION (RIGHT) OF THE SIX FL ASHES
FIGURE 5.2: XRF RESULTS OF RELEVANT HEAVY METALS CONCENTRATION OF THE SIX MATERIALS FA1, FA2, FA3, FA4, FA AND FA6. THE CONCENTRATIONS ARE OF THE EQUIVALENT OXIDES

FIGURE 5.3: FROM BOTTOM TO TOP, XRD DIFFRACTOGRAMS OF FA1, FA2, FA3, FA4, FA5 AND FA6. THE PEAK CORRESPONDING TO MOST OF THE CRYSTALLINE PHASES ARE UNDERLINED IN THE IMAGE
Figure 5.4: Results of quantitative Rietveld phase analysis of the six materials investigated in the research 6
FIGURE 5.5: PICTURES OF THE SIX MATERIALS AFTER ONE WEEK IN THE CARBONATION CHAMBER AT THE SAME CONDITIONS
FIGURE 5.6: AMORPHOUS CONTENT DETERMINED BY QXRD OF THE FLY ASHES PRE- AND POST-CARBONATION6
FIGURE 5.7: QUANTIFICATION OF CRYSTALLINE PHASES THROUGH QXRD RIETVELD REFINEMENT. FROM LEFT TO RIGHT TH PLOTS SHOW THE PHASES OF FA1, FA2 AND FA3 BEFORE AND AFTER 1 WEEK CARBONATION
FIGURE 5.8: QUANTIFICATION RESULTS OF CRYSTALLINE PHASES PRE- AND POST-CARBONATION THROUGH RIETVELL REFINEMENT OF THE QXRD PATTERNS. FROM LEFT TO RIGHT: FA4, FA5 AND FA6.
FIGURE 5.9: TG-DSC (TOP) AND DTG (BOTTOM CURVE OF FA1 (LEFT) AND FA2 (RIGHT) PRE- AND POST-CARBONATION70
FIGURE 5.10: TG-DSC (TOP) AND DTG (BOTTOM CURVE OF FA3 (LEFT) AND FA4 (RIGHT) PRE- AND POST-CARBONATION7
FIGURE 5.11: TG-DSC (TOP) AND DTG (BOTTOM CURVE OF FA5 (LEFT) AND FA6 (RIGHT) PRE- AND POST-CARBONATION7
FIGURE 5.12: (LEFT) CARBON-UPTAKE IN WT.% OF EACH MATERIAL AFTER 1 WEEK OF CARBONATION. (RIGHT) SUMMARY O THE RELEVANT HEAVY METALS' CONCENTRATIONS OF EACH MATERIAL
FIGURE 6.1: TG-DSC RESULTS OF THE ORIGINAL FLY ASH (FA1), THE CARBONATED MATERIAL AT 1% CO ₂ AND 20°C FOR DAY (FA1_C01d) AND THE CARBONATED FA1 AT 40°C, 100% CO ₂ FOR 2 H (FA1_C1_1)75
FIGURE 6.2: (LEFT) TG-DSC-DTG CURVE OF ORIGINAL FA4 AND FA4 CARBONIZED IN DRY CONDITIONS AND (RIGHT) WITH ADDITION OF 3 ML OF WATER IN 10 G OF SOLID MATERIAL
FIGURE 6.3: RATE OF REACTION THROUGHOUT THE CARBONATION EXPERIMENT OF THE FA-BINDER MIXTURE AT 1 BAR70
FIGURE 6.4: EVOLUTION OF REACTION RATE DURING THE CARBONATION OF FA1 AND BINDER AT 2 BAR
FIGURE 6.5: TG-DSC-DTG CURVES OF THE ORIGINAL FA1 AND THE CARBONATED FA1-B MIXTURE AT 1 BAR AND 2 BAR7
FIGURE 6.6: (A) FA1 AFTER PRE-CARBONATION AND (B) IMMOBILIZED FA1_C2 SPECIMEN AFTER 28 DAYS OF CURING7
FIGURE 6.7: RESULTS FROM RIETVELD REFINEMENT OF THE QXRD PATTERNS OF THE REFERENCE PASTE (FA1-B_REF PRE CURING), THE PRE-CARBONATED FA1 PRE-CURING (FA1_C2 PRE-CURING) AND THE PASTE WITH PRE-CARBONATED FA AFTER 28 CURING (FA1_C2 POST-CURING).
FIGURE 6.8: DTG CURVES OF REFERENCE SAMPLE, PRE-CARBONIZED FA MIXED WITH THE BINDER AND THE HARDENED PAST AFTER 28 DAYS.
FIGURE 6.9: (A) PICTURE OF FA1-B MIXTURE AFTER 1 DAY OF CARBONATION. (B) PICTURE DURING MIXING THE CARBONIZED MATERIAL WITH THE REMAINING WATER. (C) FA1-B_C2 SPECIMEN AFTER 28 DAYS OF CURING8
FIGURE 6.10: RESULTS FROM RIETVELD REFINEMENT OF REFERENCE SAMPLE AND THE PRE-CARBONATED PASTE OF FA1 AND BINDER BEFORE AND AFTER 28 DAYS OF CURING
FIGURE 6.11: DTG CURVES OF REFERENCE PASTE (FA1-B_REF), CARBONATED FA1-BINDER PASTE BEFORE CURING (FA1-B_C2) AND AFTER CURING (FA1-B_C2 POST-CURING)

FIGURE 6.12: (A) FA1-B_C3 AFTER 3 DAYS IN THE CARBONATION CHAMBER AND (B) AFTER 28 IN THE CARBONATION CHAMBER
FIGURE 6.13: RESULTS FROM QUANTIFICATION OF XRD RESULTS OF THE REFERENCE SAMPLE AND FA1-B_C3 BEFORE AN AFTER CURING.
FIGURE 6.14: ON THE LEFT ARE PLOTTED THE XRD PROFILES OF FA1-B BEFORE AND AFTER CURING, AND ON THE RIGHT THE PARTS OF THE SPECTRUM BETWEEN 5 AND 20 2THETA DEGREES.
FIGURE 6.15: DTG CURVES OF REFERENCE PASTE, FA1-B_C3 PASTE PRE- AND POST-CARBONATION.
FIGURE 6.16: PICTURES OF THE (A) REFERENCE MATERIAL RINSED WITH PHENOLPHTHALEIN AND (B) CARBONIZED SAMPI AFTER 28 DAYS OF EXPOSURE. THE CIRCLED PARTS INDICATE THE AREAS WHERE COLOUR CHANGED, BUT HARDLY VISIBI IN THE PICTURE.
FIGURE 6.17: COMPRESSION TESTS RESULTS OF THE REFERENCE AND THE THREE DIFFERENT MIX-DESIGNS WITH FA1. THE MAXIMUM STRENGTH DECREASES FOR THE PRE-CARBONATED FA1_C2 AND WAS NON-DETECTABLE FOR FA1-B_C2. THE AVERAGE STRENGTH OF FA1-B_C3 IS HIGHER THAN THE REFERENCE SAMPLE
FIGURE 6.18: PICTURES OF (A) REFERENCE SAMPLE POST-COMPRESSION TEST, (B) FA1_C2 AFTER COMPRESSION TEST, (C) FA1-B_C2 AFTER DEMOULDING, (D) FA1-B_C3 AFTER COMPRESSION STRENGTH TEST
FIGURE 6.19: SLAKE BEHAVIOUR OF REFERENCE PASTE AND IMMOBILIZED MATERIALS AT DAY-0, DAY-1, DAY-3 AND DAY-EACH MATERIAL IS SCORED TO A NUMBER FROM 1 TO 4, WHERE 1 IS THE MATERIAL THAT RESULTED IN LESS SLAKING AN 4 IS THE MATERIAL WITH THE LEAST STABLE SPECIMEN IN WATER
FIGURE 7.1: LEACHING BOTTLES BEFORE SHAKE TEST. FROM LEFT TO RIGHT, REFERENCE SAMPLE, FA1_C2, FA1-B_C2 AN FA1-B_C3
FIGURE 7.2: LEACHING BOTTLES IN THE END-OVER-END TUMBLER AFTER ONE DAY OF SHAKING.
FIGURE 7.3: (LEFT) RESULTS OF ELECTRICAL CONDUCTIVITY AND PH MEASUREMENTS OF THE LEACHATES. FROM LEFT TO RIGHT OF EACH GRAPH ARE DISPLAYED THE VALUES OF PURE FA1, THE REFERENCE PASTE, FA1_C2, FA1-B_C2 AND FA B_C3
FIGURE 7.4: LEACHING TEST RESULTS OF THE PURE FA1, THE REFERENCE SAMPLE AND THE CARBONIZED SAMPLES. IN THE TO GRAPH ARE DISPLAYED, FROM LEFT TO RIGHT, THE CONCENTRATIONS OF BROMIDE, CADMIUM, CHROMIUM, COPPER, AN MOLYBDENUM. IN THE BOTTOM GRAPH ARE SHOWN THE CONCENTRATIONS IN MG/KG OF DRY MATTER (DM) OF LEAL ANTIMONY, SELENIUM, VANADIUM AND ZINC.
FIGURE 7.5: LEACHING TEST RESULTS ANIONIC COMPOUNDS PRESENT IN THE PURE FA1, THE REFERENCE SAMPLE AND THE CARBONIZED SAMPLES. FROM LEFT TO RIGHT ARE SHOWN THE CONCENTRATIONS IN MG/KG DM OF BROMIDE, CHLORIDE FLUORIDE AND SULPHATE.
FIGURE 8.1: DTG PROFILES OF THE REFERENCE SAMPLE FA2-B_REF, THE PRE-CARBONATED FA2_C2 AND THE PRE-CARBONATED FA2 AFTER 28 DAYS OF CURING
FIGURE 8.2: DTG CURVES OF FA2-B_REF, FA2-B_C2 AND FA2-B_C2 AFTER CURING
FIGURE 8.3: (A) REFERENCE SAMPLE AND (B) CARBONIZED SAMPLE RINSED WITH PHENOLPHTHALEIN.
FIGURE 8.4: DTG CURVES OF THE REFERENCE SAMPLE, OF FA2-B_C3 BEFORE AND AFTER CURING IN THE CARBONATIC CHAMBER
Figure 8.5: Pictures of (A) reference sample, (B) FA2_C2, (C) FA2-B_C2 and (D) FA1-B_C3 after demoulding

FIGURE 8.6: COMPRESSION TEST RESULTS OF FA2. FROM LEFT TO RIGHT ARE REPRESENTED THE MAXIMUM STRE REFERENCE SAMPLE, FA2_C2, FA2-B_C2 AND FA2-B_C3	
FIGURE 8.7: (LEFT) RESULTS OF ELECTRICAL CONDUCTIVITY AND PH MEASUREMENTS OF THE LEACHATES. FI RIGHT OF EACH GRAPH ARE DISPLAYED THE VALUES OF THE REFERENCE PASTE FA2-B_REF, FA2_C2, FA FA2-B_C3	2-B_C2 AND
FIGURE 8.8: LEACHING TEST RESULTS OF THE REFERENCE SAMPLE AND THE CARBONIZED SAMPLES. IN THE TO DISPLAYED, FROM LEFT TO RIGHT, THE CONCENTRATIONS OF BROMIDE, CADMIUM, CHROMIUM, C MOLYBDENUM. IN THE BOTTOM GRAPH ARE SHOWN THE CONCENTRATIONS IN MG/KG OF DRY MATT ANTIMONY, SELENIUM, VANADIUM AND ZINC.	COPPER, AND ER OF LEAD
FIGURE A.O.1: LIMIT LEACHABILITY VALUES PER CHEMICAL COMPONENT (BESCHIKKING 2003/33/EG)	116
FIGURE A.O.2: SOLUBILITY OF HEAVY METAL HYDROXIDES BASED ON PH (GASSER ET AL., 2021)	117
FIGURE B.0.3: EXPERIMENTAL SETUP OF CARBONATION EXPERIMENTS IN THE GEOSCIENCE AND ENGINEERING L	
FIGURE B.0.4: CRYSTALLINE PHASES IDENTIFIED FROM QXRD ANALYSIS ON THE PURE FLY ASHES	118

List of tables

TABLE 3.1: POSSIBLE MINERAL PHASES PRESENT DURING CARBONATION AND HYDRATION OF FA WITH THE CORRESPONDIN THERMAL DECOMPOSITION TEMPERATURES IN ARGON
Table 3.2: Maximum leachable concentration in mg/kg of dry matter (DM) of anion and cationic species fo unshaped building materials (Ministerie van Infrastructuur en Waterstaat, 2022)
TABLE 4.1: LIST OF FA ANALYSED IN THIS RESEARCH.
TABLE 4.2: NOTATIONS USED FOR THE PRELIMINARY CARBONATION EXPERIMENTS
TABLE 4.3: MIXTURE DESIGNS FOR THE CASTING MATERIALS WITH RESPECT OF 1 KG OF FINAL PRODUCT
TABLE 5.1: SUMMARY OF PARTICLE SIZE DISTRIBUTION OF THE SIX FLY ASHES
TABLE 5.2: CHEMICAL COMPOSITION OF EQUIVALENTS OXIDES FOR ALL FA WITH XRF IN WEIGHT PERCENTAGE [WT.%]6
TABLE 5.3: CHEMICAL FORMULAS OF CRYSTALLINE PHASES IDENTIFIED FROM THE QXRD ANALYSIS
Table 5.4: Proportions of sulphite, silicon and calcium ions present in the amorphous phases of the si materials
Table 5.5: Crystalline phases and their chemical formulas identified pre- and post-carbonation in FA1, FA and FA36
Table 5.6: Crystalline phases and their chemical formulas identified pre- and post-carbonation in FA, FA2 an FA36
TABLE 5.7: RESULTS OF WEIGHTED SUM METHOD TO SELECT THE MOST FEASIBLE FLY ASH
Table 6.1: Carbon-uptake of fly ash after 1 and 7 days of carbonation at 20° C, 1 bar, 65% RH and 1% CO ₂ an carbon-uptake of FA1 at 40° C, 2 bar, 100% CO ₂ 7
TABLE 6.2: EFFECTIVE CARBON-UPTAKE RESULTS FROM THE CARBONATION OF THE BINDER FA4 UNDER DRY (FA4_C1_WC0 and wet conditions (FA4_C1_WC3)
TABLE 6.3: EFFECTIVE CARBON-UPTAKE OF CARBONIZED FA1-BINDER MIXTURES AT 1 BAR AND 2 BAR
TABLE 6.4: EFFECTIVE MINERAL CARBONATION OF THE FA1_C2 BEFORE AND AFTER CURING
TABLE 6.5: EFFECTIVE MINERAL CARBONATION OF THE PRE-CARBONATED PASTE FA1-B_C2 BEFORE AND AFTER CURING8
TABLE 6.7: EFFECTIVE MINERAL CARBONATION OF THE FA-BINDER PASTE FA1-B_C3 BEFORE AND AFTER CURING IN THE CARBONATION CHAMBER
TABLE 7.1: RESULTS OF DRY CONTENT MATTER AND MOISTURE CONTENT ON THE DIFFERENT MIX DESIGNS OF FA19
Table 7.2: Target M_W for each material for leaching test, real M_W for each leaching test, equivalent M_D an leachate (L) for each bottle.
Table 7.3: Immobilization I_l factor for every ion in all immobilized materials and the pure FA1, along with the final score A of the immobilization methods9

TABLE 8.1: EFFECTIVE MINERAL CARBONATION OF THE FA2_C2 BEFORE AND AFTER CURING
TABLE 8.2: EFFECTIVE MINERAL CARBONATION OF THE FA2-B_C2 BEFORE AND AFTER CURING9
TABLE 8.3:EFFECTIVE MINERAL CARBONATION OF THE FA2-B_C3 BEFORE AND AFTER CURING9
TABLE 8.4: RESULTS OF DRY CONTENT MATTER AND MOISTURE CONTENT ON THE DIFFERENT MIX DESIGNS OF FA210
TABLE 8.5: IMMOBILIZATION I_t FACTOR FOR EVERY ION IN ALL IMMOBILIZED MATERIALS AND THE PURE FA1, ALONG WITH THE FINAL SCORE A OF THE IMMOBILIZATION METHODS.
TABLE B.0.1: EXTENDED LIST OF QXRD RESULTS OF IMMOBILIZED FA1 CALCULATED THROUGH RIETVELD REFINEMENT. I THE TABLE ARE SHOWN THE RESULTS OF THE REFERENCE PASTE AND THE PASTE WITH PRE-CARBONATED FLY ASH BEFOR AND AFTER 28 DAYS OF CURING
TABLE B.0.2: EXTENDED LIST OF QXRD RESULTS OF IMMOBILIZED FA1 CALCULATED THROUGH RIETVELD REFINEMENT. I THE TABLE ARE SHOWN THE RESULTS OF THE PRE-CARBONATED PASTE OF FA1 AND BINDER BEFORE AND AFTER 28 DAY OF CURING, AND THE RESULTS OF THE SPECIMEN CURED IN THE CARBONATION CHAMBER
TABLE B.O.3: WET MASS, EQUIVALENT DRY MASS AND FINAL VOLUME OF LEACHATE FOR EACH FA1 MIX DESIGN12
TABLE B.0.4: WET MASS, EQUIVALENT DRY MASS AND FINAL VOLUME OF LEACHATE FOR EACH FA2 MIX DESIGN12
TABLE B.0.5: PURE FA1, REFERENCE SAMPLE AND IMMOBILIZED SAMPLES' LEACHATES HEAVY METALS COMPOSITION. FROM LEFT TO RIGHT ARE DISPLAYED THE CONCENTRATIONS IN MG/KG OF DRY MATTER OF ARSENIC, BROMIDE, CADMIUN CHROMIUM, COBALT, COPPER AND LEAD.
TABLE B.0.6: PURE FA1, REFERENCE SAMPLE AND IMMOBILIZED SAMPLES' LEACHATES HEAVY METALS COMPOSITION. FRO LEFT TO RIGHT ARE DISPLAYED THE CONCENTRATIONS IN MG/KG OF DRY MATTER OF MOLYBDENUM, NICKEL, ANTIMON' SELENIUM, TIN, VANADIUM AND ZINC
TABLE B.0.7: PURE FA1, REFERENCE SAMPLE AND IMMOBILIZED SAMPLES' LEACHATES HEAVY METALS COMPOSITION. FRO LEFT TO RIGHT ARE DISPLAYED THE CONCENTRATIONS IN MG/KG OF DRY MATTER OF BARIUM, CHLORINE, FLUORINE AN SULPHATE
TABLE B.0.8: PURE FA2, REFERENCE SAMPLE AND IMMOBILIZED SAMPLES' LEACHATES HEAVY METALS COMPOSITION. FROM LEFT TO RIGHT ARE DISPLAYED THE CONCENTRATIONS IN MG/KG OF DRY MATTER OF ARSENIC, BROMIDE, CADMIUN CHROMIUM, COBALT, COPPER AND LEAD.
TABLE B.0.9: PURE FA2, REFERENCE SAMPLE AND IMMOBILIZED SAMPLES' LEACHATES HEAVY METALS COMPOSITION. FROM LEFT TO RIGHT ARE DISPLAYED THE CONCENTRATIONS IN MG/KG OF DRY MATTER OF MOLYBDENUM, NICKEL, ANTIMON'S SELENIUM, TIN, VANADIUM AND ZINC
TABLE B.0.10: PURE FA2, REFERENCE SAMPLE AND IMMOBILIZED SAMPLES' LEACHATES HEAVY METALS COMPOSITION. FRO LEFT TO RIGHT ARE DISPLAYED THE CONCENTRATIONS IN MG/KG OF DRY MATTER OF BARIUM, CHLORINE, FLUORINE AN SULPHATE

I. Introduction and overview

1. Introduction

In the transition towards a circular economy, the development of technologies to recover materials from waste streams for the generation of new raw materials is accelerating. As a result, landfill disposal has decreased in Europe, and non-recoverable materials are increasingly treated in waste-to-energy (WtE) plants where waste is used as fuel to generate heat and electricity. Similarly, biomass (BM) waste streams, such as wood and agricultural wastes, are utilized in BM incineration plants to produce energy. However, energy recovery through combustion also generates residues. These residual materials are often highly concentrated with heavy metals and pollutants. Although existing technologies enable the use of some of these materials in the construction industry, the remaining materials are classified as hazardous wastes due to their high pollutant concentrations, necessitating safe environmental disposal. Since resource recovery from these materials is not yet viable, alternative strategies are needed to reduce the environmental impact of their storage and disposal. In the context of reducing carbon emissions, research and applications have increasingly focused on carbon capture in cementitious materials and the potential for immobilizing heavy metals in waste streams through carbonation. This study aimed to explore this avenue by investigating the applicability of carbonation in the immobilization and storage of hazardous fly ashes, thereby making the disposal and storage less environmentally harmful.

This report is divided into 3 major sections: Introduction and overview, Experimental Investigation and Closure. The Introduction and Overview provides a brief introduction to the relevant aspects of hazardous waste management in the Netherlands as well as the motivation for the work. The objective of the research is discussed in Chapter 2, where the research questions and outline of the thesis are described. In Chapter 3 lays the literature review on immobilization technologies, carbonation mechanisms, and Dutch regulations of hazardous waste disposal. The Experimental Investigation section is the core of the report and the research. The materials and experimental methodology are described in Chapter 4. The results of the material characterization are presented in Chapter 5, after which two fly ashes are selected for further analysis. Chapter 6 presents the results of the different carbonation and immobilization routes for the selected fly ashes and Chapter 7 shows the results of the leaching tests. In Chapter 8 the different extra experiments are discussed but it is only in the final section called Closure that the results from the literature study and the experiments are discussed and the limitations of the study evaluated. Chapter 9 discusses the results and limitation of the research and Chapter 10 traces the research questions to the developments and findings of this thesis to provide conclusions and recommendations for future work.

1.1 Background

The yearly production of hazardous waste is a threat to human health and the environment (European Court of Auditors, 2023). In Europe, 95.5 million tonnes of hazardous waste were produced only in 2020. The Netherlands produced 3.0 million tonnes of hazardous waste with an increase of ~5% compared to 2010. Of all the hazardous waste produced in Europe in 2020, only 47.5% was recovered and more than 22% ended up in a landfill or in underground storage (Eurostat, 2023).

One of the hazardous wastes produced as a by-product of several industries is fly ashes. Hazardous fly ash originates from various sources, including municipal solid waste incineration (MSWI). Fly ash from MSWI contains hazardous substances like inorganic heavy metals such as Zn, Pb, Hg, Cu, Cr, Cd, and Ni easy to leach in soil and water. Also, organic dioxins can be present in the ashes, such as polychlorinated dibenzo-p-dioxins, polychlorinated dibenzo-furans and dioxin-like hydrocarbons that are highly toxic, persistent, and bio-accumulative

organic compounds. The management of hazardous components varies by country. In Europe hazardous fly ash is either landfilled, stored in underground disposal sites, or solidified and stabilized with binders and stored in a hazardous waste landfill (Zhang et al., 2020).

Renewi is a Dutch waste management company that works in a vast sector of the waste industry. One of the aspects they operate on is to process and dispose of un-processable hazardous waste. Mineralz is a fraction of Renewi operating the Maasvlakte landfill site where Dutch hazardous waste is safely disposed. Here the material is immobilized according to Dutch regulations (Beschikking 2003/33/EG). The materials arriving at the site are non-cleanable soil and dredging sludges, asbestos-containing waste, industrial sludges, and fly ashes from municipal waste incineration and other sources (Mineralz, n.d. a). This study will focus on these last hazardous fly ashes.

The secure storage of hazardous fly ash, schematically represented in Figure 1.1, requires in the Netherlands the addition of binders to prevent leaching into the environment (Beschikking 2003/33/EG). During immobilization, the material solidifies and bonds with the solid waste containing hazardous components. The heavy metals are immobilized in the carbonates by co-precipitation or physical adsorption (Yuan et al., 2022a). As a result, the volume of the waste increases but the leaching of heavy metals is inhibited by the binding agent (Guo et al., 2017).

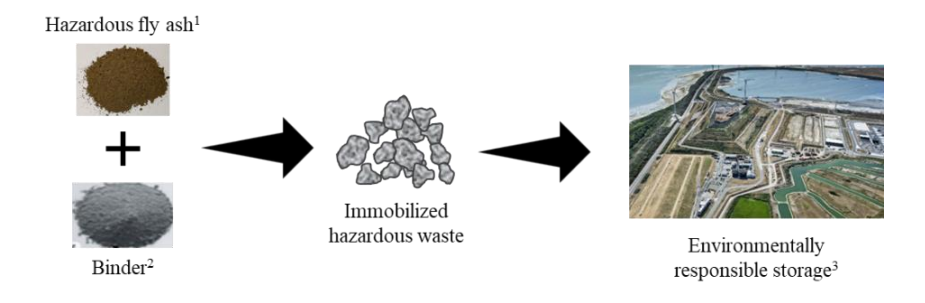


Figure 1.1: Schematic representation of the storage procedure of hazardous fly ashes used by Mineralz (¹Tomic & Ducman, 2023; ²Singh & Budarayavalasa, 2021; ³Mineralz, n.d. b).

1.2 Problem statement

The immobilization process is both material-intensive and costly, and the solidified material, with final volume larger than the initial hazardous waste, cannot be repurposed for other applications. Additionally, the high carbon dioxide (CO₂) emissions during cementation production of 1.6 billion Mt/y are another environmentally stressing aspect of the technology that is now in use (Global Carbon Project, 2023). Mineralz has already implemented its immobilization process to a lower environmentally damaging solution by replacing the binding material with a commercial by-product. One method used in the construction industry to reduce the amount of concrete and environmental impact is accelerated carbonation curing. During carbon curing, CO₂ is injected into fresh concrete to increase the strength of the material and favour mineral carbonation by the formation of CaCO₃ (El-Hazzan, 2020; Saleh, 2021). An increase in mineral carbonation has already proven to be effective in enhancing the immobilization of heavy metals. Other studies investigate the increase of mineral carbonation by injection of CO₂ into different fly ashes, resulting in higher mineralization and lower heavy metals leachability (Qin et al., 2022; Jianguo et al., 2009; Ni et al., 2017; Ren et al., 2022; Yuan et al., 2022a). To address the continuous generation of solid waste and mitigate the environmental impact of treating hazardous fly ash, a promising approach is to enhance mineral carbonation on the hazardous fly ash by carbonation.

Past research focuses on the immobilization of heavy metals from fly ash by carbonation or binder addition at different temperatures, pressures and water content (Qin et al., 2022; Jianguo et al., 2009; Ni et al., 2017; Ren et al., 2022; Yuan et al., 2022a; Singh & Budarayavalasa, 2021). However, studies have not investigated the

immobilization of hazardous fly ashes through carbon dioxide injection; instead, they primarily focus on non-hazardous fly ashes or, to a limited extent, on MSWI fly ashes. Hazardous fly ashes contain much higher heavy metals concentrations compared to coal fly ash, as well as their chemical composition is much more diverse than the other non-hazardous fly ashes (Ji & Yu, 2017). Thus, carbonation and immobilization reactions are more tedious to predict, as well as it is difficult to extend the results from previous research to the hazardous material produced in the Netherlands. Additionally, the techniques for immobilization have never been integrated into a unified process. There has been no research conducted on the carbonation potential of fly ash followed by immobilization. Furthermore, there is a lack of research on integrating binder addition and carbonation into the ash-binder mixture.

The motivation of this work is to support the development of a new solution to decrease the carbon emissions and possibly serve as long-term carbon storage. The solution has also the prospective to implement the efficiency of the industrial immobilization process of hazardous fly ashes used in the Netherlands. The focus is to bridge the gap between laboratory research and real-life application by experimenting new carbonation technologies on settings applicable to industrial applications. Increasing the immobilization efficiency by injection of carbon dioxide has the potential to reduce the use of binders for the immobilization process. Such reduction not only has the prospective of lowering the overall waste treatment costs but has also to decrease the volumes of material stored in the landfill.

1.3 Mineralz

This project is a conducted in collaboration with Mineralz. Throughout this research, the companies provided professional guidance, visits to the immobilization site, insights on real-life case and access to laboratories, materials and information. Mineralz is a sub-company of Renewi and specializes in cleaning of contaminated soils and mineral residual flows. By transforming waste materials such as bottom ashes and other industrial residues into valuable secondary materials, Mineralz contributes to the circular economy of the Netherlands and Belgium. Mineralz manages the only location in the Netherlands where hazardous waste streams can be treated in the Maasvlakte. Such wastes are asbestos-rich materials, non-cleanable sludges and soils, fly ashes from various sources, blasting agent residues and other industrial wastes.

2. Objective and scope

This research focused on the feasibility of enhancing the immobilization of heavy metals in hazardous fly ashes in the current immobilization methodology through carbonation. This work aimed at extending the understanding of current knowledge on the potential of carbonation for immobilization in industrial-scale applications. Based on an intensive literature study and consultation with the industry, the carbonization of hazardous fly ashes can occur at three different stages of the immobilization process. The processes possible are shown in Figure 2.1 below and are:

- 1. Binder mixing with pre-carbonated fly ash;
- 2. Post-carbonation of the specimens made of binder and fly ash;
- 3. Carbonation during curing;
- 4. Carbonation of fresh mixture during mixing;

Based on the equipment available for this research, this project limited its focus to only the first three possible processes (1. 2. and 3.) of carbonation timelines.

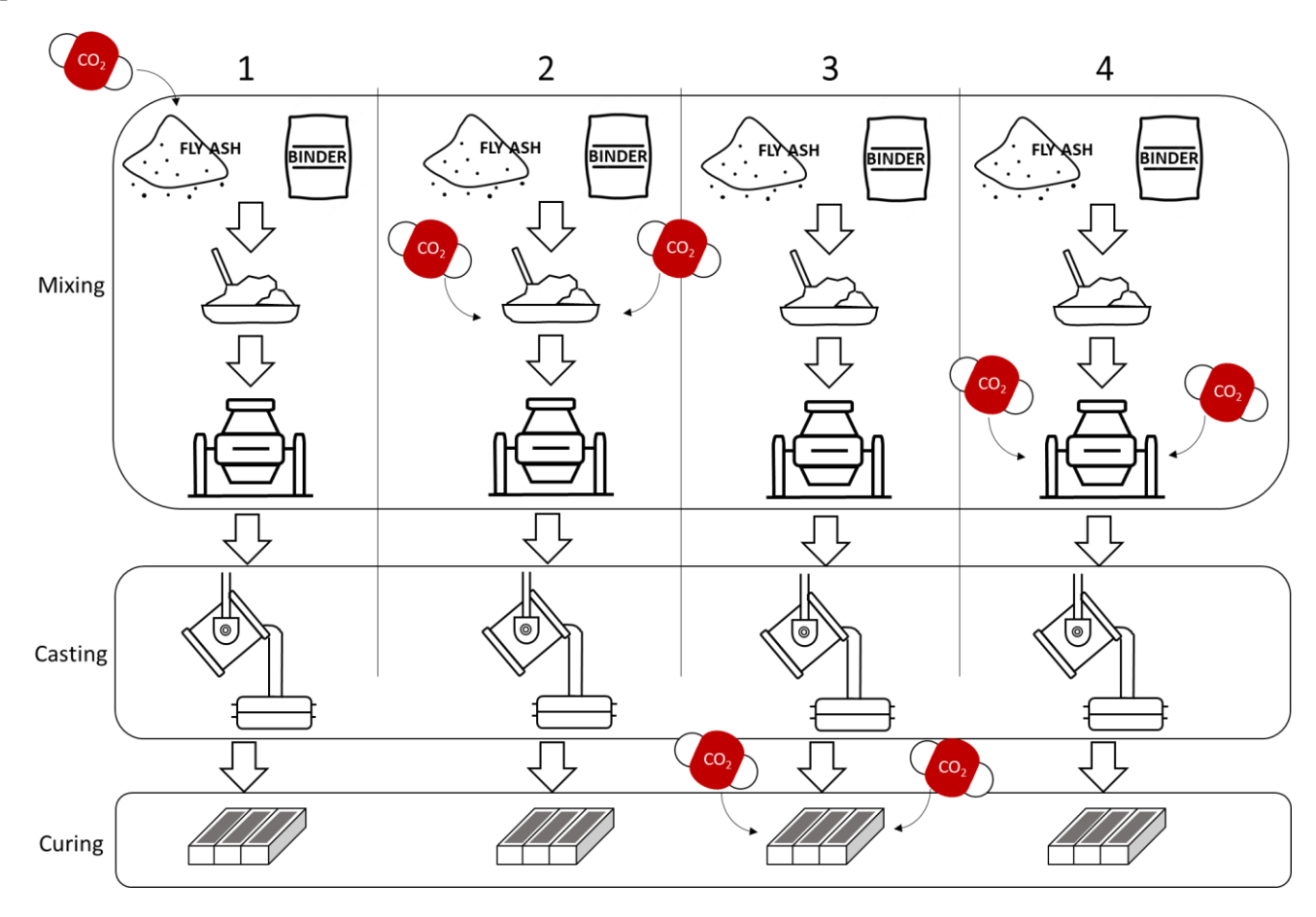


Figure 2.1: Possible carbonation routes during immobilization process of fly ashes. (1) Pre-carbonation of fly ash, (2) carbonation of the mixture fly ash and binder, (3) carbonation during curing, (4) carbonation while mixing.

2.1 Research questions

The goal of this research was to investigate the potential of mineral carbonation as supplementary immobilization process to hazardous fly ashes. Building upon the past research, this work seeked to investigate aspects of a new technology (mineral carbonation) that can be applied to the existing industrial scale immobilization process and on the real hazardous materials with high heavy metals concentrations. Following in that direction, the central question posed for this research can be broadly stated as follows:

Can the immobilization efficiency of heavy metals in hazardous fly ash improve through mineral carbonation?

This question is further subdivided into more treatable parts, each of which is addressed and tackled during this research.

RQ-1: Which fly ash is more suitable for mineral carbonation?

- a. What is the chemical composition of the available fly ashes?
- b. Which fly ashes exhibit the highest potential for carbonization and immobilization?

RQ-2: How does the binder mixing with pre-carbonated fly ash impact the selected material?

- a. Which water content and pressure are optimal for achieving higher mineral carbonation?
- b. How does the composition of the material change after the carbonation process?
- c. How does the mineral carbonation of the pre-carbonated fly ash change compared to the reference sample?
- d. How does the composition of the paste change after curing?
- e. How does the addition of the binder influence the mineral carbonation after curing?
- f. Does the final material meet the physical requirements?

RQ-3: How does the pre-carbonation of the specimens made of binder and fly ash impact the selected material?

- a. How does the composition of the mixture change after carbonation?
- b. How does the addition of the binder influence the mineral carbonation?
- c. How does the composition of the mixture change after curing?
- d. Does the final material meet the physical requirements?

RQ-4: How does the carbonation during curing impact the selected material?

- a. How does the composition of the material change after the addition of the binder?
- b. How does the composition of the mixture change after the carbonation process?
- c. How does the carbonation during curing influence the mineral carbonation?
- d. Does the final material meet the physical requirements?

RO-5: How is the leachability of heavy metals influenced by carbonation?

- a. How does the leachability vary among the different samples?
- b. Which procedure exhibits the most favourable performance in terms of avoiding heavy metals leachability?

2.2 Research outline

To answer the main research question, the study was divided into three main phases: literature study, experimental investigation and closure. An initial literature study was conducted to gain insights on the available knowledge regarding carbonation technologies for immobilization of heavy metals. Once identified the relevant research, the experimental setup was defined to answer the research questions of this project. The experimental section was further split into three main sections: characterization experiments, carbonation experiments and leaching experiments. A schematic representation of the experimental methodology of the thesis can be seen in Figure 2.2, indicating the stages at which the main questions and sub-questions are addressed. The results from the experiments are discussed and evaluated in the analysis to deliver a final outcome of the research, showing its limitation and further recommendations.

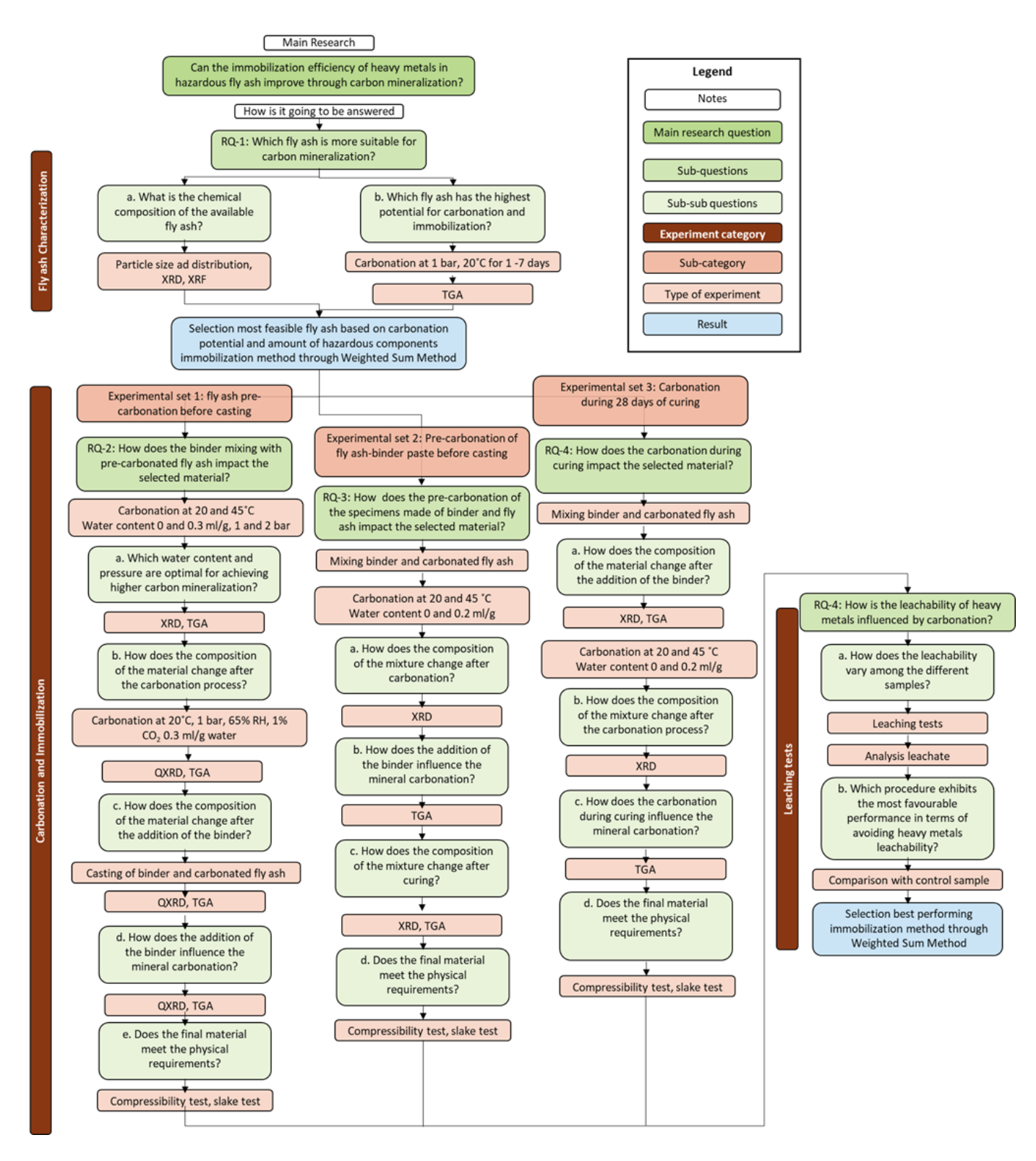


Figure 2.2: Detailed research flow diagram addressing all the questions and sub-questions identified in the methodology and in the Research Question chapter.

3. Literature review

In recent years, extensive knowledge and research on the carbonization capacity of coal fly ash (FA) have been extended to municipal solid waste incineration fly ashes (MSWI FA) (Qin et al., 2022; Jianguo et al., 2009; Ni et al., 2017; Ren et al., 2022; Yuan et al., 2022a). Previous studies have investigated the effects of time, temperature, pressure, and moisture content on carbonation processes. These factors influence both the carbonation of lime (CaO) and the immobilization efficiency of heavy metals on the tested FA.

This chapter provides a brief literature review on hazardous fly ashes and their characterization, followed by an examination of current understanding of immobilization mechanisms and existing immobilization methods and processes of heavy metals in hazardous wastes. The chapter provides an in-depth review of previous research on the potential of using mineral carbonation as immobilization process, highlighting the possible carbonation reactions and their dependence on physical and chemical factors. For this study to have a sense for the industrial practices, this chapter also gives an overview of relevant Dutch regulations concerning the disposal of hazardous waste.

3.1 Hazardous fly ashes

Hazardous FA is a by-product of industrial processes that involves the high-temperature combustion of waste materials. Incineration of waste is the ultimate method decided for the Dutch government to treat wastes once all possible recoverable materials are separated from the waste. If it is not possible to recover with the existing technologies the materials, the last thing to do accordingly to the Dutch government, is to recover some of the energy used to produce the material, using the waste as fuel for an incineration plant (Stichting LAP3, n.d.).

The Netherlands has a total of 12 waste incineration plants, spread all over the country, as shown in Figure 3.1. As from 2019, 7.4 million tonnes of waste were incinerated only in the Netherlands, resulting in a total energy production of 4010 GWh and total heat supply of 15.7 GJ. Since 2011, the amount of residual waste in Netherlands has decreased as more materials are recycled, but the total mass of incinerated waste has increased as more than 1500 kilo tonnes of waste are imported every year from other European countries (Rijkswaterstaat, 2021).



Figure 3.1: Location and names of the 12 incineration plants in the Netherlands (De Leeuw & Koelemeijer, 2022).

Waste is initially collected and dumped into a pit in the incineration plant where the waste stream is sometimes shredded, and constantly mixed to homogenise the feedstock by an overhead bridge crane. The waste material is then lifted and disposed into the combustion chamber, where the heat generated turns the water in the boiler into steam. The initial residues of waste combustion called bottom ash are collected and sent to processing plants for the recovery of precious metals and conversion into aggregates for the construction industry. This process can reduce up to 90% of the original waste volume (Setoodeh Jahromy et al., 2019). The hot air generated during combustion passes through a heat exchanger system to distribute heat to the grid and powers a steam turbine that converts mechanical power into electricity. As the hot air cools, it undergoes treatment in an air pollution control system. The gas goes through a spray dryer or electrostatic precipitator and baghouses to precipitate and collect pollutants before being released into the atmosphere. These pollutants, known as MSWI fly ash, are collected and transported to a designated landfill for the further immobilization processes, as shown in Figure 3.2 (Chester, 2016). In 2019, 183 k tonnes of total residues were produced from waste incineration, of which 100 kilo tonnes were of hazardous materials that need to be safely immobilized before disposal in a landfill (Rijkswaterstaat, 2021).

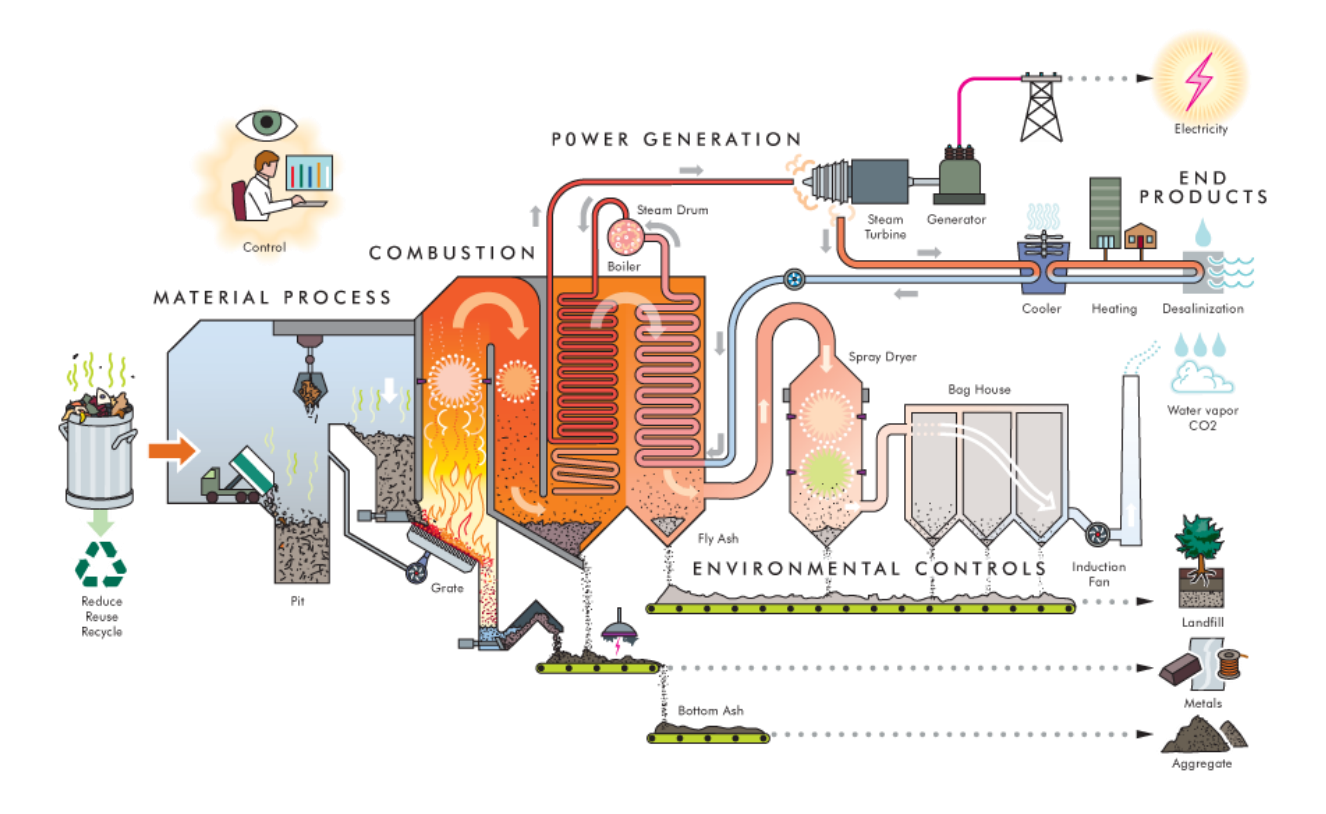


Figure 3.2: Schematic drawing of WtE plant with generation of energy, heat and residual fly ash and bottom ash (Chester, 2016).

3.1.1 Origin of fly ashes

The term of FA is typically associated with coal fly ash, the particulate produced by coal combustion and used already in the construction industry. However, hazardous fly ashes originate from combustion of waste streams and contain much higher concentrations of hazardous and toxic components. There are two main categories of fly ashes exist based on their origin: biomass (BM) FA and MSWI FA.

- BM FA is originated from combustion of organic materials. Depending on the BM plant, the burning feedstock includes wood derived from trees and forest residues, energy crops (e.g. elephant grass) and animal-based products such as livestock manure (Mida, 2009; Statista, 2024). BM is an important sector in the production of renewable energy in Europe. In 2022 electricity from BM was the third largest green source of energy after wind and hydroelectric (Statista, 2024).
- Mixed municipal solid waste (referred as "restafval" in Dutch) is another source of FA. MSWI is an alternative management method to deal with wastes from households, small businesses and institutions, excluding industrial waste. These materials, which are either heavily polluted or non-recyclable, are incinerated and MSWI FA and other residues are produced. Incineration of hazardous waste, sewage sludge and clinical wastes also creates hazardous fly ashes (Lecomte et al., 2017).

3.2.2 Composition

The composition of the residual stock in BM FA and MSWI FA is highly variable, as the original waste stream is a dynamic. Generally, the composition of FA consists of three main phases: crystalline minerals, amorphous phase

and unburnt carbon-rich particles (Ji & Yu, 2017). However, the original feedstocks for two types of FAs do not overlap, making distinguishing ashes possible based on their final FA composition.

While most materials in BM FA are organic, some inorganic and heavy metal pollutants can also be present. Wood wastes does not only consist of wood pallets and construction or demolition wood, but it also includes trees and plants used in phytoremediation projects to reclaim highly polluted areas (Mida, 2009). These wood wastes can contain residues of paints, glues, resins, plastic materials, heavy metals used in coatings, and other non-wood materials. Traces of arsenic, which was widely used in wood treatments, can still be present in demolition wastes despite its ban. The waste streams are likely to contain high concentrations of essential elements commonly found in living organisms, including carbon, calcium, and potassium (Krutul et al., 2014). BM FA contains relatively high concentrations of oxides such as CaO and MgO, but relatively low concentrations of heavy metals, as the feedstock is mainly organic matter.

The original waste contributing to MSWI FA is much more complex compared to BM FA. The large variety of different wate streams, often including hazardous wastes, results in a high variety of elements present in the FA. The principal crystalline phases present are salts like halite (KCl), quartz (SiO₂) and sulphated compounds such as anhydrite (CaSO₄). Heavy metals are generally present in much higher concentrations compared to BM FA. MSWI FA has also much lower concentrations of oxides compared to BM FA, calcium and magnesium are found mainly in the carbonized form or as sulphates (Azam et al., 2019; Shi & Kan, 2009). The carbon content is significant in MSWI FA as well due to the presence of oils and other anthropogenic organic components are present in the original feedstock (Zhang et al., 2020).

Among the various hazardous components of FA, the presence of heavy metals in the material has significant environmental and health risks. Unlike organic pollutants, which degrade over time, heavy metals are persistent in the environment and can accumulate in soils and biota, leading to long-term contamination. Their toxicity, even at low concentrations, poses serious threats to human health and ecosystems. Moreover, heavy metals can readily leach from fly ash into groundwater, further spreading contamination. Therefore, understanding and mitigating the risks associated with heavy metals in fly ash is crucial for effective waste management and environmental protection, making them a primary focus of research and remediation efforts (Tchounwou et al., 2012).

3.3 Immobilization of heavy metals

Heavy metals are naturally occurring metallic elements with atomic weight and density at least five times higher than water (Tchounwou et al., 2012). Examples include arsenic (As), cobalt (Co), chromium (Cr), titanium (Ti), nickel (Ni), cadmium (Cd), lead (Pb), molybdenum (Mo) and zinc (Zn), all located in the middle section of the periodic table. Some heavy metals are nutrients for organisms, for example iron functions as oxygen and electron transporter. Other elements in this category are highly toxic or poisonous even at low concentrations and tend to bioaccumulate. In recent years, there has been increased awareness and concern regarding heavy metals exposure due to their extensive use in various industries (European Environmental Agency, 2023). These elements are mined and produced through various chemical processes for products used in agriculture, such as pesticides and herbicides, as well as in the steel industry to produce special alloys, among numerous other applications. Elevated concentrations of heavy metals in the environment are typically caused by industrial discharges, agricultural runoff, and improper waste disposal (Tchounwou et al., 2012; Guo et al., 2017).

Contaminants are naturally retained in soils and living organisms through different mechanisms, which can limit their spread into the subsurface. From the study of these natural immobilization mechanisms, further analysis on novel materials have been investigated to develop immobilization treatments. These treatments are continuously implemented to prevent and reduce the environmental and health impacts of highly contaminated wastes.

3.3.1 Immobilization mechanisms

The main immobilization mechanisms for heavy metals are physical encapsulation and chemical stabilization (Guo et al., 2017).

Physical encapsulation involves surrounding the waste material with another material, preventing exposure to water and other leachable mediums. Heavy metals are highly leachable under certain conditions such as pH and temperature, increasing their potential to leach in the environment (Shi & Kan, 2009). By encapsulating the material in a solid matrix, heavy metals are isolated from the environment. The efficiency of this isolation depends on the porosity of the matrix; higher porosity allows more water infiltration reducing the immobilization efficiency (Singh & Budarayavalasa, 2021).

Chemical stabilization refers to changes in the chemistry of the waste material to enhance the stability of heavy metals. Hydration of calcium-rich materials such as Portland cement produces calcium silicate hydrates (C-S-H) which absorbs heavy metals in its structure, as illustrated in Figure 3.3. Heavy metals are initially adsorbed on the surface of these gels. Depending on the atomic structure, some elements can bond at (1) the edges of the silicachain, (2) become encapsulated in between layers and, with longer reaction times, (3) substitute calcium ions within the structure (3) (Vespa et al., 2014; Guo et al., 2017; Feng et al., 2024).

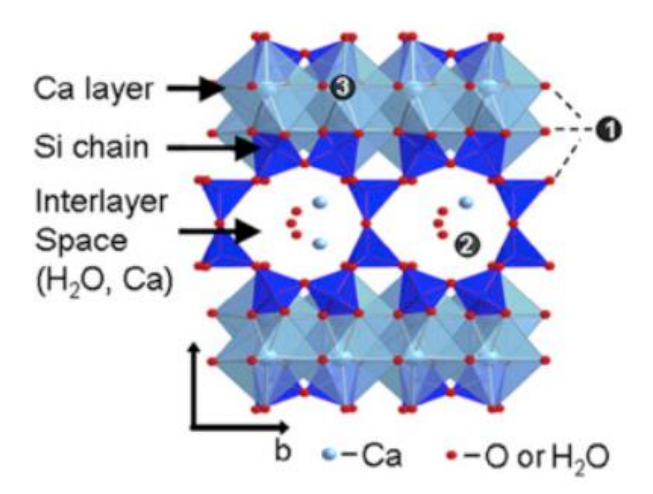


Figure 3.3: Schematic representation of the C-S-H structure and the potential locations of heavy metals. (1) Substitution on the edges of the chemical structure, (2) physical encapsulation between interlayer space, (3) substitution of Ca ions into structure (Vespa et al., 2014).

More specifically, chemical stabilization occurs in cement-like materials and through acid-base reactions.

- Heavy metals in contact with cement-like materials can also bound with a secondary hydration product of ettringite (3CaO·Al₂O₃·3CaSO₄·32H₂O), another reaction product of cement hydration. Ettringite can transform into monosulfate (3CaO·Al₂O₃·CaSO₄·12H₂O), where heavy metals can replace certain positions in the structure (Segni et al., 2006). Heavy metals such as lead, zinc, chromium and copper can also react with hydrated species to form precipitates widely described by Guo et al. (2017).
- Acid-base reactions can occur in presence of acid phosphate solutions. The phosphate solution reacts with heavy metals cations to form stable precipitates. Metal oxides such as hematite (Fe₂O₃), gibbsite (Al₂O₃·H₂O) react with phosphoric acid (H₃PO₄) to generate chemically bonded phosphate ceramics (CBPS) (Wagh, 2016).

Another method to stabilize heavy metals is through a phase transformation. At high temperatures, waste materials can vitrify, incorporating heavy metals into the matrix at the atomic level and forming strong bonds within the newly formed glass. Heavy metals with similar atomic radii (e.g. Cr^{3+} and Al^{3+}) can migrate and replace other atoms in the structure (Li et al., 2019). These strong inter-atomic bonds allow heavy metals to be permanently immobilized in the matrix. The immobilization efficiency in vitreous material depends significantly on the initial composition of the waste form, as the presence of other heavy metals can increase the solubility of the glass in water. Additionally, high temperatures can facilitate the formation of new stable crystal phases. Zinc, aluminium, and copper can bind with aluminium, iron, and oxygen to form new oxides, resulting in a reliable stabilization process (Guo et al., 2017).

3.3.2 Immobilization techniques

Several methods are employed to immobilize heavy metals in contaminated soils, sediments, and industrial wastes. These methods include solidification and stabilization of the waste followed by safe storage, thermal treatments and other new technologies in development since recent years (Guo et al., 2017; Shang et al., 2020).

3.3.2.a Solidification/stabilization and safe storage

Solidification and stabilization (S/S) of heavy-metal bearing waste is the methodology employed in the Netherlands and in other European countries to physically encapsulate and chemically stabilize hazardous material already treated before disposal (Chen et al., 2009). Hazardous wastes such as MSWI FA, contaminated soils and sludge are mixed with a binding agent like cement to form a monolithic or granular solid material, altering the leaching properties of the waste (Li et al., 2006). The hazardous components are fixed to the matrix and the final material is easier to handle and store in a secure landfill. Two major drawbacks of this immobilization technology are the high costs of the binder material and the increased final volume of disposed material that goes to the landfill compared to the non-treated hazardous waste (Chen et al., 2009).

Landfill regulations differ by country, but a schematic representation of them can be seen in Figure 3.4. Immobilized waste (shown as drummed waste in the figure) is arranged in stacked with some soil in between. The mound is insulated from groundwater sources through impermeable geotextile liners, preventing the leachate to percolate in the soil and water reservoirs. The leachate is continuously collected through a collection system, and the waters are further treated in a water treatment plant. Monitoring wells are positioned around the site to constantly monitor the groundwater levels to avoid flooding of the bottom part of the landfill and prevent a failure of the mound (Liu et al., 2018; Nathanson, 2020). Other countries like Germany do not use the S/S technique before storing but instead place the hazardous wastes in underground disposal sites such as old salt mines (Zhang et al., 2020).

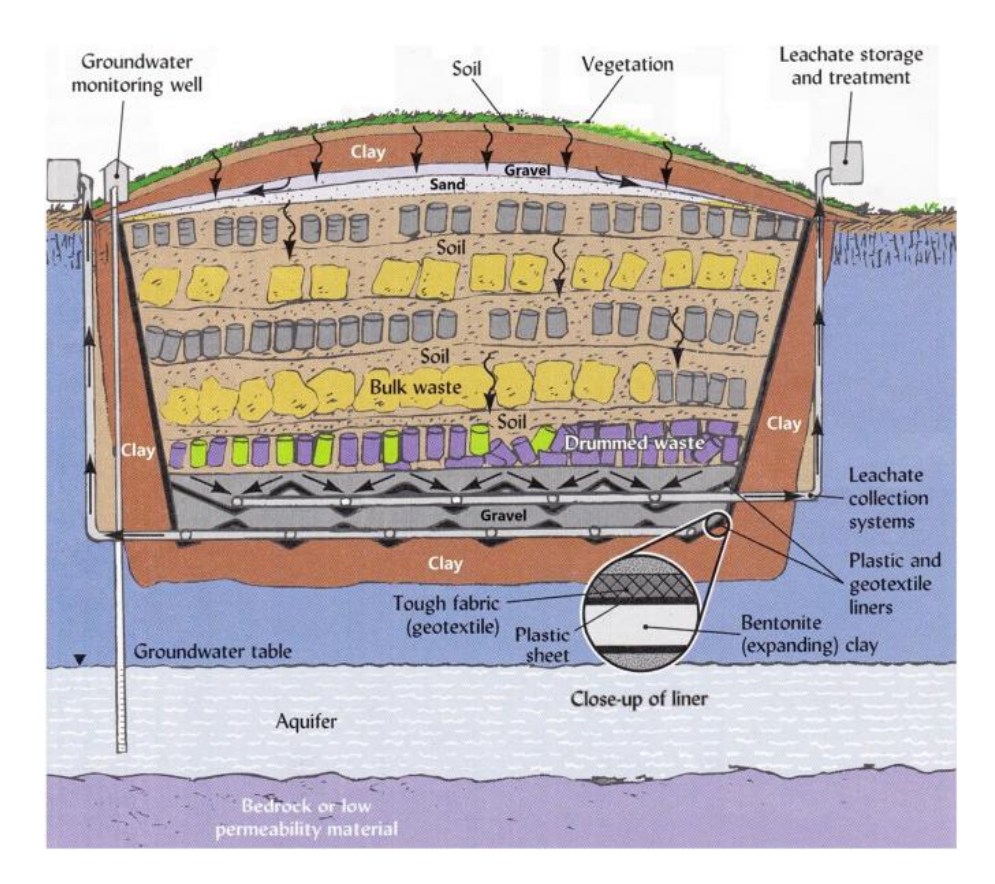


Figure 3.4: Cross-sectional drawing representing a secured landfill and safe storage site (Liu et al., 2018). In the case of the Netherlands, the hazardous waste in the image referred as drummed waste is instead a stabilized monolithic waste.

3.3.2.b Thermal Treatment

Sintering and vitrification are the primary thermal treatments used in waste treatment processes (Guo et al., 2017). During sintering (Figure 3.5a), the feedstock is deposited onto a sintering bed, where an overhead belt transports the material through the ignition jet. The heating temperatures can reach between 900°C and 1000°C, the melting point of some wastes. This process converts the chemical phases into a ceramic material, thereby immobilizing the heavy metals within the structure. Vitrification of waste streams (Figure 3.5b) is achieved by mixing glass forming raw materials and heating the mixture until it liquefies. The heating temperatures range between 1000°C and 1500°C (Guo et al., 2017). Wastes are heathen up by electrodes in a steel cylindrical chamber. The inner core melts and is collected separately to solidify, while the surface of the material inside the chamber is maintained at lower temperature to ensure thermal insulation from the surroundings. Wastes rich in silica and alumina do not require the addition of glass-forming precursors (Bernardo et al., 2012). Through a controlled solidification temperature and time, the final stabilized product of vitrification can be a glass-ceramic material with potential industrial applications due to its mechanical properties being comparable to equivalent products made from raw materials (Park & Heo, 2002). Despite the potential to stabilize waste materials, thermal treatments are not widely used due to the high operational costs and energy demand. These technologies are currently employed only in countries such as Sweden and Korea (Li et al., 2006).

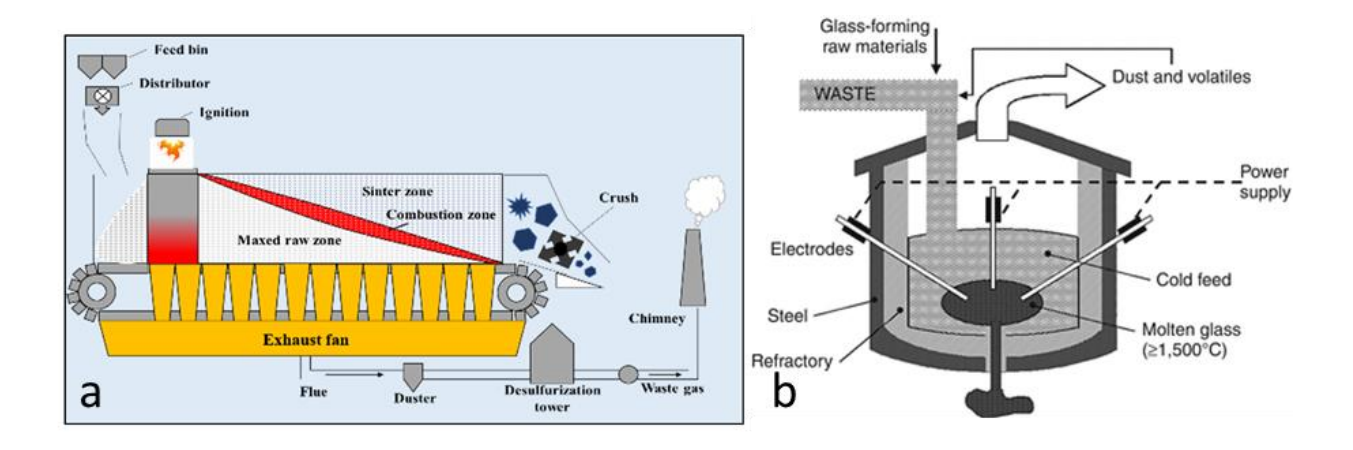


Figure 3.5: (a) Schematic representation of sintering (Gao et al., 2022) and (b) cross-sectional drawing of a vitrification chamber (Bernardo et al., 2017).

3.3.2.c New technologies

Two new technologies have been at the centre of research in the recent years to immobilize heavy metals: utilization of geopolymers as substitute to cement and carbonation of the waste stream.

Geopolymers are amorphous inorganic polymers, used as alternatives to cement in the construction industry (Singh & Budarayavalasa, 2021). The production of geopolymers involves the reuse of by-products such as slag and coal fly ash generated by industrial activities. Following in that direction, geopolymers have also been investigated as materials for the immobilization of toxic wastes rich in heavy metals. During the geopolymerisation process, heavy metals can be trapped inside the complex polymer structures. In environments rich in calcium and silicon, through alkaline hydrolysis the Si-O, Al-O and Al-O-Si bonds break. The dissolution of aluminosilicate in alkaline environment originates aluminate and silicate that are then incorporated in the aqueous phase through gelation. Depending on the pH of the solution, different Al-OH complexes form and precipitate, reorganizing into more stable gels that also include silicon. These compounds polymerize and harden, eventually precipitating, as shown schematically in Figure 3.6. Similar reactions occur for low calcium materials that form sodium aluminosilicate hydrate (N-A-S-H) or potassium aluminosilicate hydrate (K-A-S-H) gels (Vu & Gowripalan, 2018, Guo et al., 2017).

Immobilization using geopolymers is under investigation. The immobilization efficiency is highly dependent on the long-term stability of the product as well as factors such as the alkali activator used and the nature of the waste stream (Vu & Gowripalan, 2018).

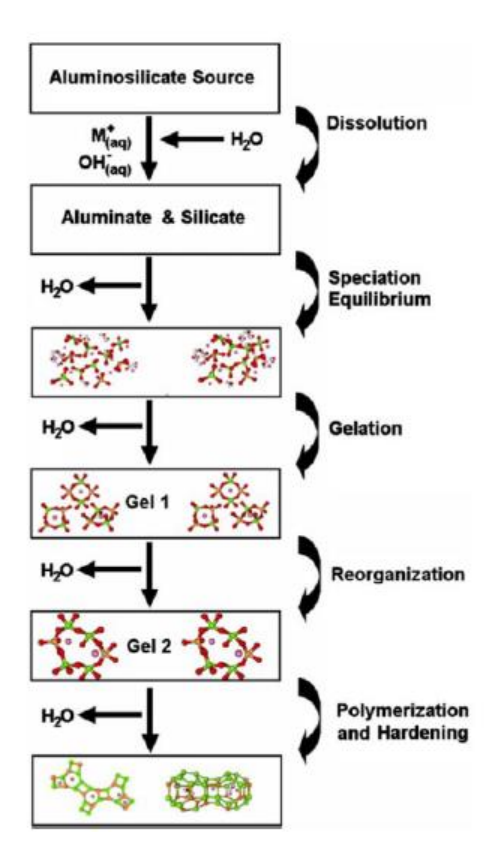


Figure 3.6: Schematic representation of geopolymerisation mechanism (Vu & Gowripalan, 2018).

The other promising technology for enhancing the chemical stabilization and physical encapsulation of hazardous material is carbonation. Mineral carbonation is already used in the construction industry as an accelerated curing process to decrease carbon dioxide emissions. CO₂ is injected into fresh concrete to enhance the carbonation reactions of components containing calcium (El-Hazzan, 2020). Additionally, carbonation of coal FA has been on the spotlight of several researchers including Li et al. (2006), Quin et al. (2022) and Yuan et al (2023). The alkali content and oxides in FA make it suitable for carbonation (Quin et al., 2022). Carbon capture can be achieved through the mineralization of CO₂ in the waste stream. Simultaneously, carbonation can trap the heavy metals through four main mechanisms studied by Yuan et al. (2023) and represented in Figure 3.7:

- Physical encapsulation
- Chemical reaction
- Adsorption precipitation
- Speciation transformation

Heavy metals can be equally physically encapsulated by a carbonate layer formed around the fly ash, a process that is non-selective for the type of element. Lead, zinc, and copper are more likely to be physically adsorbed in the new carbonate layer, or to chemically react with the carbon dioxide. Pb, Zn, Cd and Ni are likely to create speciation as a consequence of the newly formed carbonate minerals, forming hydroxides precipitates such as Zn(OH)₂. The carbonation of hazardous waste streams has the potential to both reduce global carbon dioxide emissions and increase the immobilization efficiency of heavy metals, potentially lowering the usage of binders.

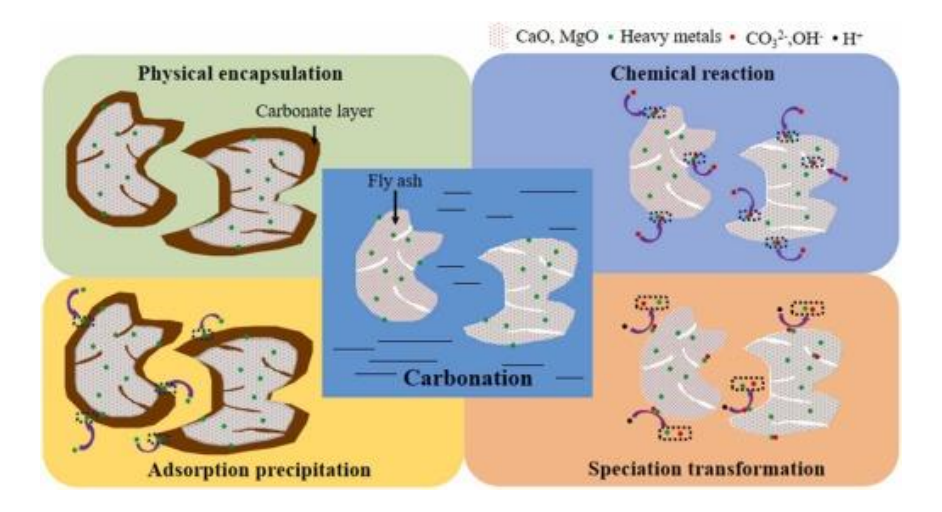


Figure 3.7: Mecahnisms of heavy metal immobilization by carbonation of fly ashes (Yuan et al., 2023).

3.4 Carbonation

Effective carbonation of fly ashes depends on several factors that have been investigated by previous researchers. Only certain minerals and compounds can carbonize within the fly ashes under hydrated or dehydrated conditions and providing that the environment is favourable for the reaction to occur. Carbonation reactions are highly influenced by temperature, time, water content, gas pressure and pH of the FA (Li et al., 2012; Quin et al., 2022; Mazzella et al., 2016; Yuan et al., 2022a; Yuan et al., 2023). These factors have been studied and investigate under different conditions and are evaluated in the following subchapters.

3.4.1 Carbonation reactions

The initial chemical composition of both the amorphous phase and the crystalline phase of fly ashes determines the carbonation potential of the FA. Generally, the main mineral phases likely to react with carbon dioxide are lime (CaO), portlandite (Ca(OH)₂), brucite (Mg(OH)₂) and periclase (MgO) (Ji & Ju, 2018). Mineralogical studies revealed that carbonation of these phases occur spontaneously at ambient pressure and temperature and the newly formed carbonates are mainly aragonite or calcite (CaCO₃), Mg-Calcite or magnesite (MgCO₃) and dolomite (CaMg(CO₃)₂) (Ji & Ju, 2018).

In complex environments more mineralogical complex can carbonize. Zhao et al. (2015) investigates the carbon sequestration of anhydrite (CaSO₄). In weak basic environment with ~9 pH compounds such as ammonia can react with water and carbon dioxide worming ammonium carbonate, that then reacts with anhydrite to form calcium carbonate or calcite as shown in Eq. (1).

$$CaSO_4(s) + CO_2(g) + H_2O(1) + 2NH_3 \rightarrow CaCO_3(s) + (NH_4)_2SO_4(aq) + H_2O(1)$$
 (1)

Another carbonation reaction that can occur with a weak basis is the reaction of magnesium sulphate with carbon dioxide shown in Eq. (2) (Xu et al., 2019).

$$MgSO_4(s) + CO_2(g) + H_2O(l) + 2NH_3(g) \rightarrow MgCO_3(s) + (NH_4)_2SO_4(aq)$$
 (2)

Lime can also be produced from decalcification of calcium-bearing compounds. Wang et al. (2010) investigated the production of titanium oxide (TiO₂) from perovskite (CaTiO₃). In sodium-rich aqueous solution sodium ions

replaces calcium ions in the perovskite. The titanium salts can be dissolved in chloride-rich solutions forming TiO_2 and CaO, as shown in Eq. (3), Eq. (4) and Eq. (5).

$$CaTiO_3 + 2NaOH \rightarrow Ca(OH)_2 + Na_2TiO_3$$
 (3)

$$Ca(OH)_2 \rightarrow CaO + H_2O$$
 (4)

$$Na_2TiO_3 + 2HCl \rightarrow TiO_2 + 2NaCl + H_2O$$
 (5)

In aqueous solutions, hydration products can form, as the fly ash reacts with water. In Figure 3.8 are represented the different phases formed depending on the pH of the liquid solution as well as the hydromagnesite concentration (Winnefeld, 2019).

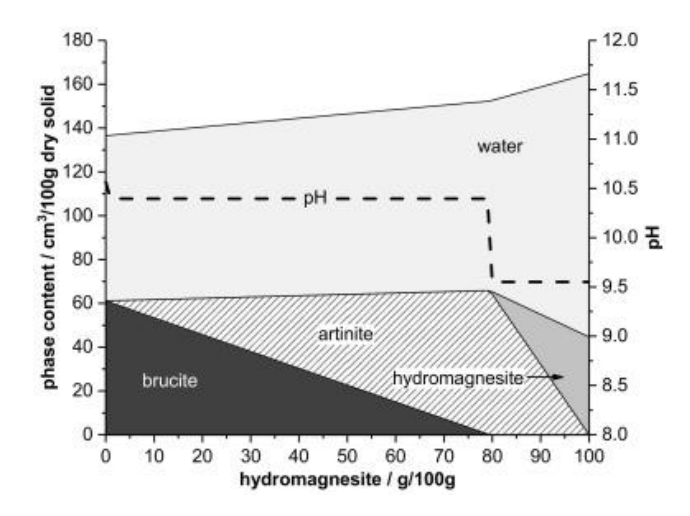


Figure 3.8: Thermodynamic modelling of the stable hydrate assemblage in MgO-hydromagnesite blends hydrated at 20°C using a water/solid ratio of 1.20 (Winnefeld, 2019).

The presence of Mg-carbonates in water can originate several different chemical structures including huntite $(CaMg_3(CO_3)_4)$, Artinite $(Mg_2(OH)_2(CO_3)(H_2O)_3)$, hydromagnesite $(Mg_5(OH)_2(CO_3)_4(H_2O)_4)$ and nesquehonite $(MgCO_3(H_2O)_3)$ (Hollingbery & Hull, 2010; Winnefeld, 2019). All these species are intermediate phases from the carbonation and hydration and thermogravimetric analysis (TGA) is commonly used to identify exactly which phase has formed. The non-chemically bound water can also be easily measured from the TGA. In TGA, samples are heated, and the mass of the specimen is constantly monitored. The mass loss at specific temperature corresponds to the thermal degradation of a compound. Thanks to extensive research on pure materials, literature has now a vast database on the decomposition temperature of every species. The carbonized and hydrated products and their thermal decomposition are reported in Table 3.1.

Table 3.1: Possible mineral phases present during carbonation and hydration of FA with the corresponding thermal decomposition temperatures in argon.

Mineral	TG - decomposition temperature
Anhydrite (CaSO ₄)	1300°C
Calcite (CaCO ₃)	670-900°C (Ji et al., 2017)
Brucite (Mg(OH) ₂)	400°C (dhy) (Winnefeld et al., 2019)
Magnesite (MgCO ₃)	617°C (dcr) (Gabrovšek et al., 2006)
Huntite (CaMg ₃ (CO ₃) ₄)	570°C (dcr) (Hollingbery & Hull, 2010)
Artinite $(Mg_2(OH)_2(CO_3)(H_2O)_3)$	219°C (dhy) – 355°C (dcr) - 429°C (dcr) (Frost et al., 2008)
Hydromagnesite (Mg ₅ (OH) ₂ (CO ₃) ₄ (H ₂ O) ₄)	270°C (dhy) – 400°C (dhy) – 520°C (dcr) (Winnefeld et al., 2019)
Nesquehonite (MgCO ₃ (H ₂ O) ₃)	200°C (dhy) - 380°C (dcr) – 500°C (dcr) (Werner et al., 2013)

3.4.1 Water content

The presence of water is one of the factors that positively influences the speed of reaction and carbonation efficiency. As shown in Figure 3.9, the water surrounding the solid particles can play an important role, as it allows the gas to diffuse and react with the solid surface in the ionic state. Carbonation products form on the surface of the particle while, an increase in heat or humidity makes the surface water evaporate, leaving the fly ash surrounded by the carbonated layer (Wang et al. 2021).

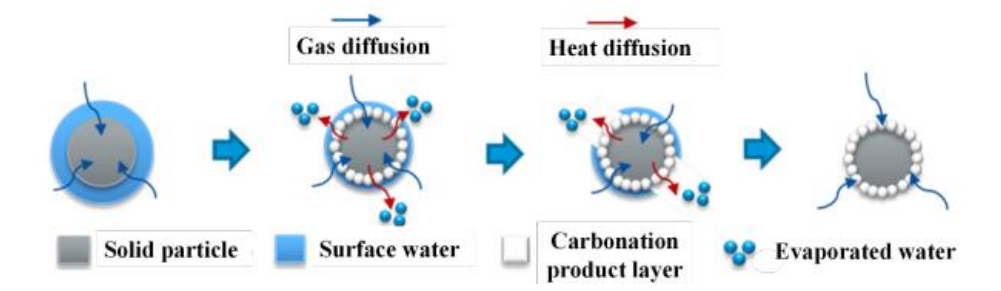


Figure 3.9: Representation of carbonation dissolution and mineralisation in low-water environment (Wang et al., 2021).

Previous research investigates the optimal liquid/solid (L/S) ratio for the best carbonation efficiency of fly ash. The ideal L/S ratio for a medical waste FA is 0.3 ml/g within a range between 0 and 0.6 ml/g, as can be seen in Figure 3.10(a) (Li et al., 2007; Baciocchi et al., 2009). Carbonation with low water content or no water results in much slower kinetics as the dissolution of carbon dioxide is only driven by temperature and pressure. However, at a higher L/s ratio, carbonation efficiency is also lower as the reaction is blocked by the resistance of CO_2 diffusion in the water. Hydration and dissolution of CO_2 is a faster process than diffusion in a solid surface, as calcium and magnesium ions dissolve in water and are more prone to react with the carbon oxide in the ionic form (Li et al., 2007; Ju & Yu, 2018). However, Baciocchi et al. (2009) shows that at higher pressure and temperature conditions, the carbonation reaction can also occur at a solid/gas interface.

3.4.2 Dependence on temperature and pressure

The efficiency and kinetics of carbonation are highly influenced by the temperature and pressure of the reaction environment. Higher temperatures typically lead to a higher carbonation rate and faster kinetics in fly ash, as the reaction activity of calcium-based materials increases (Li et al., 2012; Quin et al., 2022; Mazzella et al., 2016; Ni et al., 2017; Yuan et al., 2023; Ji & Yu, 2017). Mazzella et al. (2016) demonstrated that carbon uptake in direct contact between gas and solid is doubled at 45°C compared to a carbonation temperature of 25°C. In the presence

of water, the dissolution of the solid increases at higher temperatures; however, excessively high temperatures can limit the dissolution of CO_2 in water resulting in lower carbon uptake and reduced immobilization efficiency (Ni et al., 2017). As shown in Figure 3.10(b), carbonation is faster at higher temperatures and slower at lower temperatures (Baciocchi et al., 2009).

The immobilisation of heavy metals is also influenced by the reaction temperature. Rising temperatures enhance not only the dissolution of calcium, but also the ionization of heavy metals in water, such as Pb²⁺ and Zn²⁺. These metal ions react more easily with the carbon to form precipitates or are adsorbed by the newly formed carbonated minerals, lowering the final leaching concentrations (Vermilyea, 1969; Ni et al., 2017, Yuan et al., 2022a). According to researchers, the optimal temperatures for both effective carbonation and immobilization of heavy metals range between 45°C and 100°C (Baciocchi et al., 2009; Ni et al., 2017).

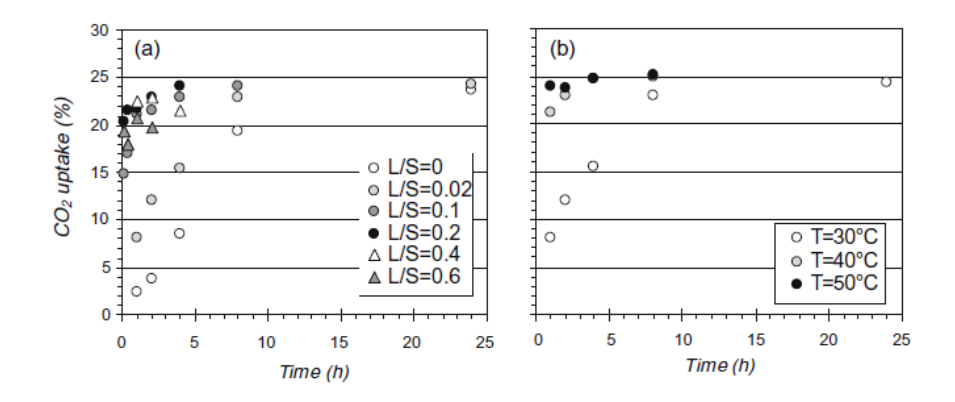


Figure 3.10: Carbon uptake as a function of S/L (a) and temperature (b) (Baciocchi et al., 2009).

The carbon uptake increases with the increase in pressure within the vessel. Following Henry's law, the solubility of a gas in a liquid is proportional to its pressure, higher pressure results in greater gas solubility. As solubility increases, more CO₂ molecules are available in the ionic state for carbonation, leading to faster reactions (Ji & Yu, 2017). When the gas reaches its supercritical state, the carbonation efficiency experiences the most significant increase, as shown in Figure 3.11. In the supercritical state, the diffusion coefficient is much larger than a liquid or a gas, as no surface tension prevents diffusion through the pores of the solid material. Diffusion of CO₂ becomes easier on the surface of the solid particles, resulting in carbonation efficiency up to 8% higher than in low-pressure conditions (Mazzella et al., 2016; Yuan et al., 2022a, Yuan et al., 2023).

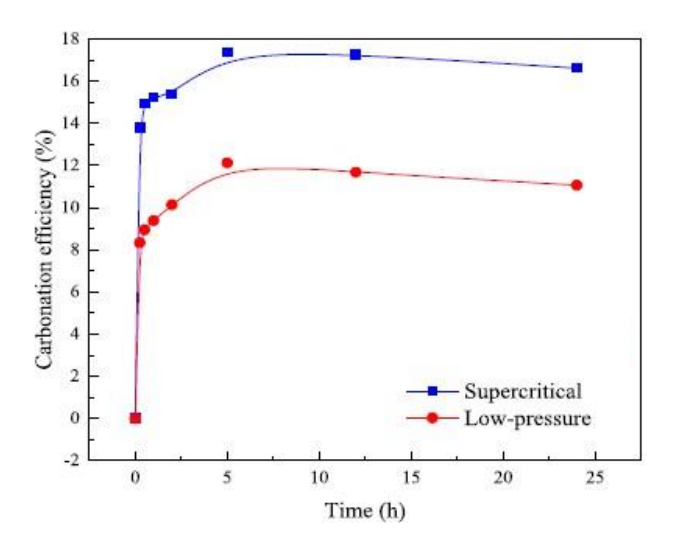


Figure 3.11: Carbonation efficiency of fly ash under supercritical conditions (80 bar) and low-pressure (40 bar) conditions (Yuan et al., 2022a).

3.4.3 Time dependency

The hydration and carbonation reactions of calcium-rich materials evolve differently over time due to the different reaction kinetics.

Hydration, nucleation and crystalline growth times vary depending on the mineral phase, as demonstrated by several researchers (Mitchell et al., 2010; Li et al., 2012; Ji & Yu, 2017). An example of different kinetics in hardening reactions is the hydration of cementitious materials. Cementation hydration reactions are divided into five main stages: dissolution, induction, acceleration stage, deceleration stage and diffusion stage. Dissolution occurs in the first minutes, during which calcium, silicon oxides and sulphates dissolve in water. In the induction stage, reaction time slows to a few hours until it accelerates again due to the nucleation and growth of hydration products. This reaction is exothermic; speeding the reaction time this stage completes after approximately 6 h. As the availability of free water decreases, the reaction slows again, and the formation of hydrate products continues, controlled mainly by diffusion, typically lasting 30 h. During the final stage, only diffusion occurs, and the reactions continue until all water has been consumed for cementation (Guang, 2024).

Carbonation and curing times are important aspects for efficient carbonation and immobilization of heavy metals. While carbon dissolution is a relatively fast process, mineralization has much slower kinetics (Mitchell et al., 2010). Altree-Williams et al. (2017) also studied the phase formation during the carbonation of anhydrite at a constant temperature over time. While anhydrite carbonates, aragonite and calcite are formed. Once all anhydrite is consumed, the crystalline phases continue to transform until they reach equilibrium only after 10 days, as shown in Figure 3.12. This extended reaction period highlights the importance of sufficient exposure and curing times to ensure complete carbonation and hardening of the material.

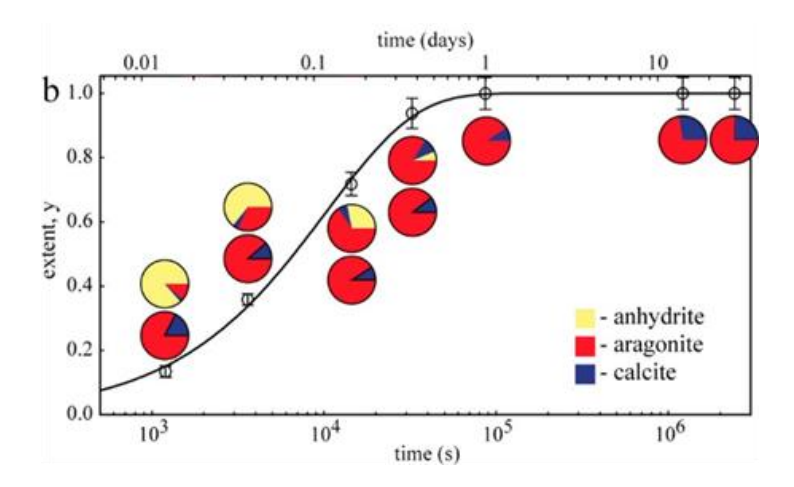


Figure 3.12: Kinetics of reaction for carbonation of anhydrite at 80°C (readapted from Altree-Williams et al., 2017).

The leachability of heavy metals is also influenced by the duration of exposure to carbonation. Qin et al. (2022) analysed coal plant FA revealing that the leachability of heavy metals decreases effectively only during a carbonation period between 1 and 4 h, as shown in Figure 3.13. Ashes carbonated for periods outside this interval show an increase in heavy metal leachability. For shorter carbonation times a significant amount of material remains unreacted, thus heavy metals have not been immobilized in the matrix. On the contrary, longer carbonation times can trigger more chemical reactions that may lead to the decalcification of calcium silicate hydrate (C-S-H) minerals (Saleh, 2021), releasing some of the heavy metals back into the environment.

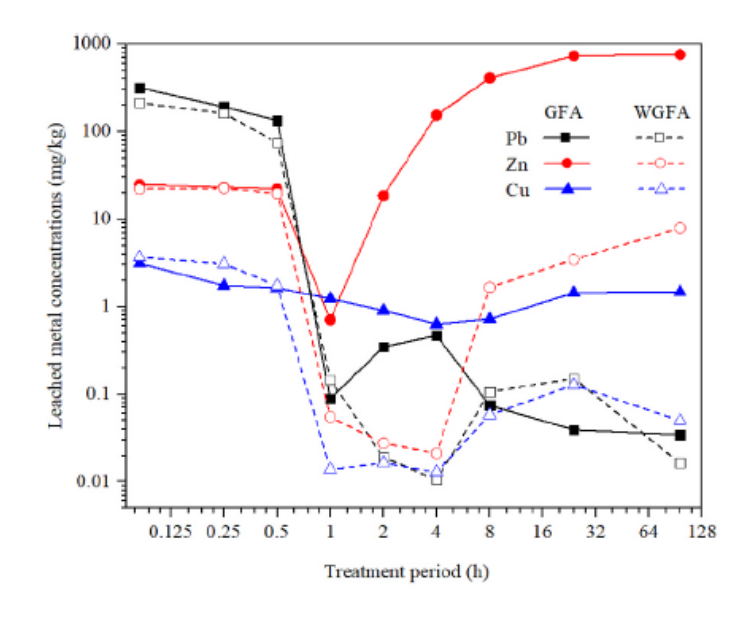


Figure 3.13: Leachability of lead, zinc and copper for FA carbonized for times in between 0.125 and 128 h (Quin et al., 2022).

3.4.5 Dependence on pH

The carbonation capacity of FA is highly dependent on the pH of the reaction environment. In alkaline conditions, the solubility of carbon dioxide increases, forming carbonate ions (CO₃²⁻). As carbon dioxide dissolves in water, the pH of the solution decreases, facilitating the dissolution of calcium and magnesium ions in the FA, which are more prone to carbonation (Ji & Yu, 2017). Higher mineral carbonation also results in higher immobilization of heavy metals, not only because of the physical encapsulation and chemical stabilization but also because the pH lowers (Bertos et al., 2004). Other dissolved species, such as sulphur and potassium in the form of H₂SO₄ and HNO₃, can react with the heavy metals to form other insoluble minerals, as shown in Figure 3.14. The minerals that form are lead sulphates, copper sulphates, zinc nitrates and others, which are not immobilizable by the carbonation of calcium and magnesium (Ni et al., 2017).

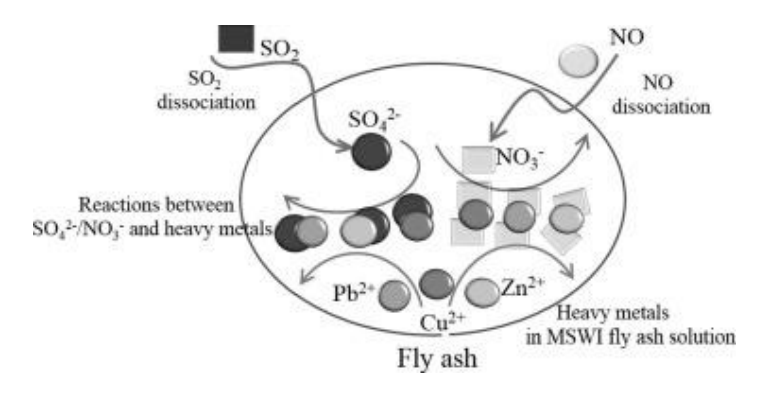


Figure 3.14: Mechanisms of reactions of H₂SO₄ and HNO₃ with lead, copper and zinc to form insoluble salts (Ni et al., 2017).

The final pH and solubility of the hardened immobilized material also influence the leachability of the heavy metals. Heavy metals generally have lower solubility in the pH range between 7 and 10, resulting in minimized leaching (Mazzella et al., 2016; Quin et al., 2022). However, this range is not the most efficient for some heavy metal such as cadmium, which shows reduced leachability only at pH levels greater than 10 (Baciocchi et al., 2009). As shown in Figure 3.15, other heavy metals such as molybdenum, chromium, arsenic, selenium and antimony, are less soluble at pH lower than 6 (Dijkstra, 2007; Król et al., 2020). A specific pH environment can both prevent heavy metals from leaching as well as favouring others. As an example, at pH between 9 and 10, cadmium, aluminium, copper, and zinc do not leach, whereas the leachability of chromium and molybdenum is at its highest (Król et al., 2020). The solubility of heavy metals hydroxides can vary from 1 mg/l to 100 mg/l with changes of only 0.5 pH and vice-versa, as reported from previous studies also shown in the Appendix (Figure A.0.2). The decrease in solubility of some heavy metal hydroxides of a factor of 10, can lead to solubilities even 100 times higher for other compounds.

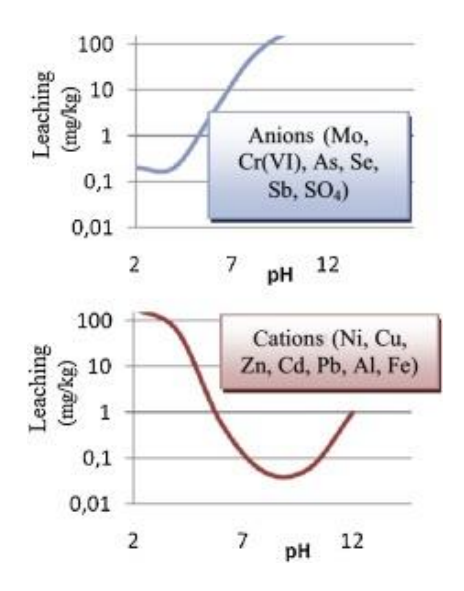


Figure 3.15: General leaching behaviour of two sets of heavy metals as function of pH (Król et al., 2020).

3.4 Dutch regulations on hazardous waste disposal and landfilling

3.4.1 Regulations

Hazardous waste management and disposal is established by European directives that are singularly applied per country. The Waste Framework Directive (2008/98/EC) is the European directive that specifies criteria to identify hazardous wastes from other wastes. In Hazardous Waste Directive (2008/98/EC) proper waste management guidelines are specified to minimize risks to human health and the environment for all European countries. In the Netherlands, the European directives have been implemented into a series of regulations included in the Wet Milieubeheer (2024). The law enforces that hazardous materials already deprived of valuable components and used for energy conversion, must be stabilized through an immobilization method and safely disposed in a specialized landfill. According to the Dutch legislation for the safe containment of hazardous waste (Beschikking 2003/33/EG), the final product must meet certain physical requirements. These regulations include specific requirements such as a designated compressive strength (1.0 N/mm²) and maximum allowable leachable components shown in Figure A.0.1 (Appendix). Besides the maximum allowable leachable components, another parameter that is necessary for the safe disposal is the stability in water. The stability is determined visually by a slake test where the material is immersed in water for several days to determine if slaking occurs (Franklin & Chandra, 1972).

Another regulation that was active until recent years is the Dutch Soil Quality Decree and Regulation (Ministerie van Infrastructuur en Waterstaat, 2022). The passed regulation states the leachability values of "niet-vormgegeven" materials. Table 3.2 below reports the limit concentrations of the leachates that were allowed by the Soil Decree for unshaped building materials.

Table 3.2: Maximum leachable concentration in mg/kg of dry matter (DM) of anion and cationic species for unshaped building materials (Ministerie van Infrastructuur en Waterstaat, 2022).

	Unformed [mg/kg DM]
Sb	0.32
As	0.9
Ba	22
Cd	0.04
Cr	0.63
Co	0.54
Cu	0.9
Hg	0.02
Pb	2.3
Mo	1
Ni	0.44
Se	0.15
Sn	0.4
V	1.8
Zn	4.5
F	20
Br	616
Cl	55
SO ₄ ² -	2430

3.4.2 Standardized tests

NEN 7375 is the standardized procedure applied in the Netherlands to determine the leachability of inorganic components applied to immobilization sites for hazardous wastes (Stichting Koninklijk Nederlands Normalisatie Instituut, 2003). The standard requires 64 days of leaching tests which might be too long given the duration of this project. However, being a time-consuming procedure, previous publications examine the possibility of comparing faster leaching tests to slower procedures (Ram et al., 2006).

An example of a standardized faster leaching test is NEN-EN 12457, used for MSWI bottom ash and highly contaminated soils. The standard includes a shaking test to fasten the leaching procedure of heavy metals for high solid-content materials and granular wastes. NEN-EN 12457 has four different variations -1, -2, -3, -4 that differ for the size of the average particle size and the S/L ratio. The first two versions are representative of material with more than 90% of the total heap with a maximum particle size of 4 mm. Version -3 and -4 are intended for materials with 90% of the particle size smaller or equal to 10 mm, but it also allows for material with bigger grain size, for size reduction. The S/L ratio considered in the four standards are of 2 l/kg and 10 l/kg, that simulate respectively the leaching behaviour of the material after 5 and 50 years (Stichting Koninklijk Nederlands Normalisatie Instituut, 2002; Stichting Koninklijk Nederlands Normalisatie Instituut, 2002b; Eurofins, n.d.). The test is also used to determine the leachability of unshaped building materials unstable under normal conditions defined in the past Dutch Soil Decree (Ministerie van Infrastructuur en Waterstaat, 2022).

II. Experimental Investigation

4. Materials and methods

An overview of previous research on mineral carbonation and sequestration is discussed in the Literature Review and it was used to identify the optimal experimental conditions to answer the research questions. At the beginning of the study, it was essential to determine the parameters relevant for this research, given that previous research analysed different fly ashes and binders as well as the immobilization efficiency at specific conditions. It was also necessary to reassess the experimental parameters selected based on the results of the first experiments. The final methodology used for this research study is described in this chapter.

This chapter lists the experimental and analysis method used in this study to answer the research questions. To determine whether carbonation influences the immobilization of heavy metals in hazardous fly ashes, the research is divided in three main experimental phases: material characterization, carbonation and leaching experiments. Chapter 4.1 describes how the composition and carbonation potential of the fly ashes are determined, to select the most appropriate material for further experiments. The selected material is used to prepare different mix designs for the immobilization process and carbonation, as explained in Chapter 4.2. the materials are also tested for their relevant physical properties, still described in Chapter 4.2. Finally, Chapter 4.3 contains the methodology to determine the leachability of the materials to finally select the most optimal immobilization process.

4.1 Material characterization

The initial phase of experiments, defined as 'Fly Ash Characterization' in Figure 2.2, aimed to address **RQ-1** and identify the most appropriate sample out of all fly ashes available for subsequent carbonation and immobilization experiments. This phase involved analysing the relevant chemical composition of the ashes, assessing the carbonation potential of each ash, and ultimately selecting the most suitable fly ash through a statistical evaluation process.

This research investigated six different hazardous fly ashes from various industrial sources. FA1, FA5 and FA6 are originated from a MSWI plant. FA2 is a BM-FA, whereas FA3 comes from another W-t-E plant. The binder used in industrial applications for the immobilization of the fly ashes is denoted as FA4 or B, and it is a by-product of paper incineration. A summary with the notation and source of the fly ashes can be seen in Table 4.1.

Name	Origin
FA1	MSWI - FA
FA2	BM - FA
FA3	E-Ash from WtE plant
FA4 and B (binder)	By-product of paper incineration
FA5	MSWI - FA
FA6	MSWI - FA

The six fly ashes not only differed in their origin, but also appear different in their colour and texture. FA1, FA5, and FA6 were of a similar shade of grey, as shown in the pictures in Figure 4.1. The colour of FA2, FA3, and FA4 tended towards brown and was generally lighter under the same light (not visible in the pictures). The grain size

of the ashes was visually similar; however, FA2, FA5, and FA6 contained light black flakes of unburnt material in the heap.



Figure 4.1: From left to right pictures of FA1, FA2, FA3, FA4, FA5 and FA6 used in this research.

4.1.1 Chemical composition

The particle size distribution is an important physical property in characterizing the material as the particle surface influences the degree of reaction (McIlvried & Massoth, 1973). Particle size distribution was carried out using a Malvern Panalytical particle size analyser through a Mie scattering model. All the fly ash samples were previously dried in an oven at 105°C for 7 h to eliminate the free water in the sample and ensure proper results.

An X-ray fluorescence (XRF) analysis was conducted to determine the elements' composition in the solid sample of the amorphous and non-amorphous phases. XRF is a non-destructive analytical technique used to determine the heavy metal content and provides a broad overview of other heavier elements present in the FA. The sample was irradiated with an X-ray beam and each element emits secondary X-ray characteristics for specific elements. Through XRF analysis was not possible to detect light elements such as hydrogen, carbon and lithium (Nakai, 2017); but combining the results with other qualitative and quantitative analysis it was possible to map the composition of the material. The sample preparation for XRF analysis required drying the material for at least 7 h at 105°C and griding the FA in a mortar until reaching a homogenous particle size smaller than 5 µm. Following the indications of the analyser Bruker S2 PUMA A35X1 ED-XRF, 4 g of fine powder were mixed with 1 g of Cereox wax (C₃₈H₇₆O₂N₂) and pressed into a pellet of 4 cm diameter and 0.25 cm thick. The loss of ignition (LOI) of the material was also determined to quantify the water and carbon dioxide content not measurable by the XRF. The LOI was necessary to calibrate and total the oxide analysis to 100% mass fraction total. NEN-EN 196-2:2013 is the standard method to determine the LOI. The sample was heated at 950±25°C for 1 h (Stichting Koninklijk Nederlands Normalisatie Instituut, 2013). The final LOI was determined as shown in Eq. (6), where $m_{pre-ignition}$ is the mass of the sample before placing it in the furnace, and $m_{post-ignition}$ is the mass after the experiment (Robertson, 2011). Following recommendations from previous studies at TU Delft, TGA in air is another approach used to estimate the LOI. However, as the results showed different values, the standardized method was chosen for this study.

$$\%_{OM} = \frac{m_{pre-ignition}[g] - m_{post-ignition}[g]}{m_{pre-ignition}[g]} * 100$$
 (6)

The crystalline structure of the fly ashes was determined through an X-ray diffraction (XRD) scan D8 Advanced Diffractometer (Bruker AXS) with a Lynxeye detector, shown in Figure 4.2C. The instrument operated at 40 kV and 40 mA with Cu K α radiation at room temperature. Phase identification of the fly ashes was determined combining the results from the XRF and XRD tests. The identification was carried using the Bruker Diffrac-plus software and the Crystallography Open Database. The fly ashes were prepared by drying for 7 h at 105°C and grinding the material until reaching maximum particle size of 5 μ m in a stone mortar, as shown in Figure 4.2A.

The material was placed inside the sample holder (Figure 4.2B) and spread as evenly as possible in the available space with the help of a small opaque glass to level the surface of the material. The analyses were executed between a 2Theta angle of 5° and 85° . The first set of experiments was conducted on a time step of 0.045° /s. To detect the amorphous phase present in the FA, the semi-quantitative analysis QXRD was conducted to quantify the amorphous content as well as the composition of the crystalline phases. 10% wt. of silicon powder was added to the samples as internal standard by weighing the material on a Mettler Toledo precision scale with accuracy of ± 0.1 mg. To improve the results and reduce the background noise, a longer step size of 0.02° /s. The results were analysed using Profex and the Crystallography Open Database through the Rietveld refinement process (**RQ-1.a**).

By combining the results from the XRF and XRD analysis it was also possible to identify the elements in the amorphous phase. The difference between the XRF [wt.%] and the equivalent sum of the crystalline phases identified resulted in the amount of non-crystalline phases. An example on how to determine the amorphous calcium ($\%_{Ca-amorphous}$) is shown in Eq. (7), where the equivalent calcium content of the crystalline phases detected through QXRD ($\%_{CaCO_3}^{XRD}$) are subtracted from the total equivalent calcium determined in wt.% through XRF($\%_{CaO}^{XRF}$).

$$\%_{Ca-amorphous} = \frac{40.1}{56.1} \%_{CaO}^{XRF} - \frac{40.1}{56.1} \%_{CaO}^{XRD} - \frac{40.1}{100.1} \%_{CaCO_3}^{XRD} - \frac{40.1}{136.2} \%_{CaSO_4}^{XRD}$$
 (7)

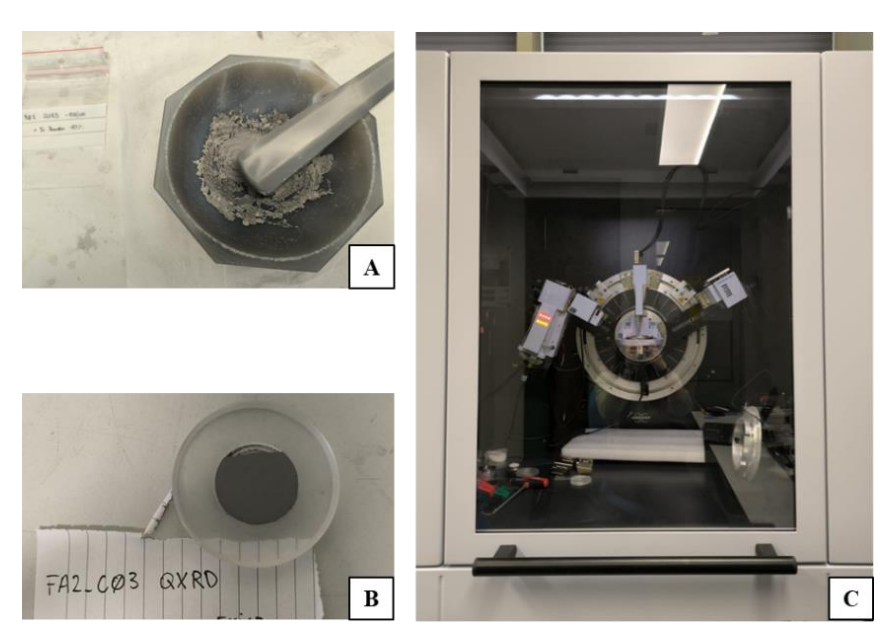


Figure 4.2: (A) Sample preparation for QXRD analysis by grinding the FA and mixing it with Si-powder. (B) sample in the sample holder that was analysed by the (C) D8 Advanced Diffractometer.

4.1.2 Carbonation potential

As discussed in the Literature Review, only some chemical compounds are likely to react with carbon dioxide to form carbonates. The chemical composition can already give an indication of the materials with the highest carbonation potential as fly ashes with no lime, portlandite, brucite and periclase are less likely to carbonate. However, the CO₂ binding capacity of each fly ashes can vary as the structure of chemical compounds is complex. The final carbonation potential of each ashes cannot be assessed merely from the amount of the crystalline phases just mentioned.

Based on previous experimental studies (Nedeljković, 2019; Yuan et al., 2022), the effective binding capacity of the six materials, defined as carbonation potential, was determined by carbonizing the samples at the same conditions and comparing their final carbon-uptake through a set of analytical methods including XRD/QXRD and TGA. It is to notice that the quantifications are only an indication of the performance of the experiment. Only one test per experiment was executed on every sample, thus the results are not representative for a larger batch of material, but only for the selected small batch tested.

Accelerated carbonation was performed in the carbonation chamber shown in Figure 4.3A. Temperature, pressure, relative humidity (RH) and CO₂ concentration were controlled and kept constant for the whole time. The temperature was fixed at 20°C, the pressure was maintained at 1 bar and the RH at 65%, at 1% by volume CO₂ environment. The fly ashes were dried at 105°C and mixed with demineralized water at a L/S ratio of 0.3 ml/g, as it was proven to be the optimal value for carbonation, as explained in the Literature Review. To ensure that all material was wetted, the powder was kneaded by hand, wearing gloves, until all powder was equally darkened. As sown in Figure 4.3B, the material was placed in plastic trays in thin layers to ensure that the maximum available surface was in direct contact with the reaction gas. Differently from previous research (Nedeljković, 2019), the material was kept at its original texture (not grinded) to prevent the liberation of physically trapped materials. The first batch of samples was carbonized for 24 h (CO_1d), but to ensure that all samples carbonize, the exposure time of the second batch was extended to 7 days (CO_7d).



Figure 4.3: (A) Carbonation chamber at fixed temperature of 20°C, pressure of 1 bar, RH of 65% and 1% CO₂. (B) Sample holder for the fly ashes to ensure maximum contact surface to the environment.

The carbonation reactions and the degree of carbonation were investigated through QXRD and TGA. To ensure that the carbonation and hydration were at an advanced stage and detectable, only the samples carbonized for 1 week were tested with QXRD. A few grams of each fly ashes were dried, grinded, and mixed with the internal standard to be analysed for their crystalline composition and the change in mineral phases and amorphous content. The carbon uptake of each sample was determined through a TG-DTG-DSC measure, where the TGA was combined with differential scanning calorimetry (DSC) to quantify the carbon uptake. The solid raw and carbonized materials were dried and grinded and around 30 mg placed in the alumina crucible represented in Figure 4.4A/B. An initial blank curve was performed by heating an empty crucible from 40°C to 1100°C at a

heating rate of 5°C/min in the Netzsch STA 449 F3 Jupiter simultaneous thermal analyser shown in Figure 4.4C. The fly ashes were tested under the same conditions, and the mass weight loss was systematically subtracted from the measure. The degradation peaks and the weight difference of the carbonized samples were compared to the TG-DTG-DSC curves, combining the results from the QXRD and previous literature studies to identify and quantify the mineralized CO₂ in the fly ashes.

The total mineralized carbon (m_{CO_2}) corresponds to all new carbonized phases in the fly ash. The degradation temperatures differ depending on the phase, as explained in the Literature Review, as well as the start and end temperature of decomposition. The weight loss between the non-carbonated and carbonated sample in the range of the decomposition indicates the carbon uptake for each species. Following Ji et al. (2017), the weight loss in carbonated sample is due to the decomposition of carbonated species in the fresh sample $(\Delta m_{x-y^{\circ}C})$ and the decomposition of the newly formed carbonated species $(\Delta m'_{x-y^{\circ}C})$. Thus, the total carbon uptake was calculated as shown in Eq. (8), where $\Delta m_{x-y^{\circ}C}$ is the mass loss of the sample in the temperature range characteristic for each compound decomposition and determined by the experimental results from the TG-curves.

$$m_{CO_2}[\text{wt. \%}] = \sum (\frac{\Delta m_{x-y^{\circ}C}}{m_{105^{\circ}C}} - \frac{\Delta m'_{x-y^{\circ}C}}{m'_{105^{\circ}C}}) \times 100$$
 (8)

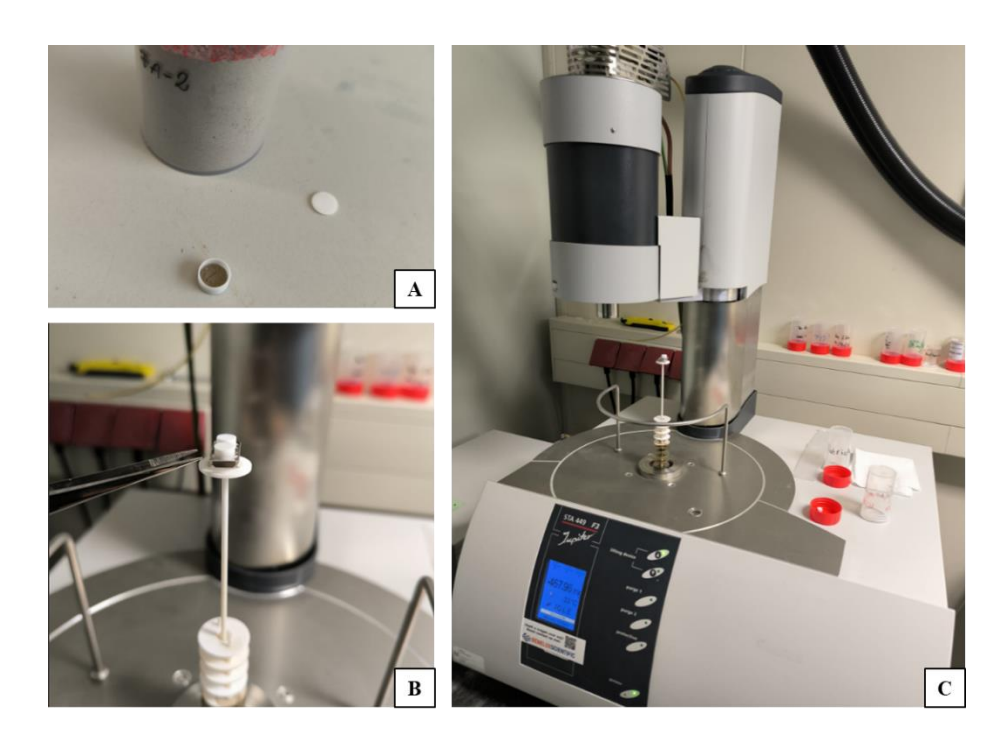


Figure 4.4: (A) Alumina crucible with on average 30 mg of grinded and dried sample. (B) Closed picture of the crucible with the sample placed next to the reference thermocouple. (C) Netzsch STA 449 F3 Jupiter simultaneous thermal analyser.

4.1.3 Selection process

The objective of the study was to immobilize heavy metals; therefore, it was important to immobilize fly ash that contains a substantial amount of hazardous components. The selection of the most feasible fly ash for this research was done by applying a simple Weighted Sum Method (Kolios et al., 2016) to each sample, assigning a value to

the alternatives (A_{FA}) as shown in Eq. (9). The total percentage of heavy metals ($\%_{HM}$) was given higher importance than carbonation efficiency, with weights of 0.55 and 0.45 respectively. The highest value of A_{FA} resulted in the optimal fly ash for this research (**RQ-1.b**).

$$A_{FA} = 0.55 \times \%_{HM} + 0.45 \times m_{CO_2} \qquad (9)$$

4.2 Carbonation and immobilization

The second phase of the research study named 'Carbonation and Immobilization' consisted of immobilizing the waste material and assessing its physical stability to answer RQ-2, RQ-3 and RQ-4.

A set of initial experiments was conducted in a small carbonation chamber to determine the ideal carbonation exposure conditions based on possible industrial applications. Carbonation of larger amount of sample, testable for physical strength, was only possible in one reaction chamber where pressure, temperature, RH and carbon dioxide concentration were fixed and not representative of the industrial conditions. The two carbonation chambers are shown in Figure 4.5; temperature, pressure and gas concentration were controlled in the cylindrical chamber in Figure 4.5A. The same experimental setup was also used to determine the influence of temperature, pressure and water content on the carbon uptake. Once selected the carbonation conditions, the three different mix designs were prepared together with a reference sample to immobilize the waste material. After 28 days at defined curing conditions, the final specimens were tested for their physical stability, as described further in the chapter.

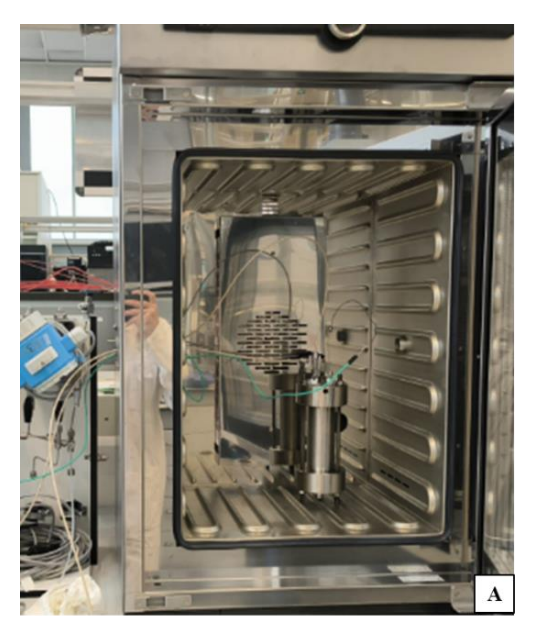




Figure 4.5: (A) Small carbonation chamber from the Geoscience and Engineering laboratory at TU Delft. P, T and CO₂ concentration were controlled in the reaction chamber. (B) Larger carbonation chamber in Stevin I laboratory at TU Delft where carbonation happened at fixed T, P, RH, and CO₂ concentration.

4.2.1 Preliminary carbonation

The preliminary carbonation experiments were divided into three main experiments. The notation used is summarized in Table 4.2

Table 4.2: Notations used for the preliminary carbonation experiments.

Notation	Experiment	Carbonation conditions
FA_C1_1	Selection of carbonation conditions	100% CO ₂ , 40°C, 1 bar, 0.3 ml/g FA, 2 h
FA_C1_WC	Influence of water content of carbon-uptake	100% CO ₂ , 40°C, 1 bar, 0-0.3 ml/g FA, 2 h
FA_C1_P	Influence of pressure on carbon-uptake	100% CO ₂ , 40°C, 1-2 bar, 0.3 ml/g FA, 2 h

4.2.1.a Selection carbonation conditions

In industrial applications, to ensure that the heap of fly ashes is homogenously distributed, the materials are mixed in a large industrial mixer. Even if the mixer is exposed to the outside air, the temperatures inside the tank body easily reach 40°C. Additionally, in case of further industrial applications, the material is preferably treated with higher carbon dioxide concentrations to maximise the contact and reaction between the gas and the material. The carbonation chamber at the Stevin I laboratory at TU Delft shown in Figure 4.5B could only operate at fixed temperature of 20°C and at 1% CO₂. As explained in the Literature Review, at these carbonation conditions the carbonation of the material occurs at much lower rate, thus carbon-uptake was slower than in a possible industrial condition at 100% CO₂ and 40°C.

As the equipment in the Stevin I laboratory was the only carbonation chamber at which significant amount of materials could be carbonized, the small setup at geoscience engineering laboratory was used to estimate an appropriate exposure time of the material in the other carbonation chamber. Figure 4.6 shows the schematic representation of the experimental setup in in the Geoscience and Engineering laboratory, and pictures of the real setup can be found in Appendix B. 10 g of FA were homogeneously mixed with 3 ml of demineralized water in a cylindrical plastic container and spread on its surfaces. The sample holder was switched to an HDPE plastic bottle as in an initial experiment a stainless steel was used but the material reacted with the steel sticking to the surface of the cylinder. Additionally, the contact surface between the gas and the vessel was limited by the diameter of the cylinder, thus it was important to maximise it by spreading the sample along the walls of the plastic cylinder. The sample holder was placed inside the cylindrical vessel with 2 cm diameter and 10 cm long, and properly connected to the system. Before the beginning of the experiment, the exhaust valve was closed, and the system flooded with N₂ gas. All connections were rinsed with the specific Snoop liquid leak detector, a surfactant that, in case of a gas leak, generates small bubbles. Once the system was properly insulated, the exhaust gas valve was opened, and all liquid was dried from the equipment. The vessel was placed inside the oven that was turned on to the desired temperature of 40°C. Through a pressure regulator in between the carbon dioxide cylinder and the reaction chamber, the gas was de-pressurize to 1 bar. Once the temperature inside the vessel was equal to the one in the oven, the inlet valve was opened until the absolute pressure gauge reaches 1 bar. The temperature in the closed cylinder raised in less than one hour to the desired value, whereas the pressure, once the gas valve was opened, taking less than two second to reach the target. Based on the relevant research discussed in the Literature Review, the material was exposed for 2 h to carbon dioxide. At the end of the experiment, the inlet gas and oven were turned off. The carbon uptake of the sample was measured through TGA and compared with the carbon uptake after 1 day and 7 days (C0_1d, C0_7d).

The optimal exposure time (t_x) was determined by interpolation as shown in Eq. (10), where the carbon uptake after 1 day $(m_{CO_2}^{7d})$ and 7 day $(m_{CO_2}^{7d})$ was compared to the carbon uptake at 40°C $(m_{CO_2}^{40°C})$ (1d and 7d stands for 1 day and 7 days). For simplicity, it was assumed that the carbon-mineralization is linearly proportional to exposure time in between 1 day and 7 days.

$$\frac{t_x - 1d}{m_{CO_2}^{40^{\circ}C} - m_{CO_2}^{1d}} = \frac{7d - 1d}{m_{CO_2}^{7d} - m_{CO_2}^{1d}}$$
(10)

Experimental set-up carbonation fly ash

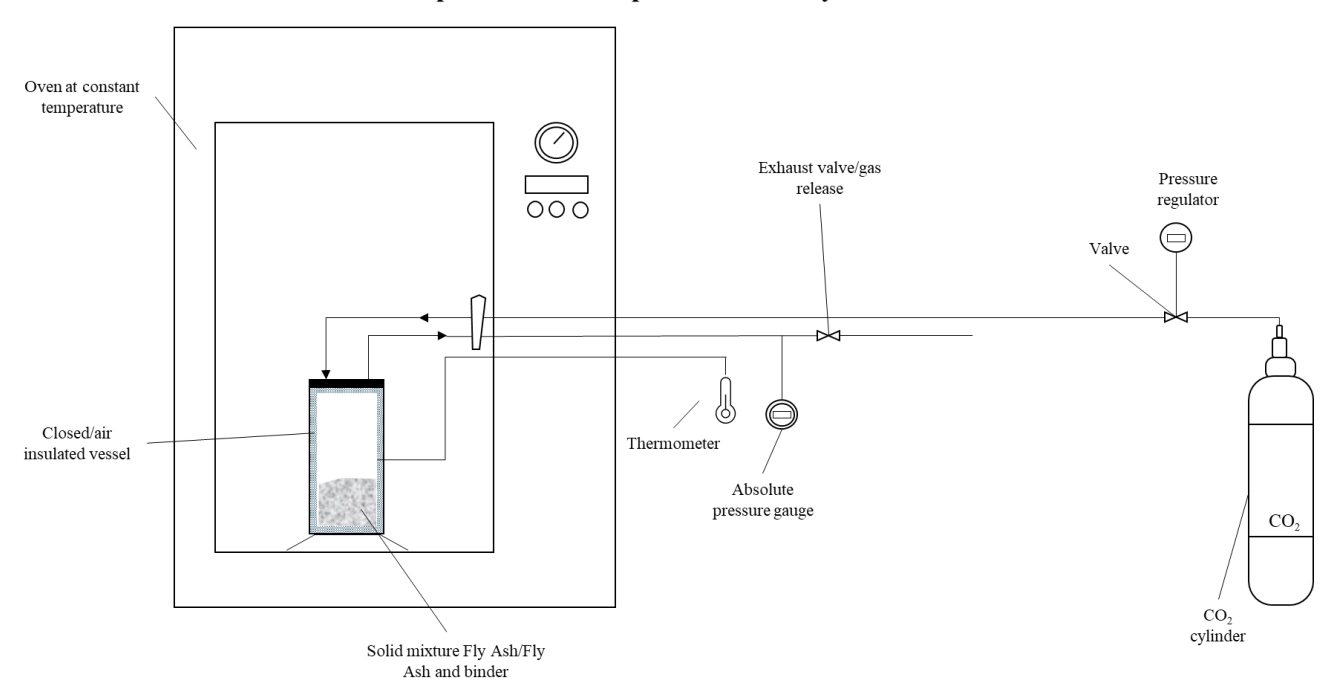


Figure 4.6: Experimental setup of carbonation chamber from the geoscience and engineering laboratory at TU Delft. A cylinder containing pressurized CO₂ was connected through capillary plastic tubes to an insulated stainless-steel vessel placed inside an oven. Temperature and pressure inside the vessel were monitored, and the gas was released through a valve outside the oven.

4.2.1.b Carbonation conditions and carbon-uptake

The experimental setup shown in Figure 4.6 was also used to determine the influence of water, pressure and binder presence on the carbonation reaction (**RQ-2.a**). Carbon uptake was investigated at water contents of 0 ml/g and 0.3 ml/g, at pressures of 1 bar and 2 bar and with or without the addition of binder to the fly ash. This aimed to comprehend the influence of these factors on both the mineral carbonation as well as the rate of reaction.

Influence of water-content on carbon-uptake

The binder, FA4 was used as referece to assess the impact of water on the mineral carbonation. Following on the previous studies presented in the Literature Review, this research investigated the carbonation efficiency in the absence of water and at a water to FA ratio of 0.3 ml/g. In case sufficient carbonation on the selected fly ash occurs without the addition of water, the process would become even less material intensive. However, it was important to compare the mineral carbonation without the addition of water with the optimal L/S ratio of 0.3 ml/g, established by the previous studies. While carbonation is known to be faster in the presence of water (Tominic & Ducman, 2023), the absence of a stirrer inside the reaction vessel might reduce the contact surface between the gas and the fly ash, potentially compromising the reaction and preventing the ash from reaching its maximum carbonation potential. Therefore, the chosen reaction at 100% CO₂ at 45°C and 15 bar should aim for a maximum carbonation efficiency, as demonstrated by Mazzella et al. (2016). This procedure also helped mitigating the risk of equipment damage due to the entrapment of liquid in some vessel cavities. In absence of water, 10 g of dried raw fly ashes were directly placed in the sample holder. The operational steps were the same as explained before, besides the exhaust gas valve was closed before the cylinder valve was opened. The temperature of the oven was set to 45°C and the CO₂ cylinder was depressurized until 15 bar.

Influence of pressure on reaction rate and carbon-uptake

The same experimental setup and operational conditions were used to determine the influence of pressure on the reaction rate and mineral carbonation. For this experiment, a mixture of the selected fly ash and binder was chosen to ensure that the carbonation rate is detectable. The FA alone had less components that can mineralize compared to the large amount of lime present in the binder. Additionally, the scope of the experiment was to determine how both materials together behave to the carbonation, as the larger amount of mineralized carbon was expected from the carbonation of lime from the binder.

The ratio FA/binder/water was maintained constant for the mixture, where 10 g of FA were mixed in the plastic sample holder with 3 g of binder and 3 ml of demineralized water. Following Çengel & Boles (2005), carbon dioxide behaves as an ideal gas at 40° C, 1 bar and 2 bar. Considering isothermal conditions and the fixed volume inside the vessel, the number of CO_2 moles reacted (n_{CO_2}) as function of time could be monitored as shown in Eq. (11) (see Appendix B for detailed calculations). In the equation, $P_f(t)$ represents the pressure inside the vessel at a specific time, P_i is the initial pressure inside the vessel and n_i is the initial amount of CO_2 moles present in the vessel.

$$n_{CO_2}(t) = n_i - \frac{P_f(t)}{P_i} \times n_i$$
 (11)

The reaction rate (R) was calculated by differentiating the number of moles of CO_2 reacted (dn_{CO_2}) with respect to time (dt), as shown in Eq. (12). This gave the rate at which CO_2 was consumed in the reaction for the different experiment. The carbonation rates at low and higher pressure were compared to the mineralized carbon of each process determined by TGA. As explained previously in the Carbonation Potential chapter, the carbon uptake was this time balanced for the proportions of FA and binder. In Eq. (8) the mass drop of the fresh samples $\Delta m_{x-y^\circ C}$ was rescaled as 77% mass of FA was present in the total material, as only 3 g of binder were present in 13 g of total FA-binder mixture.

$$R = \frac{dn_{CO_2}}{dt}$$
 (12)

4.2.2 Mix designs

Continuing with the procedure employed at the Maasvlakte site, the hazardous components in the ashes needed to be immobilized by adding the binder used by the company. Three different fly ash/binder mix designs were prepared to answer the research questions **RQ-2**, **RQ-3** and **RQ-4**. In this study, the baseline for the research on the immobilization process was to maintain the fly ash-binder-water ratio constant.

A reference sample (FA-B_Ref) was initially prepared to define the FA/binder/water ratio for all mix designs. This was necessary as in industrial applications the ratio varies as the composition of the FA is also variable. Generally, the FA/binder ratio was maintained constant at 100:30. In the industry, the water content varies based on the behaviour of the material in the mixer, if the mixture is too dry, water is added until it reaches the earth-moist like texture desired. In industrial applications, the FA-water varies between 300 and 450 g/kg of FA.

The reference sample of the selected FA was prepared initially mixing it with binder at a ratio of 100:30 and water at a FA-water ratio of 100:30. For the preparation of the refence sample, 577 g of fly ash were weighted in a Mettler PM 16 scale shown in Figure 4.7A and poured in the 51 laboratory bench mixer from Hobart, as shown in Figure 4.7B. The corresponding amount of binder (173g) was added, and the dry materials mixed for 10-15 seconds at low mixing settings. A small plastic cylinder was filled with 300 ml of demi-water and added while mixing, still at low-speed settings. Water was poured until the material reached the ideal consistency and texture shown in

Figure 4.7C. After 10-15 seconds, the mixing speed was increased to the medium settings for 1 to 2 minutes, until all the material was homogeneously mixed. The additional water added to the system was recorded, resulting to a final FA-water ratio of 100:43.3. The material was casted in polystyrene moulds $40x40x160 \text{ mm}^3$, compressing the paste by hammering the material inside the mould. As the material was highly porous, it was important to compress it to consolidate the material. The mould was wrapped in plastic foil and stored for 28 days in standard curing conditions at $20 \pm 2^{\circ}\text{C}$, and RH in between 98 and 95%.

The final FA-binder-water ratio was maintained constant for all casting designs, shown in Table 4.3. It is to note that the mixtures were not optimized for all the cases, as the texture of the material texture and its composition varied for the pre-carbonated compared to the raw materials. The earth-moist texture of the reference sample was not obtained in all mix-designs.

Table 4.3: Mixture designs for the casting materials with respect of 1 kg of final product.

	FA Carbonized [g/kg]	Binder Carbonized [g/kg]	FA [g/kg]	Binder [g/kg]	Water [g/kg]	FA:Binder	FA:Water
FA-B_Ref	-	-	577	173	250	100:30	100:43.3
FA_C2	577	-	-	173	250	100:30	100:43.3
FA-B_C2	577	173	-	-	250	100:30	100:43.3
FA-B_C3	-	-	577	173	250	100:30	100:43.3

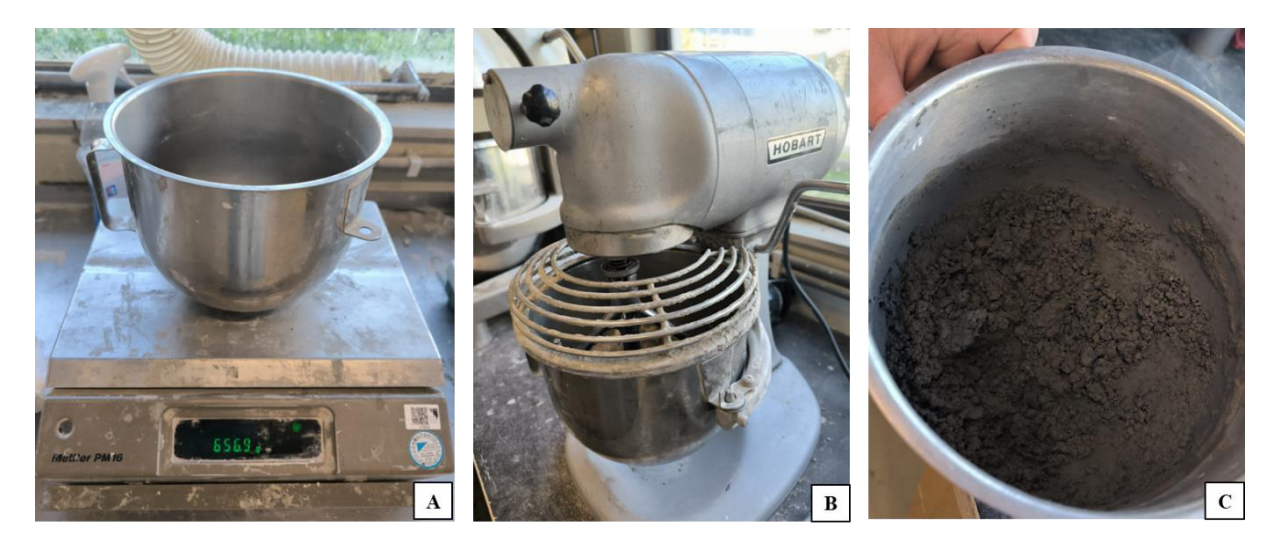


Figure 4.7: (A) Measuring scale for preparation of fly ash-binder-water mixture. (B) Hobart industrial mixing device used for mixing the materials before casting. (C) Ideal earth-moist texture of reference sample after mixing.

4.2.2.a Pre-carbonated fly ash

In the second mix design (FA_C2), carbonation was carried out on the selected hazardous fly ash before the addition of the binder. The fly ash was weighted in the same Mettler PM 16 scale shown in Figure 4.7A and 0.3 ± 0.01 ml/g of demi-water were added to the FA. The material was mixed by hand until homogeneously wetted. The FA-water mixture was placed in large plastic trays and spread all over the surface, as shown in Figure 4.8A, to ensure the highest contact surface in the carbonation chamber. The carbonation time was defined from the previous experiments and the reaction conditions were maintained constant at 20°C, 65% RH, 1 bar and 1% CO₂. Heavy metals immobilization can occur during the mineralization of CaCO₃ and later during the addition of binder. Pre-carbonation of the ash had less components that could mineralize compared to the calcium and manganese

present in the binder. However, the pre-treatment of the material had the potential to effectively immobilize part of the hazardous compounds.

At the end of the exposure time, mineral carbonation and residual water content in the sample were measured through TGA. To monitor changes in the mineral composition the sample was also analysed under QXRD (**RQ-2.b**). Even if 0.3 ml/g of water were already added to the system, during carbonation some water evaporates. The remaining effective water was determined from the TG mass drop at 105°C. The carbonized material, once removed from the carbonation chamber, was weighted, and poured in the same bench mixer shown in Figure 4.7B. The corresponding amount of binder was added, and the dry materials were mixed at the same settings as for the preparation of the reference sample. The evaporated water was slowly re-added to the system together with the remaining 76.9 g/kg of liquid. Once the material was properly mixed, the material was casted and cured following the procedure of the reference sample. Characterization through QXRD and TGA was done also right before curing (**RQ-2.c**) and after 28 days of curing (**RQ-2.d**).

4.2.2.b Pre-carbonated fly ash-binder mixture

The fly ash and the binder were mixed together with the same water-to-fly ash ratio and placed in the carbonation chamber for the second mix design (FA-B_C2). During this second procedure mineral carbonation was enhanced as more lime is present due to the binder addition. However, it is to note that to maintain constant the fly ash-to-water, the total L/S ratio was lower than for the first experiment. Less water was available to dilute the carbon dioxide and the material remains drier compared to the previous carbonation, as shown in Figure 4.8B. A lower water content during carbonation might result in a lower carbonation efficiency, at the same time, pre-carbonation of the binder might result in weakening of the sample. The water retained in the sample was quantified through TGA and the material was transferred to the Hobart mixer where it was combined with the remaining demi-water until the mixture reaches the ratio in Table 4.3. Samples were casted and cured following the procedure of the reference sample. To determine the mineral carbonation at each stage of the immobilization process as well as the mineral phases formed, TGA and QXRD were performed right after carbonation (RQ-3.a; RQ-3.b) and after 28 days of curing time (RQ-3.c).

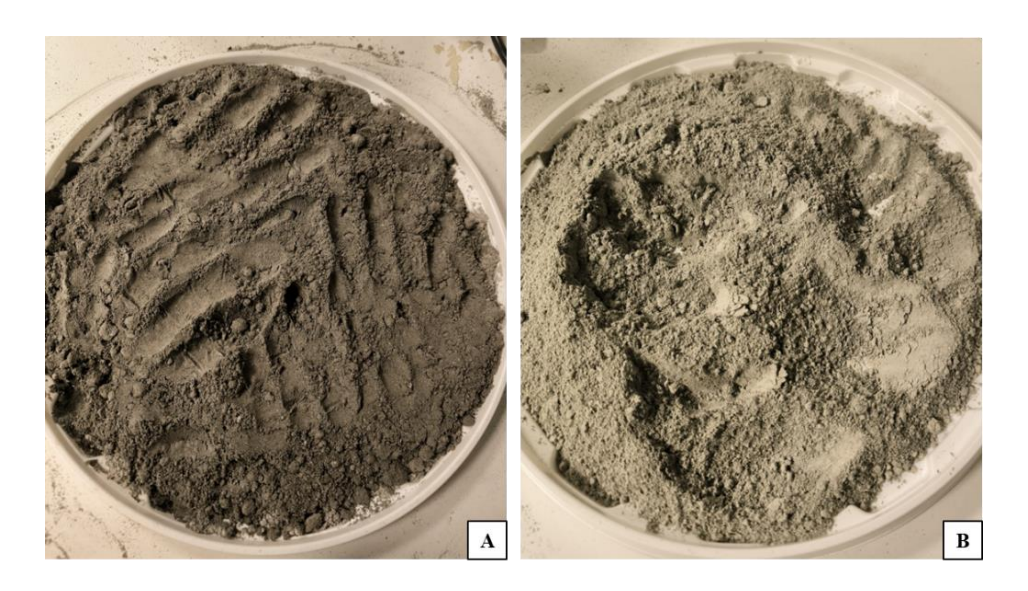


Figure 4.8: (A) FA and water mixture in large plastic tray before placing in the carbonation chamber. (B) Mixture of FA, binder and water before carbonation.

4.2.2.c Curing in carbonation chamber

The last mix design consisted of carbonizing the material during casting. The immobilized sample was prepared as the reference sample, but, after casting, it was placed in the carbonation chamber for 28 days. The evolution of the crystalline phases was monitored through QXRD and TGA pre-carbonation (**RQ-4.a**) and after 28 days in the carbonation chamber (**RQ-4.b**).

Carbonation on this last mix design might be inhibited by the polystyrene mould. As the mould surrounded the immobilized fly ash, carbon dioxide could only penetrate from the upmost top surface exposed to the gas. Even if both the mould material as well as the immobilized FA were highly porous compared to other cementitious materials, a quick carbonation test was executed to ensure that the gas penetrated the sample. The sample was cut perpendicular to the exposure plane, as shown in Figure 4.9. The phenolphthalein solution is a pH indicator that turns purple when in contact with a basic and remains colourless for pH values less than 10. In the concrete industry the indicator is used to detect the carbonated (pH<9) from non-carbonated area (pH>9). The solution turns purple in non-carbonated areas whereas it remains colourless where the sample is carbonated (Lo & Lee, 2002). As the effectiveness of the test was dependent on the pH of the solution and the final material was not concrete, the reference sample was also rinsed. This is to ensure the validity of the test and to compare the colour change for the two specimens.

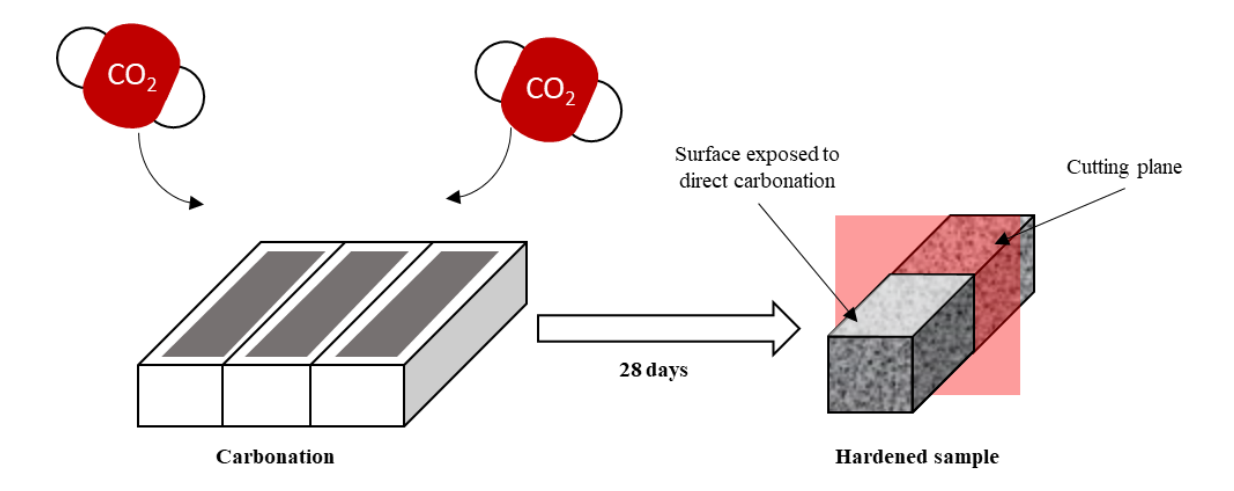


Figure 4.9: Schematic drawing of cutting plane (red) on FA-B_C3 for carbonation depth test. After 28 days, the sample was removed from the polystyrene mould and cut perpendicularly to the plane exposed to carbonation. The new surface was sprayed with phenolphthalein to determine the carbonation depth.

4.2.3 Physical stability

The final materials were tested after 28 days of curing for physical stability through flexural, compressive strength test and the slake test (**RQ-3.**; **RQ-3.**; **RQ-3.**). The final material needs to provide sufficient stability for the safe storage, also described previously in the Literature Review. The results from these tests were already and indication for the long-term stability of the immobilized material.

4.2.4.a Physical strength

Initially the flexural strength based on NEN-EN 196-1:2016 (Stichting Koninklijk Nederlands Normalisatie Instituut, 2016) was performed on the demoulded samples. The specimens with size of 40x40x160 mm³ were tested after 28 days in a Matest compression and flexural machine shown in Figure 4.10A. The prisms were placed in the testing equipment with the plane exposed to air facing the operator, as shown in Figure 4.10B. As the material was weak compared to concrete samples, the starting load point was initially chosen at 0.100 kN, at 0.100 kN/s. It was afterwards lowered to the minimum of the machine at 0.050 kN and the rate set at 0.050 kN/s, with stop load at 20%. The broken specimens were further testes in the same machine for compression test by switching the sample holder to the apparatus shown in Figure 4.10C. Following NEN-EN 12390-3 (Stichting Koninklijk Nederlands Normalisatie Instituut, 2019), at least 40x40 mm² of contact surface had to be smooth and not damaged by the previous test. The plane exposed to air during curing had to face the operator and not one of the contact surfaces as it was not evenly smooth, to ensure that the load was evenly distributed on the surface. The starting load and rate used were of 0.100 kN and 0.100 kN/s, with stop load set at 20%.

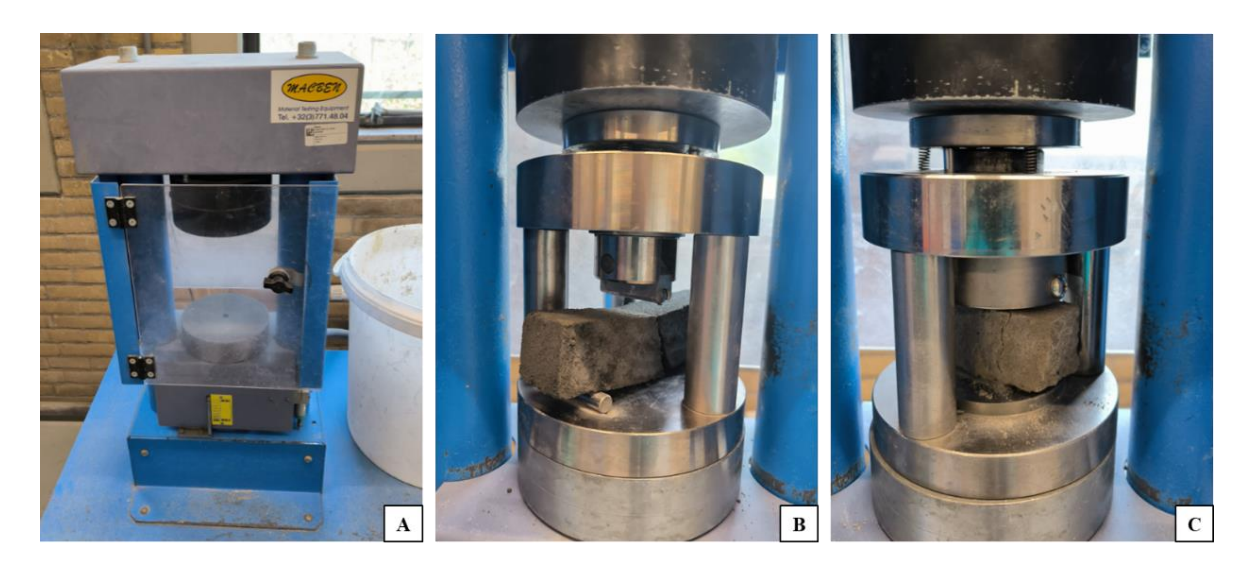


Figure 4.10: (A) Dual flexural and compressional Maset strength test. (B) Material under flexural strength test. (C) Specimen tested for compression strength test.

4.2.3.b Slake test

The stability in water of the material was another important factor to determine the durability and integrity of the final immobilized material exposed in the open air. The slake test was a rapid test used widely in soil investigations to demonstrate the performance of stabilized soils and other construction materials (Hartono et al., 2019). Through the test it was possible to assess the material's resistance to water-induced degradation that could enhance the leachability of pollutants and heavy metals in the water bodies.

The immobilized material was placed as shown in Figure 4.11 A and B on a mesh to hold the sample. The mesh was located inside a 1 litre glass beaker filled with demineralised water to ensure that all surfaces of the samples were covered with the liquid. As a proper wire mesh was not available, a perforated alumina tray was used instead for the experiment to keep the sample suspended in water. It was important to refill the water level after a few days to ensure that the samples were constantly fully covered with water. Pictures of the evolution of the samples were taken at the beginning of the experiment, after 1 day, 3 days and 7 days to detect the slake behaviour of each immobilized material.

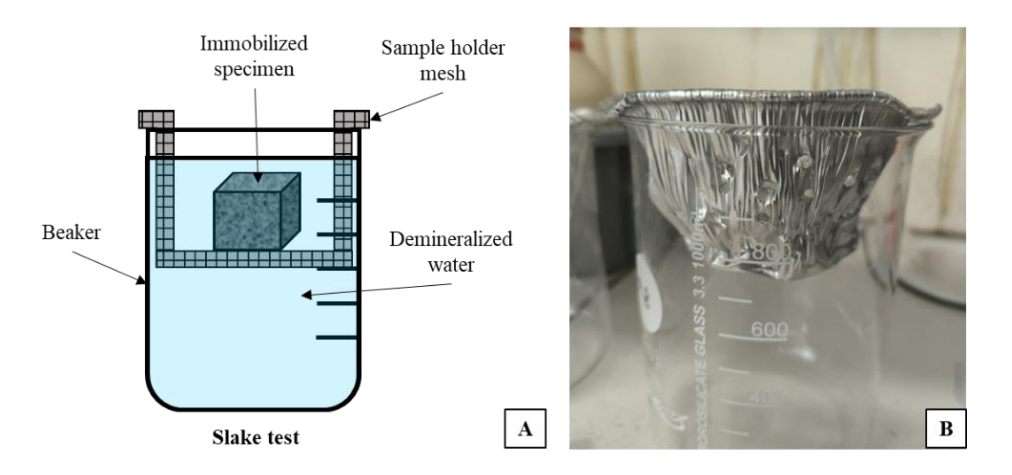


Figure 4.11: (A) Schematic representation of experimental setup used for the slake test. (B) Real equipment used for the tests.

4.3 Leaching experiments

The purpose of this study was to determine whether the final material was still highly toxic or if the heavy metals were efficiently immobilized. Therefore, the final experimental step consisted on leaching tests to evaluate the potential release of contaminants from the immobilized materials.

In industrial application, as mentioned earlier in the Literature Review, the immobilized materials are tested for leaching following the standardised procedure defined by the Dutch government NEN 7375 (Stichting Koninklijk Nederlands Normalisatie Instituut, 2004). Even considering the reliability of the method and the fact that is the real final judge of whether the immobilization process is successful or not, two main limitations do not make the standard feasible for this study. The first problem is the stability of the material. The procedure requires a monolithic sample for the leaching column test, stable in water. However, this research focussed on maintaining the final S/L ratio of FA and water constant. Favouring a constant ratio results for some samples in a non-stable final product, the structural resistance of some materials might be influenced by the prolonged carbonation before casting. Another issue is the long testing time required by the norm. The test requires at least 64 days of testing, which would correspond to half of the Master thesis' time. As the goals of the research were multiple and defined in the Objective and Scope, this study considered other normalised leaching procedures also presented in the Literature Review. The leaching test preferred allowed all the carbonated samples to be tested with the same procedure and within the times of this project.

NEN-EN 12457 resulted in the most applicable standard leaching tests given the material and time restrictions of this research (Stichting Koninklijk Nederlands Normalisatie Instituut, 2002). Both monolithic materials as well as unstable materials could be tested through size reduction in only one day, with some extra time required for the filtration and analysis on the leachate. This chapter explains the preparation of the leaching material, the leaching procedure and the final analysis on the leachate.

The variant of the standard used in this research was NEN-EN 12457-4:2002, for materials with grainsize below 10 mm and L/S ratio of 10 l/kg. By using this variant, both structurally stable samples as well as non-stable and weaker specimens were tested under the same conditions. Additionally, the largest L/S ratio was chosen as it predicts the leaching behaviour over a longer time period, as explained in the Literature Review. Following the standard, the leaching tests was divided into three main phases: preparation of leaching material, leaching test, leachate separation and analysis of the leachate.

4.3.1 Leaching material

For correctness and reliability of the results, the standard contains a procedure for the preparation and initial characterization of the sample. The material was weighted on the ±0.1 g precision scale from Sartorius shown in Figure 4.12A. The heap was sieved through the sieve in Figure 4.12B from W.S. Tyler Company and the final sieved portion weighted again. The sieve used for this study had grid size 0.577 mm smaller than the standard requires, but it was the closest to the 10 mm available in the laboratories at TU Delft. In case the sieved material was composed of at least 95% mass with grain size less than 10 mm, the material went directly through the leaching procedure. If less than 95% of the original heap complied with the particle size requirement, the whole heap was collected and crushed by hammering. The crushing procedure used for all the samples was the same to reduce differences in the leaching behaviours. The heap was not fully crushed to powder, but until more than 95% of the blocks passed through the sieve, as shown in Figure 4.12C. In case the moisture content in the sample was too high for the material to be sieved and crushed, the material was dried at 40°C for 7 h. To avoid contamination of the sample during sieving, the sieve had to be always cleaned of the residues from the previous materials.







Figure 4.12: (A) Sartorius weighing scale with precision of ± 0.1 g used to measure the material for the leaching tests. (B) Sieve used to separate the material with particle size larger than 10 mm. (C) Immobilized material after hammer crushing.

The dry matter content ratio (DR) and moisture content (MC) based on the dry matter are estimated to determine the amount of leachate necessary for each sample, as well as the solid content. A separate portion of each sample was dried at 105±5°C overnight and its DR and MC were calculated as follows in Eq. (13) and Eq. (14).

$$DR\left[\%\right] = \frac{m_d}{m_w} \times 100\tag{13}$$

$$MC \left[\%\right] = \frac{m_w - m_d}{m_d} \times 100 \tag{14}$$

Following the procedure in the standard, three samples of 0.090 ± 0.005 kg of dry mass each from all the immobilization processes were prepared based on each DR content (Eq. (12)). The split material was placed in 1 l glass bottles, with caps of inert high density polyethylene material. The leachant (L) used in the leaching experiments was distilled water at 7 pH in $20\pm2^{\circ}$ C. The amount of liquid necessary for each sample was also dependent on the moisture content, as the L/S ratio had to remain constant at 10 ± 0.2 l/kg. Eq. (15) shows how to determine the volume in litres of demineralized water necessary for each sample experiment.

$$L = (10 - \frac{MC}{100}) \times m_d \tag{15}$$

Water was measured through a 1 l measuring cylinder from Duran[®] with ± 5.0 ml accuracy, pictured in Figure 4.13A. The leachant was slowly poured in the glass bottles in Figure 4.13B, properly closed with the non-reactive lid. For repeatability and a better evaluation of the behaviours of the materials, three different bottles containing samples for all immobilization procedure were prepared.

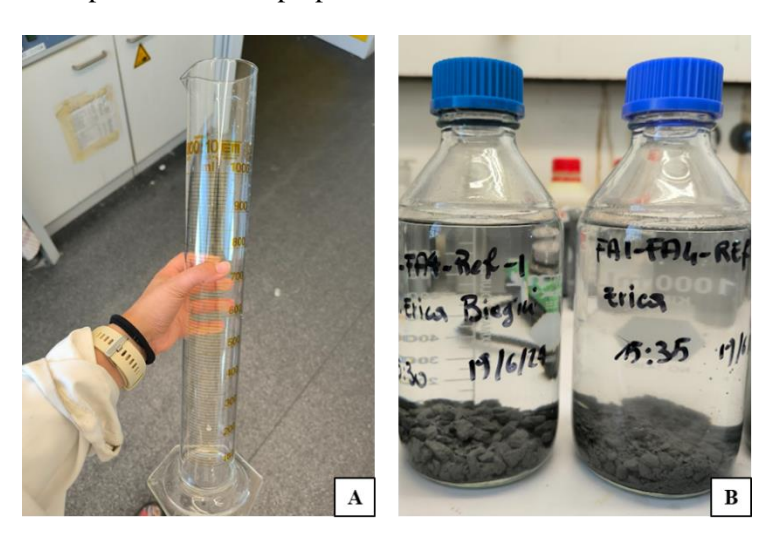


Figure 4.13: (A) Measuring cylinder to measure the correct amount of leachant. (B) 1 litre glass bottles used for the leaching experiments as denoted from the standard NEN-EN 12457-4:2002.

4.3.2 Leaching procedure and extraction of leachate

The standard provides two specific types of shaking devices, as previously explained in the Literature Review. In this study an end-over-end tumbler was used, schematically represented in Figure 4.14A. The glass bottles were fixed to the rotating device and, in case, a small volume was added to ensure that the bottle did not slip during shaking. Before the start of the test, the device was run at 1 rpm for a few rotations to ensure that all bottles remained in place and no material leaked. Once the safety of the personnel was secured, the end-over-end tumbler was set at rotation speed of 5 rpm for 24±0.5 h. At the end of the shaking experiment, bottles were retrieved, and the material was left to settle for 15 minutes.

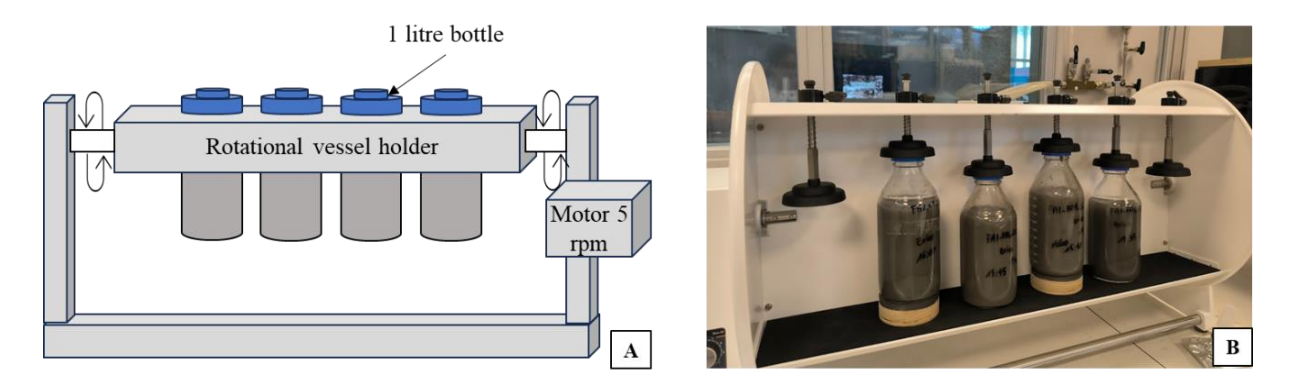


Figure 4.14: (A) Schematic representation of end-over-end tumbler and (B) real device used for the shake test.

At the end of the leaching test, the water had a turbid texture as can be seen from Figure 4.14B. To further test the liquid for the leaching of anions and cations, the eluate was filtered to remove all suspended materials. Membranes with 0.45 μ m pore size from Macherey-Nagel were used together with a vacuum filtration device shown in Figure 4.15. The membrane was placed in a filtering funnel of the appropriate diameter and fixed in a glass conical flask of at least one litre. The funnel with the membrane was rinsed with distilled water and the system sealed with a rubber rig placed in between the funnel and the flask. The pump was turned on and the material in the leaching bottle was slowly poured through the funnel. As the membrane available for the filtering were only of 70 mm diameter, they soon got saturated with the material. Filtration stopped, and the membrane was replaced with a new one.

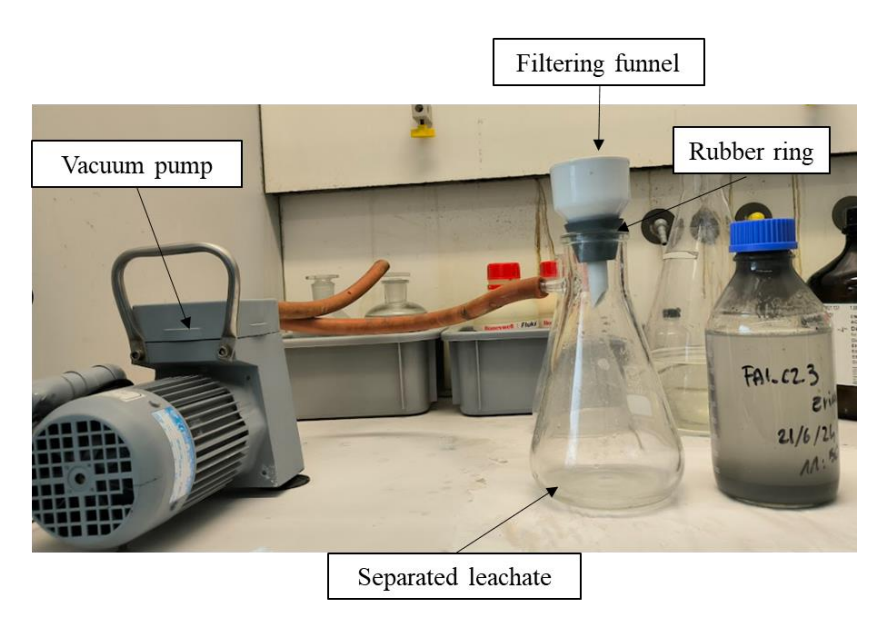


Figure 4.15: Filtering equipment used to separate the leachate from the suspended material.

4.3.3 Analysis of the leachate

The temperature, electrical conductivity and pH of the leachate were immediately tested after the solid-liquid separation as determined by the standard. Two thermometers were used to measure the difference in temperature between the liquid and air. The leachate was transferred to a smaller glass beaker and the fluid was mixed with a magnetic stirrer. After prior calibration of the measuring devices following the standard procedures, the pH of the

leachate was tested with the 827-pH lab from Metrohm, until the pH reading stabilized for at least five seconds. The electrical conductivity in mS/m was measured through a Philips portable conductivity meter.

The heavy metals composition of the leachates was characterized by an external company (SGS) to assess its composition and adherence to permissible levels of leachable compounds (**RQ-5.b**). The waters were analysed for their anions and cations concentrations. Fluoride, sulphite, and chlorine concentrations were measured following the standard NEN-EN-ISO 10304-1 (Stichting Koninklijk Nederlands Normalisatie Instituut, 2009) in mg/kg of dry matter (DM), whereas cations concentrations were determined as stated in NEN-EN-ISO 17294-2 (Stichting Koninklijk Nederlands Normalisatie Instituut, 2023). The last elements determined were arsenic, antimony, barium, cadmium, chromium, cobalt, copper, lead, molybdenum, nickel, selenium, tin, vanadium and zinc.

Since the leaching tests in this research study did not follow the Dutch regulation (Beschikking 2003/33/EG), it was also not possible to compare the results to the limit values. Thus, two control samples were used to determine the immobilization efficiency of the immobilization processes (1), (2) and (3) in Figure 2.1. The control samples were the virgin selected fly ash and the fly ash immobilized following the current immobilization procedure used in the Netherlands. It is important to have an idea of the magnitude of the expected leachability of the raw sample as well as the leaching behaviour of the procedure used in industrial sites. The results of the control sample (x_c) were compared for each chemical component with the leachability results (x_i) of every immobilization process tested, to determine the immobilization efficiency I_i as shown in Eq. (16).

$$I_i = \frac{x_i}{x_c} \quad (16)$$

The immobilization efficiency was only estimated for the elements detected above the detectable limit. The optimal immobilization procedure was then determined by following the Weighted Sum Method and assigning a value (A_I) to the alternative immobilization processes as shown in Eq. (17). In this case, N corresponds to the number of chemical components that were analysed. Each chemical component was normalized by (w_i) to ensure that ions present in small quantities did not interfere majorly with the results. All ions were assigned the same weight since all parameters must conform to the limits stipulated by Dutch regulations governing the criteria and procedures for the acceptance of waste at landfills (Beschikking 2003/33/EG).

$$A_I = \sum_{i=1}^{N} I_i \times w_i \tag{17}$$

The assigned values of all experiments were ordered and the immobilization process with the smallest A_I resulted in the best procedure (**RQ-5.b**). An A_I value smaller than one resulted in an immobilization procedure better than the reference sample.

The results from the leaching test were also compared to the Soil Quality Regulation (Ministerie van Infrastructuur en Waterstaat, 2022) which describes the maximum leachable material allowed in unstable building materials. The values do not represent the requirements for the acceptance of waste at landfills. However, as the experiments were conducted with the same leaching standard, the comparison could give an insight on how far the process deviates from a construction product.

4.4 Extra experiments

One limitation of the tests previously chosen is that the selection of fly ash was primarily based on its the heavy metal concentration. Although this criterion is the main research scope, it overlooks the potential benefit of a higher carbonation capacity on the physical stability and possibly immobilization of the material. To validate the methodology and expand on possible applications of carbonation, it is interesting to select fly ash with the highest carbonation potential. Even if it remains out of the scope of this study, the fly ash with the highest carbonation

potential was immobilized using the same mix designs presented in Table 4.3. After 28 days the samples were tested for compressional strength to compare the results with those of the initially chosen FA.

The carbonized materials, FA_C2, FA-B_C2, and FA-B_C3 were all tested for leaching and compared to the reference sample of the same fly ash. The final leaching behaviour of the materials are compared to the corresponding samples of the chosen fly ash to determine whether carbonation results in better immobilization. The testing procedure used were the same as previously described in this chapter. Comparing the final results of the physical stability tests and leaching tests helped selecting guidelines for future research and industrial applications.

5. Material characterization

This chapter contains the results of the characterization of the six different materials used for the study. The chapter is divided into three main sections. In the first part the results of the chemical composition of the materials are presented, followed by findings from the carbonation potential tests. The chapter ends with the results of the selection of the fly ash that is used further for the immobilization process.

5.1 Chemical composition

Table 3.1 and Figure 5.1 show the particle size distribution of the fly ashes analysed as described in the Methodology. The specific surface area (SSA) of FA4 was the largest at 463 m²/kg followed by FA3 with 330 m²/kg, being the materials with the highest surface reactivity. Whereas the SSA of FA2, FA5 and FA6 ranged between 200 and 300 m²/kg. Table 3.1 presents the particle size distribution D10, D50 and D90 values. The D10 value indicates the particle diameter below which 10% of the sample's mass is contained. The D50 value indicates the particle diameter at which 50% of the sample's mass is fine. The value at D90 expresses that only 10% of the sample's mass has particles coarser that this value. Said that, FA1 showed the finest particle size of D50 and D90 of 11.60 μ m and 19.22 μ m respectively. FA3 and FA4 also contained smaller particles, with 50% of the material having particle sizes smaller than 17.9 μ m and 17.1 μ m. Half of the heap of other fly ashes was composed of larger particles, with diameter >37.2 μ m and D90 >223 μ m. As previously investigated and pointed out by past research, the smaller particle size results in higher specific surface area, increasing the surface of reactivity and the rate of reaction of the materials (Nedeljković, 2019).

Table 5.1: Summary of particle size distribution of the six fly ashes.

	FA1	FA2	FA3	FA4	FA5	FA6
SSA [m²/kg]	123.7	232.9	329.8	463.0	211.6	295.5
D10 [µm]	3.99	4.09	3.36	1.73	4.42	2.98
D50 [µm]	11.60	37.2	17.9	17.1	37.6	41.9
D90 [µm]	19.22	223	89.0	165	229	240

In Figure 5.1 the particle size distributions of the six fly ashes are visually represented. FA2 and FA5 had a similar particle size distribution, with the majority of the particles with particle size of $60 \mu m$ or $75 \mu m$. All the particles in FA3 ranged between $50 \mu m$ and $70 \mu m$, whereas in FA4 most of the particles had diameter of $47 \mu m$ or $70 \mu m$.

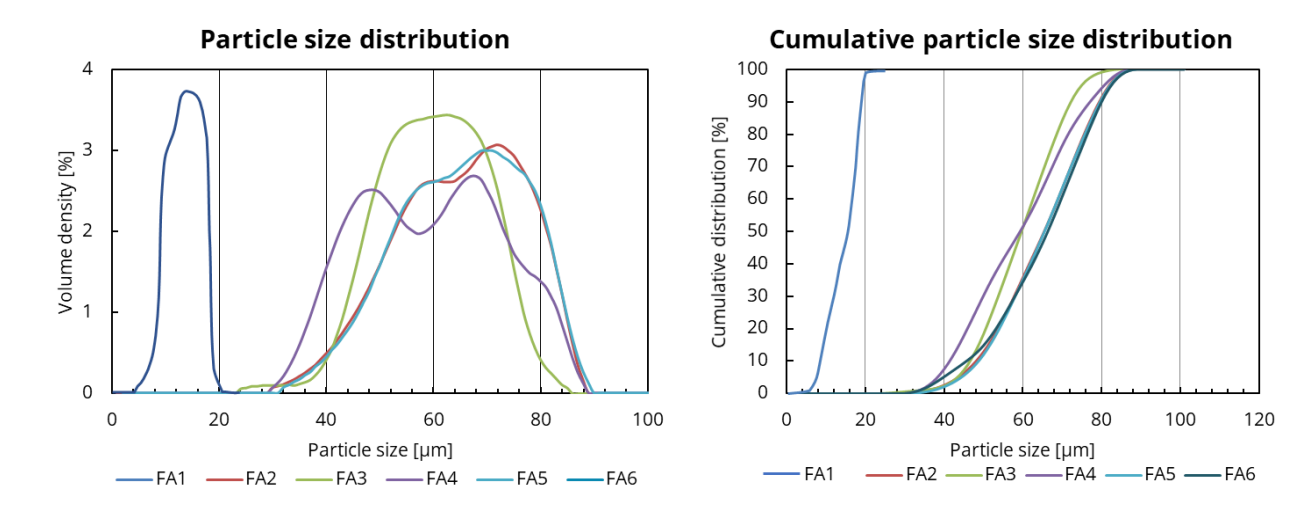


Figure 5.1: Cumulative particle size distribution (left) and particle size distribution (right) of the six fly ashes.

5.1.1 Elemental analysis

The XRF analysis was used to identify the elemental composition of the solid fly ash and quantify the heavy metals composition in the materials. The results from the XRF test can be seen in Table 5.2. The results are presented as weight percentage (wt.%) of equivalent oxides and are normalised for the LOI, as explained in the Materials and Methods section. FA1, FA2, FA5 and FA6 all had comparable and lower Al₂O₃ and SiO₂ proportions, compared to FA3 and the binder FA4. Calcium was present in the highest proportions in the binder FA4 and in FA2, the BM FA, containing respectively 57.3% and 47.1% of equivalent CaO. The weight percentages of magnesium for all samples were not higher than 3%, with FA2 and FA3 containing the highest proportions of 2.9% and 2.1%.

FA3 showed the highest concentration of Fe_2O_3 , TiO_2 and ZnO_2 . FA1, FA5, FA6, the MSWI FA, and FA2 had the second highest amount of equivalent titanium oxide of above 1%. The binder FA4 contained the least amount of TiO_2 , less than 0.5% but it presented more than 2.5% of Fe_2O_3 . The fly ash from incineration of municipal solid waste, FA1, FA5 and FA6 presented the highest concentrations of equivalent Cl and Na_2O . Cl quantities larger than 16% indicates that the ashes are rich in salt. FA2 and FA3 contained some salts, as the Cl was present in 3.7% and 7.3% respectively, whereas FA4 had less than 1% chloride ions. Differently from the other materials, the binder FA4 had also almost no potassium and sulphites. FA2 presents the highest K_2O percentages, higher than 9%, whereas FA1, FA5 and FA6 portions ranged in between 4.4% and 6.6%, with FA3 containing less than 2% of potassium. All hazardous fly ashes contained more than 9% of sulphides.

Even though most of the elements described are heavy metals, the Dutch regulation on the disposal of immobilized material specifies leachability limits for only a selection of heavy metals, as can be seen in the Appendix (Beschikking 2003/33/EG). Of the list in the Dutch regulation, Figure 5.2 shows the heavy metals detected in the fly ashes. The materials contained vanadium, chromium, copper, zinc, arsenic, bromide, cadmium, tin and lead. As the materials originated from different sources, also their concentrations in the final fly ash differs. Overall, zinc lead and copper were detected in all fly ashes in the highest quantities, with exception of FA4 that had almost no equivalent PbO. The MSWI FA, FA1, FA5 and FA6 contained the highest amounts of these heavy metals, having the highest percentages of these oxides compared to FA2, FA3 and FA4. CuO, PbO, Br and ZnO were all present in concentrations higher than 0.2% for all the MSWI FA. FA3 also presented high lead and vanadium concentrations of respectively 0.83% and 0.04%, but the weight percentages of the other heavy metals were not as high as for FA1, FA5 and FA6. FA2 contained all the heavy metals in the graph except for cadmium, but they

were all in lower quantities compared to the others. The binder contained almost none of the heavy metals listed in the regulation, if not for zinc and copper.

It is important to note that even if in the table the compounds are expressed as equivalent oxides, the XRF analysis could only detect the elemental composition, thus it cannot detect the molecular phase. In the case of MgO and CaO, the phases could be present as both oxides as well as sulphates and carbonates.

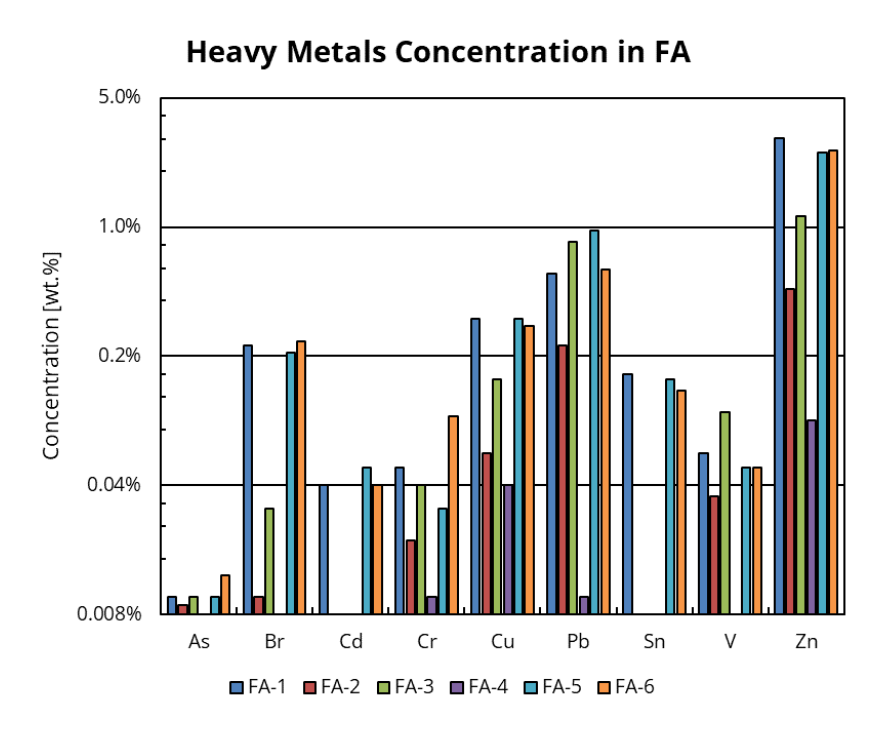


Figure 5.2: XRF results of relevant heavy metals concentration of the six materials FA1, FA2, FA3, FA4, FA5 and FA6. The concentrations are represented in the equivalent oxides.

Table 5.2: Chemical composition of equivalents oxides for all FA with XRF in weight percentage [wt.%].

Element	FA1	FA2	FA3	FA4-B	FA5	FA6
Al_2O_3	2.76	2.05	5.04	7.30	2.75	3.78
As_2O_3	0.01	0.01	0.01	-	0.01	0.01
Br	0.23	0.01	0.03	-	0.21	0.24
CaO	21.50	47.10	39.36	57.29	24.70	25.29
CdO	0.04	-	-	-	0.05	0.04
Cl	16.04	3.67	7.32	0.18	16.53	15.69
Cr_2O_3	0.05	0.02	0.04	0.01	0.03	0.10
CuO	0.32	0.06	0.15	0.04	0.32	0.29
Fe_2O_3	1.77	2.31	3.39	2.66	1.82	2.91
K_2O	6.60	9.53	1.37	0.41	4.43	5.16
MgO	1.05	2.87	2.12	1.71	0.76	1.42
MnO	0.06	0.43	0.23	0.05	0.05	0.08
Na_2O	10.62	0.41	0.32	0.14	8.23	7.72
P_2O_5	0.86	2.86	0.55	1.87	0.84	1.00
PbO	0.56	0.23	0.83	0.01	0.96	0.59
Rb_2O	0.01	0.02	0.01	=	-	0.01
SiO_2	7.47	8.82	9.02	11.55	7.69	8.98
SnO_2	0.16	-	-	_	0.15	0.13
SO_3	15.85	9.31	13.87	0.62	16.82	11.72
SrO	0.07	0.14	0.10	0.09	0.07	0.08
TiO_2	1.53	1.43	5.18	0.46	1.05	1.80
V_2O_5	0.06	0.04	0.10	-	0.05	0.05
ZnO	3.05	0.46	1.14	0.09	2.55	2.59
ZrO_2	0.02	0.03	0.03	0.02	0.02	0.02
LOI	9.30	8.20	9.80	15.50	9.90	10.30

5.1.2 Crystalline phases

To determine the phases in which the elements detected in the XRF analysis were present, a qualitative XRD analysis was conducted on all the samples. Figure 5.3 shows the XRD patterns of the six fly ashes with the relevant peaks detected. As can be seen from the patterns, the fly ashes showed a lot of peaks that might be mistaken for noise. However, even increasing the timestep analysis, as explained in the methodology, the small peaks in the graph were still present. As expected from the XRF results, the five hazardous fly ashes FA1, FA2, FA3, FA4 and FA5 presented a lot of various crystalline phases, whereas the XRD pattern of FA4 was cleaner and with less peaks than the others. From the stacked patters it was possible to identify repeating peaks and, in some cases, also the different intensities, indicating the different proportions. Quartz and calcite were present in all the samples. FA1, FA3, FA5 and FA6 showed large peaks of anhydrite, halite and sylvite. Lime was detected with clear peaks only in the patters of FA2, FA3 and FA4.

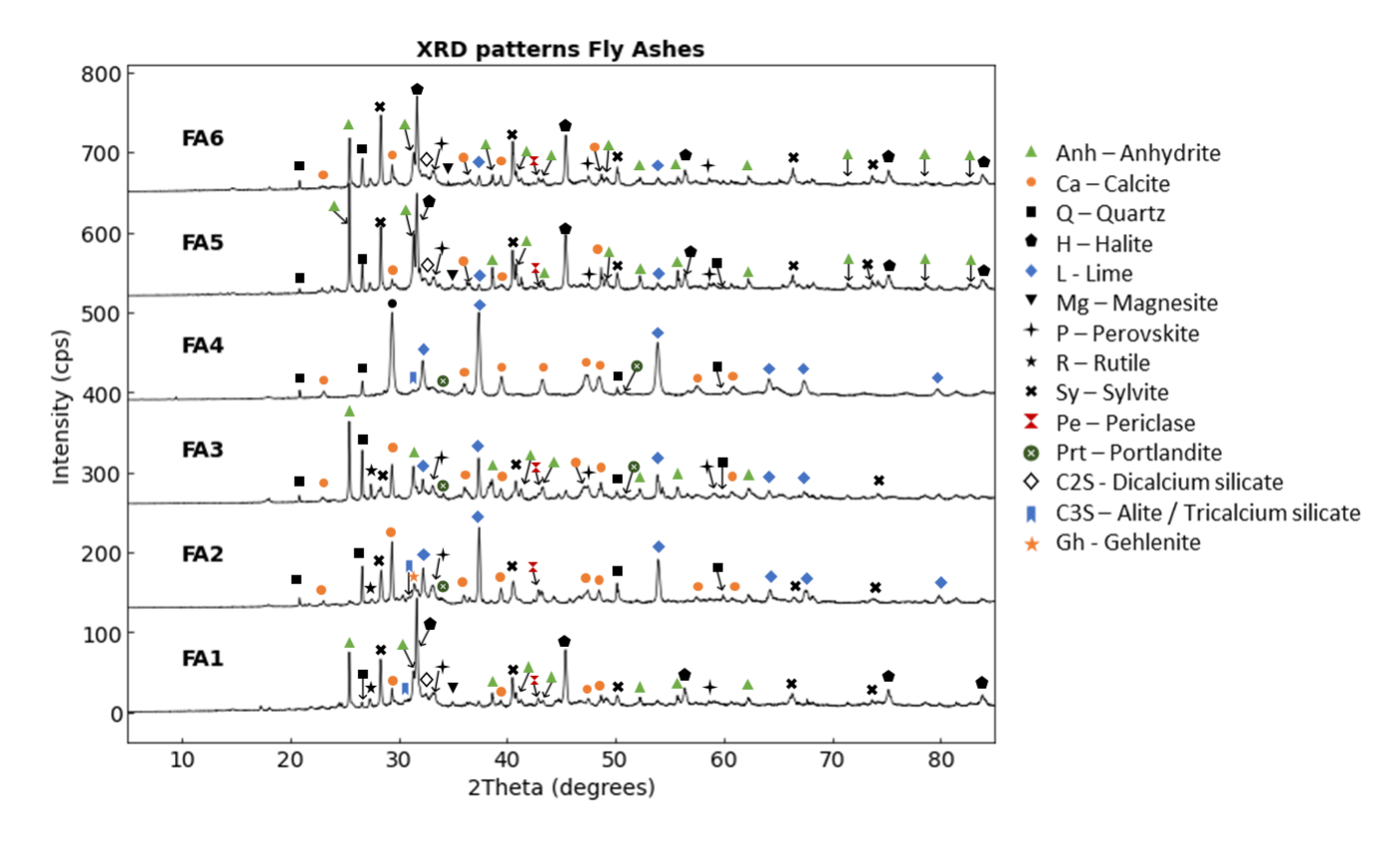


Figure 5.3: From bottom to top, XRD diffractograms of FA1, FA2, FA3, FA4, FA5 and FA6. The peaks corresponding to most of the crystalline phases are underlined in the image.

To quantify the crystalline phases and the amorphous content of the material, silicon powder was added to the system as explained in the methodology. The peak identification and analysis were executed through Rietveld analysis through Profex, with the results shown in Figure 5.4. The amorphous phase on the materials was around half of the total mass percentage of FA2, FA5 and FA6. FA1 and FA3 contained a large portion of amorphous phase of 43.7% and 35.0%, whereas FA4 had only 24.4% of amorphousness. The large amounts of calcium identified in the XRF was spread over three main crystalline phases: anhydrite, calcite and lime. Anhydrite is a form of calcium sulphate whereas calcite is carbonated calcium.

Table 5.3 contains the names and chemical formulas of the main crystalline phases identified in the XRF and QXRD analysis.

Table 5.3: Chemical formulas of crystalline phases identified from the QXRD analysis.

Anhydrite	Calcite	Lime	Halite	Quartz	Magnesite	Perovskite	Rutile
CaSO ₄	CaCO ₃	CaO	NaCl	SiO ₄	MgCO ₃	CaTiO ₃	TiO ₂
Sylvite	Periclase	Vaterite	Mayenite	Wollastonite	Portlandite	C2S	C3S
KCl	MgO	μ-CaCO ₃	$Ca_{12}Al_{14}O_{32}$	CaSiO ₃	Ca(OH) ₂	(CaO) ₃ SiO ₂	(CaO) ₂ SiO ₂

As previously explained, the crystalline phases with the highest carbon potential identified also in the fly ashes were lime, periclase and portlandite. Even if all materials showed in the XRF results CaO equivalents content higher than 30%, only FA2, FA3 and FA4 contained significant amounts of lime. The fly ashes contained 7.4%, 3.9% and 14.8% by weight respectively, as well as periclase but in less than 2%. FA2 and FA3 also contained

around 1% of portlandite and FA4 almost 3%. FA1, FA5 and FA6 had less than 1% of free lime, magnesium oxide and no portlandite. All the calcium identified from the XRF in these fly ashes wass present in the form of anhydrite and calcite, being a total of 18.3% in FA1, 17.8% in FA5 and 13.1% in FA6.

Overall, the non-amorphous composition of FA1, FA5 and FA6 was similar, showing all large amounts of anhydrite, calcite, halite, perovskite and sylvite. The high quantities of NaO, Cl and K₂O identified in the XRF were present in the ashes as halite and sylvite salts. The MSWI FA contained all 11% of total halite and sylvite salts, as can be seen from the detailed results in Figure B.0.4 of the Appendix.

In construction material, carbonation and high quantity of salts are problematic for the structural strength as they enhance corrosion. Some studies showed that carbonation capacity is not directly affected by the presence of salts (Whan et al., 2012). However, their precipitation during carbonation can obstruct the pores available for the gas flow. This might lead to the reduction of the effective carbon uptake (Li et al., 2024). FA3 contained less than 2% of salts whereas FA2 and FA4 do not contain any halite of sylvite. Titanium was present in all materials mainly as perovskite, another compound that has also the potential to react with CO₂ as described in the Literature Review. FA2 contained 5.2% of perovskite, followed by FA3 with 4.5% and FA1, FA4, FA5 and FA6 containing 3.7%, 3.3%, 1.1% and 3.5% respectively.

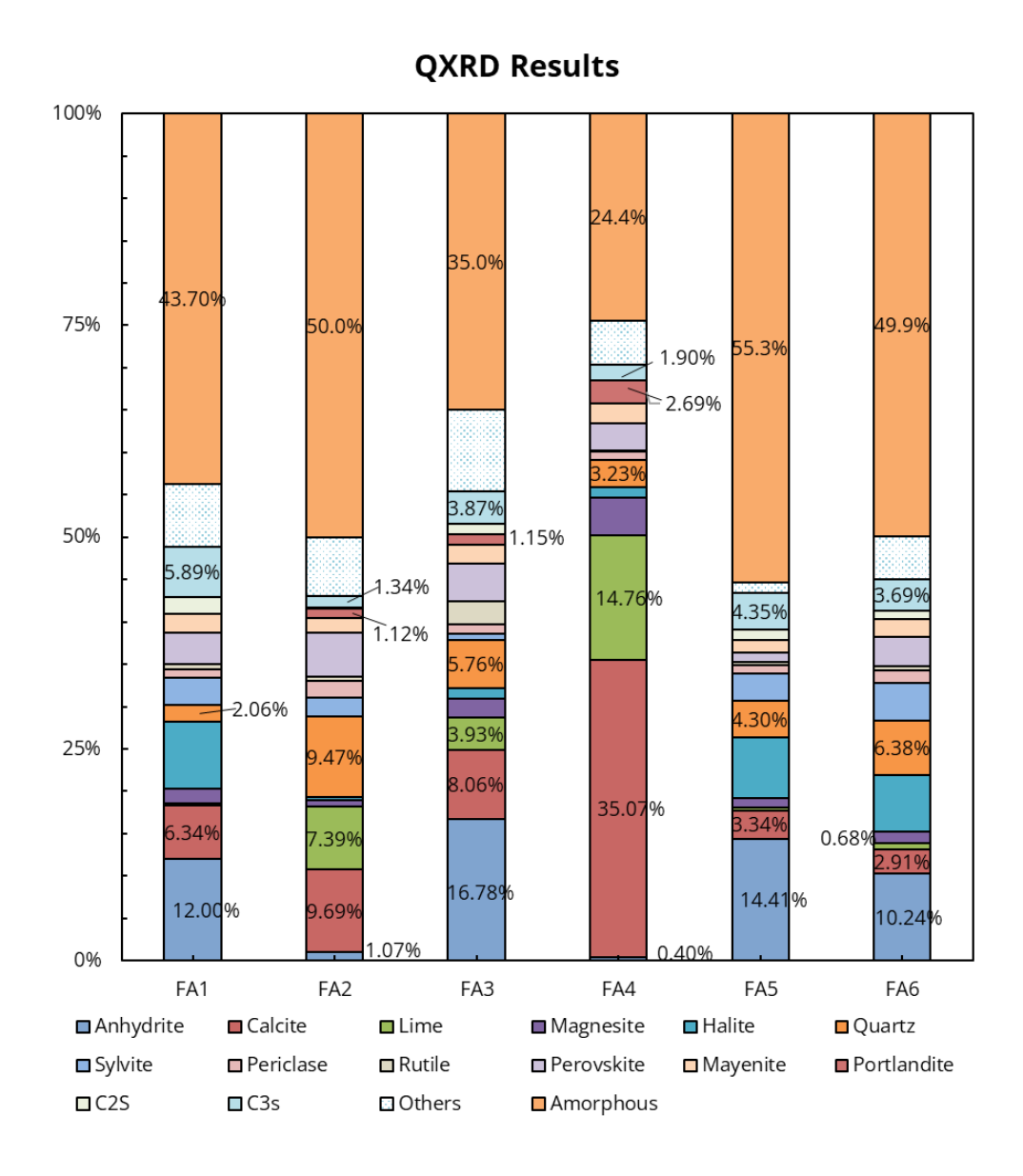


Figure 5.4: Results of quantitative Rietveld phase analysis of the six materials investigated in the research.

Even though the MSWI FA did not contain any free lime, the fly ashes contained the highest portions of dicalcium silicate (C2S) and tricalcium silicate (C3S). C2S and C3S are two crystalline phases of calcium silicates well known to carbonize during hardening of cement (Zajac et al., 2022). FA1, FA3, FA5 and FA6 show a total of C2S and C3S of 8%, 5%, 5.5% and 4.7%, higher compared to FA2 and FA4 containing respectively 1.5% and 1.9%.

The difference in the solid phases obtained by XRD and XRF indicates that not all elements were present in the crystalline phase. The three ionic groups with the highest difference are shown in Table 5.4 and were sulphite, silicon and calcite ions. The predicted composition showed that FA1, FA2, FA3, FA5 and FA6 contained respectively 8.8%, 8.7%, 4.0%, 8.4% and 5.7% of sulphite ions in the amorphous phase. Using Eq. (7), the calcium in the amorphous phase was also present in large quantities. FA2, FA3 and FA4 had high calcium in the amorphous phases, corresponding to 24.2%, 17.2% and 16.2% of the total mass of the material. FA1, FA5 and FA6 contained 9.1%, 11.9% and 13.4% of calcium in the amorphous part.

Table 5.4: Proportions of sulphite, silicon and calcium ions present in the amorphous phases of the six materials.

	FA1	FA2	FA3	FA4	FA5	FA6
SO ₃ -	8.8%	8.7%	4.0%	0.4%	8.4%	5.7%
Si^{4+}	2.5%	0.0%	1.5%	3.9%	1.6%	1.2%
Ca^{2+}	9.1%	24.2%	17.2%	16.2%	11.9%	13.4%

Based on the results of the particle size distribution, XRF and XRD it was tedious to predict the behaviour of the fly ashes. FA1 had the highest potential reactivity but its high salt content as well as low lime content might result in a non-reactive material to carbonation. Similarly, FA5 and FA6 presented even lower potential than FA1 as their SSA was much lower than the other FA. However, the C2S and C3S concentrations of the three MSWI FA might result in effective carbonation. FA2 and FA4 contained the largest content of free lime, together with the binder, but also the lowest heavy metals concentrations. Investigation on the carbon uptake was necessary to validate and confirm the predictions from the analysis on the chemical composition of the fly ashes.

5.2 Carbonation potential

After carbonation, the carbonation potential of each fly ashes was determined in two steps. Firstly, through QXRD the evolution of the crystalline phases in the hydrated and carbonized material were identified. Secondly, through TGA, the final carbon uptake was determined. After 1 week carbonation under the same conditions, the fly ashes showed very different textures, as shown in the pictures in Figure 5.5. FA1, FA5 and FA6 hardened and changed colour. Even if it is hard to perceive form the pictures, a small white layer formed on the surface of the materials. FA2 and FA3 also hardened and agglomerate, but not as much as the MSWI FA. The binder did not look much different than the original material if not for the coarser grain texture, still much finer than the other materials.

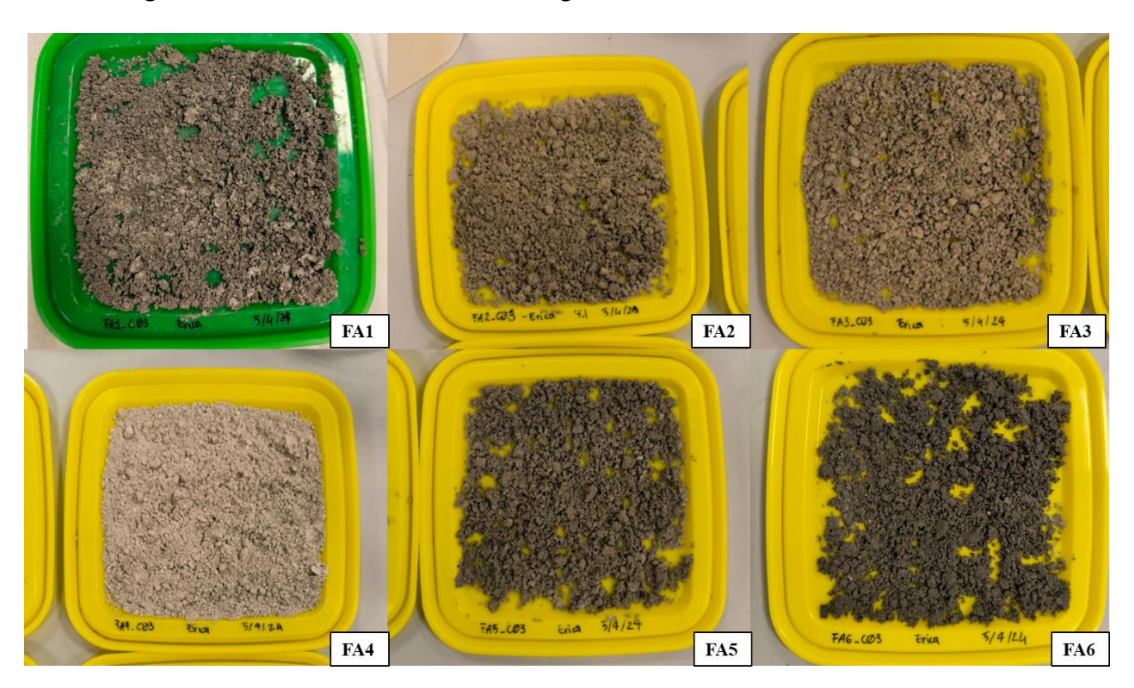


Figure 5.5: Pictures of the six materials after one week in the carbonation chamber at the same conditions.

5.2.1 Crystalline phases

After 1 week of carbonation, all fly ashes were analysed through QXRD. The amorphous content of all materials decreased noticeably, as shown in Figure 5.6. The amorphous phase of FA1, FA4 and FA6 showed the lowest decrease of 15.7%, 15.9% and 14.6%. The phase dropped from 50.0% to 9.0% in FA2, it decreased from 35.0% to 4.6% in FA3 and from 55.3% to 17.1% in FA5. The drop in this phase indicated that the chemical compounds in the amorphous part of the material reacted to form crystalline structures.

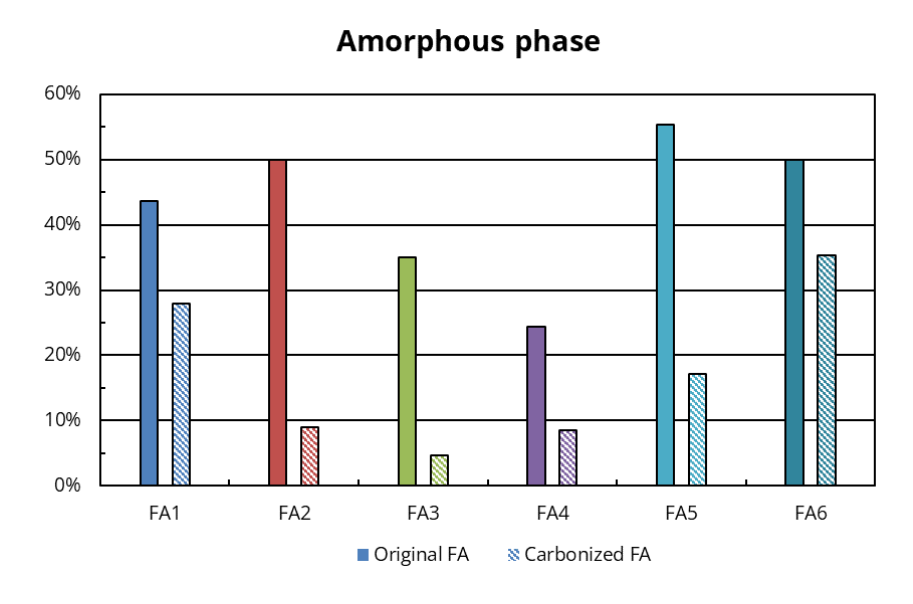


Figure 5.6: Amorphous content determined by QXRD of the fly ashes pre- and post-carbonation.

As can be seen in Figure 5.7 and Figure 5.8, new crystalline phases were formed in all fly ashes. Some phases were consumed, but overall, the amounts of new phases do not justify the consumed crystalline compounds. As explained in the previous chapter with the results of the Crystalline Phases, large proportions of calcium and sulphite ions were present in the amorphous phase. In FA1 all lime, mayenite and C3S were consumed, whereas calcite, anhydrite, magnesite and C2S were produced. Other phases present in the fly ash in concentrations between 0.5% and 4% are shown in Table 5.5. Hydromagnesite and brucite formed during hydration and carbonation of FA1, suggesting that not enough time has passed from the magnesium to carbonize in magnesite. Titanite was consumed probably relating to the small increase of perovskite in the FA. The aluminium-rich mayenite reacted during hydration and carbonation to form mullite and anorthite.

After carbonation of FA2, almost all original lime and all C2S, C3S and portlandite present were consumed to produce calcite and vaterite. As shown in Table 5.5, aragonite and dolomite also formed, other carbonated minerals of calcium and magnesium. The amount of quartz also increased as well as calcium silicates such as wollastonite, merwinite and titanite. After hydration and carbonation mullite was detected in the BM FA, as the concentration of mayenite decreases.

FA3 showed also a significant increase of carbonized species. Even if the initial lime content was not as high as FA2, almost 45% of carbonated calcium was formed as calcite and vaterite. The newly formed carbonates were the result of the initial high calcium content in the amorphous phase, also justifying the high drop in amorphous phase of the final carbonated material. Portlandite, C2S and C3s were also fully consumed. Periclase was not detected anymore in the carbonized material, but instead huntite, another form of carbonated magnesium and calcite was formed.

Table 5.5: Crystalline phases and their chemical formulas identified pre- and post-carbonation in FA1, FA2 and FA3.

		FA1	FA1_C07d	FA2	FA2_C07d	FA3	FA3_C07d
Aragonite	CaCO ₃	-	-	-	✓	-	-
Dolomite	$CaMg(CO_3)_2$	-	-	-	\checkmark	-	-
Hydromagnesite	$Mg_5(CO_3)_4(OH)_2 \cdot 4H_2O$	-	\checkmark	-	-	-	-
Huntite	$Mg_3Ca(CO_3)_4$	\checkmark	-	\checkmark	-	\checkmark	✓
Brucite	$Mg(OH)_2$	-	\checkmark	-	-	-	-
Merwinite	$Ca_3Mg(SiO4)_2$	-	-	-	\checkmark	-	-
Titanite	CaTiSiO ₅	\checkmark	-	-	\checkmark	-	-
Anorthite	$CaAl_2Si_2O_8$	-	\checkmark	-	-	-	-
Mullite	$3Al_2O_3 \cdot 2SiO_2$	-	\checkmark	-	-	-	-
Syngenite	$K_2Ca(SO_4)_2 \cdot H_2O$	-	-	-	\checkmark	-	-
Archerite	$(K,NH_4)H_2PO_4$	-	-	-	-	-	✓
Ilmenite	$Fe^{2+}TiO_3$	\checkmark	-	-	-	-	-
Chalcopyrite	$CuFeS_2$	✓	-	-	-	-	-

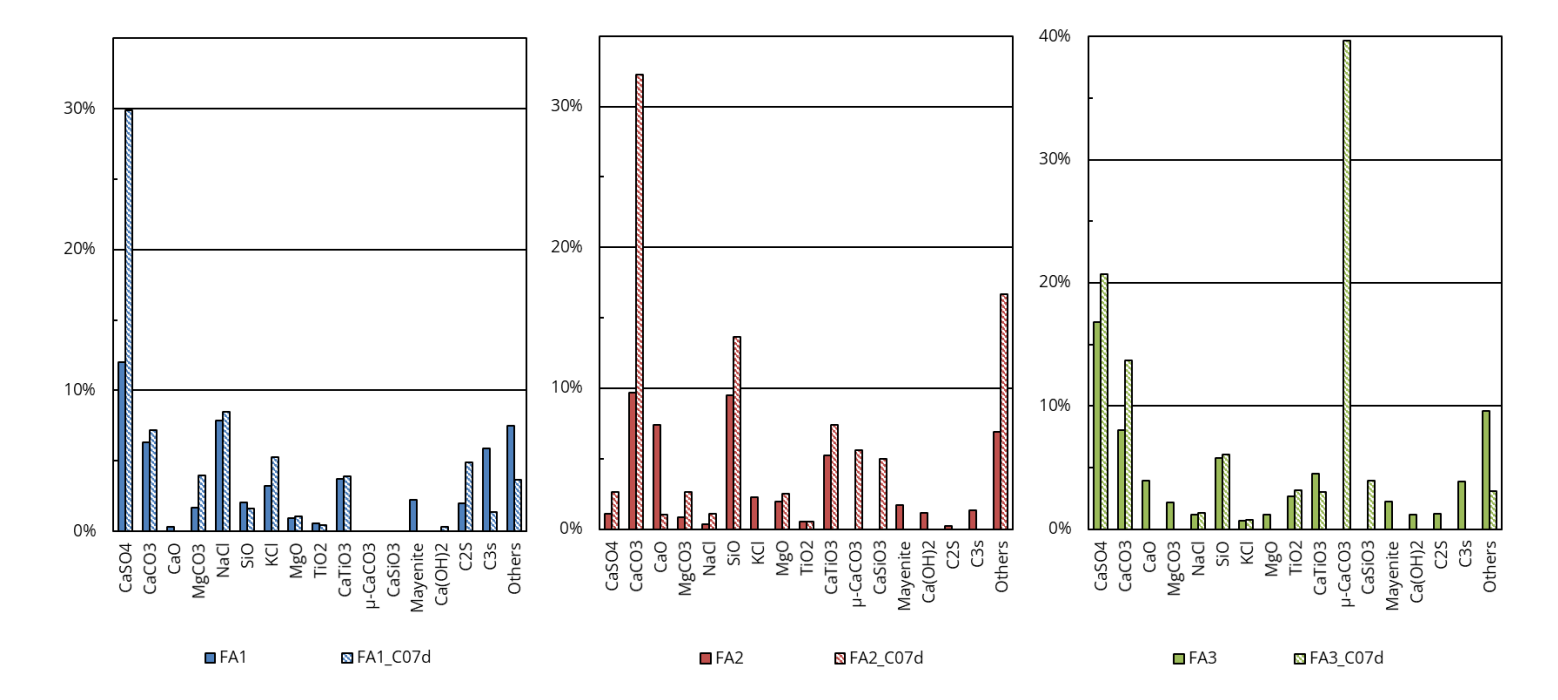


Figure 5.7: Quantification of crystalline phases through QXRD Rietveld refinement. From left to right the plots show the phases of FA1, FA2 and FA3 before and after 1 week carbonation.

The results from the QXRD analysis of FA4, FA5 and FA6 are shown in Figure 5.8. Table 5.6 shows the crystalline phases detected but in concentrations between 0.5% and 4% for the three fly ashes pre- and post-carbonation. All initial lime and C3S initially present in FA4 were consumed after carboantion, generating new calcite. The binder, having almost no sulfites in the amorphous phase (Table 5.4), did not produce new anhydrite. Magnesite and periclase both disappeared in the crystalline phase, but instead merwinite was formed. Differently from what expected, portlandite was not consumed for carbonation, but instead the proportions remained constant. In the binder, pervskivite was fully consumed but some recrystallized as titanite and titanium oxyde, suggesting that a small amount of CaO might have been liberated for carbonation.

The change in the major crystalline phases of FA5 and FA6 was similar to FA1, where calcite was formed togheter with large quantities of anhydrite, from the crystallization of the amorphous sulphites. Differently from FA1, in FA5 mayenite was produced after hydration and carbonation, whereas grossular, another calcium-aluminium-silicate disappeared. Differently from FA1 and FA5, C3S was not consumed in FA6 during carbonation, suggesting that carbonation and hardening was inhibithed. The concentrations of MgO decreased in FA5 and FA6, but hydromagnesite formed in slightly less than 4% for both materials.

Table 5.6: Crystalline phases and their chemical formulas identified pre- and post-carbonation in FA, FA2 and FA3.

		FA4	FA4_C07d	FA5	FA5_C07d	FA6	FA6_C07d
Huntite	Mg ₃ Ca(CO ₃) ₄	✓	-	✓	-	✓	-
Hydromagnesite	$Mg_5(CO_3)_4(OH)_2 \cdot 4H_2O$	-	-	-	✓	-	\checkmark
Brucite	Mg(OH)	\checkmark	-	-	-	-	-
Magnesium Chlorate Hydrate	$Mg(ClO_3)_2(H_2O)_x$	-	-	\checkmark	-	-	-
Merwinite	$Ca_3Mg(SiO_4)_2$	-	✓	-	-	-	-
Titanite	CaTiSiO ₅	-	✓	-	-	-	-
Grossular	$Ca_3Al_2(SiO_4)_3$	-	-	\checkmark	-	-	-
Sodalite	Na ₈ Al ₆ Si ₆ O ₂₄ Cl ₂	-	-	-	✓	-	-
Archerite	$(K,NH_4)H_2PO_4$	-	-	-	✓	-	✓
Hematite	Fe_2O_3	\checkmark	\checkmark	-	-	-	-
Ilmenite	Fe ²⁺ TiO ₃	-	-	-	-	-	\checkmark
Apatite	$Ca_5(PO_4)_3(F,Cl,OH)$	-	-	✓	-	-	

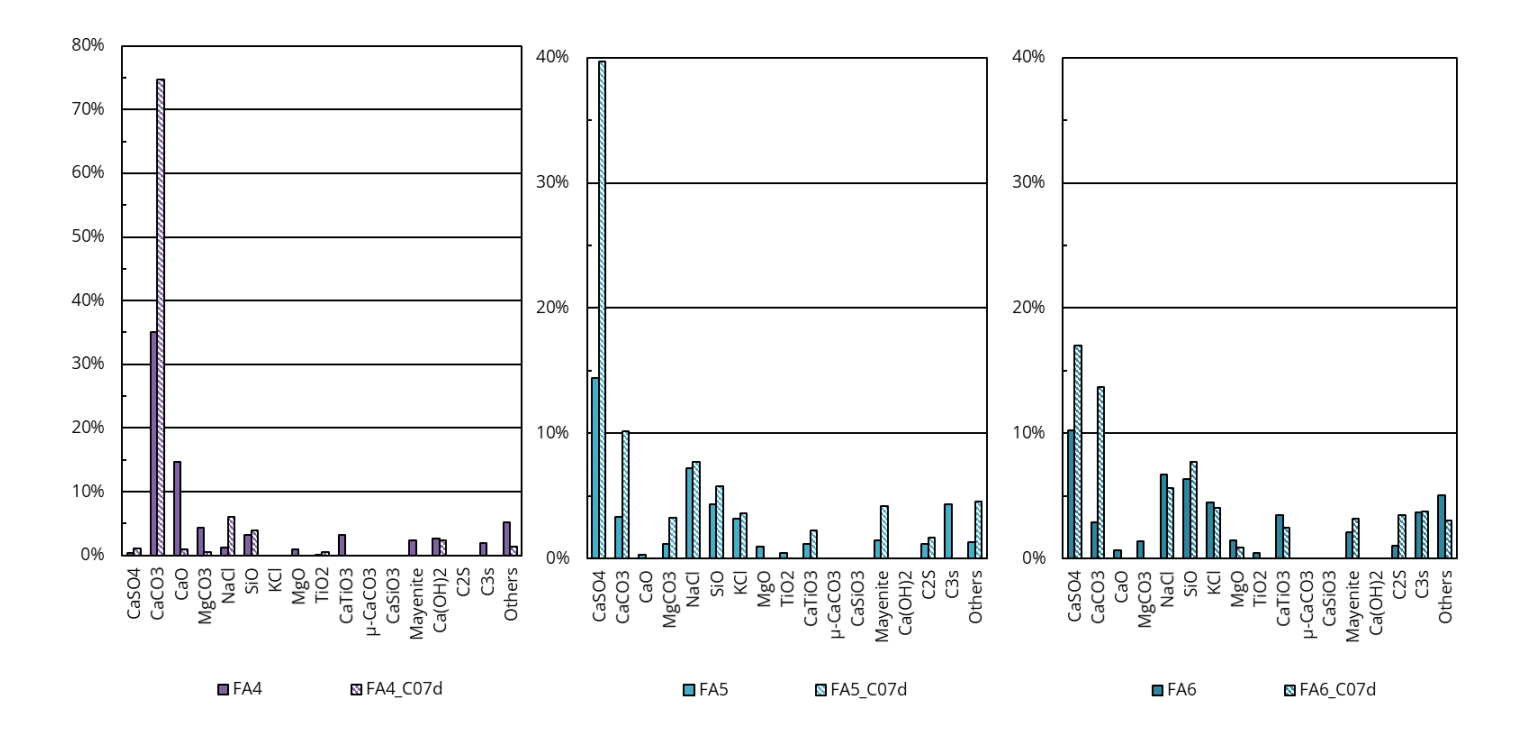


Figure 5.8: Quantification results of crystalline phases pre- and post-carbonation through Rietveld refinement of the QXRD patterns. From left to right: FA4, FA5 and FA6.

In FA1, FA5 and FA6 the large amounts of newly formed anhydrite originated from the amorphous sulphides in the materials. Differently from what predicted from the literature study, anhydrite did not carbonize in these fly ashes but instead the amorphous calcium and sulphites crystallized after hydration and carbonation. In FA3 the percentage of amorphous sulphites was lower than the other MSWI FA, whereas the amorphous calcium was higher than the others. As a result, the anhydrite production was not as enhanced as for the previous case, but instead large amounts of calcium carbonates were formed, not in the form of calcite but as vaterite.

Titanium oxide was generally consumed, and more perovskite produced, on the contrary of what predicted. Even if the changes in percentages was minimum, carbonation of perovskite did not occur. In this system, less than 1% of the available calcium was also consumed to form new perovskite.

As expected, the hydration and carbonation reactions for each fly ashes varied significantly, even within fly ashes from similar origin (FA1, FA5 and FA6).

5.2.2 Carbon-uptake

The quantification of the crystalline phases from the QXRD gave a good indication on the new crystalline phases formed in the materials after hydration and carbonation. However, it was not possible to determine wheter the newly carbonated phases were fromed from the carbon uptake or were re-arranged amorphous phases. For this reason, TGA analyses were conducted on all materials to quantify the real mineral carbonation of the materials pre- and post-carbonation.

Figure 5.9, Figure 5.10 and Figure 5.11 show the TG-DSC-DTG curves of the six materials before and post carbonation along with the relevant peaks of dehydration and decarbonation. CCA stands for the decarbonation reaction of calcite and HMG represents the decarbonation and dehydration of hydromagnesite. In Figure 5.9, the

carbonized curve shows a similar trend compared to the non-carbonated material. However, from the DTG curve the peak at 570°C confirms the XRD results on the formation of hydromagnesite. The enhanced peak at 900°C indicates that more calcite was formed. Similarly, the TG curves of FA2 and FA2_C07d show a big drop in between 670°C and 900°C. The TG-DSC-DTG curves of FA3 and FA4 in Figure 5.10 show similar trend to FA2. The curves of FA5 and FA6 are similar with each other's and both show the degradation peak of hydromagnesite and, only for FA6, also of calcite.

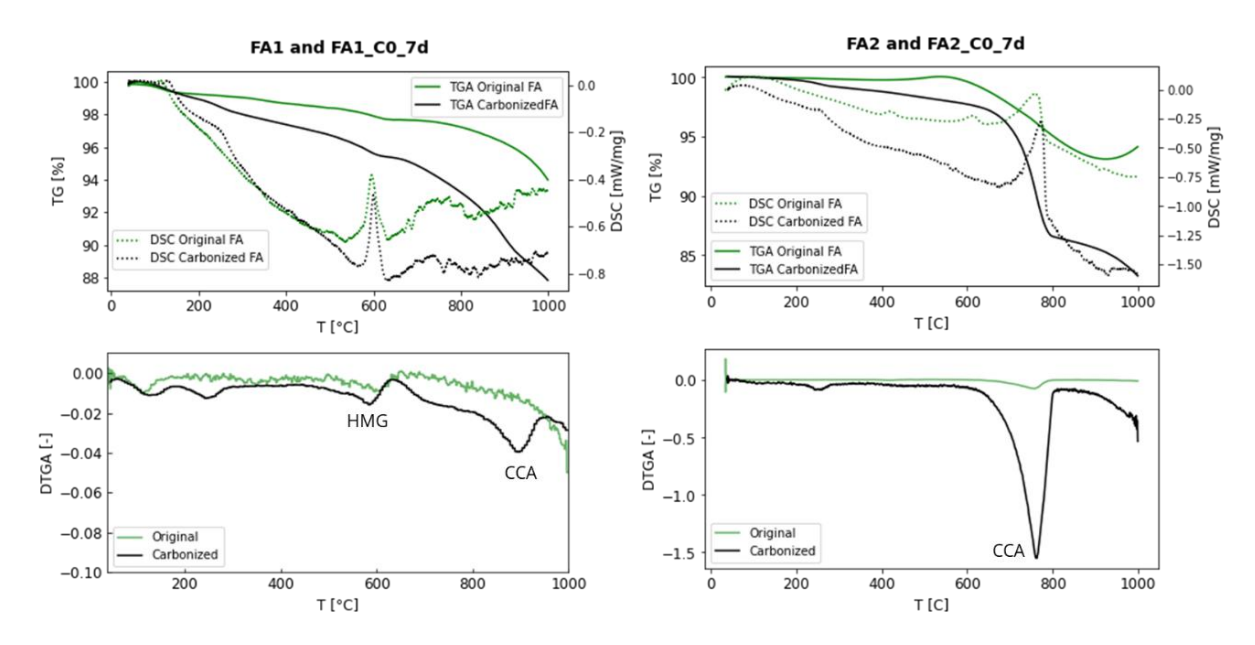


Figure 5.9: TG-DSC (top) and DTG (bottom curve of FA1 (left) and FA2 (right) pre- and post-carbonation.

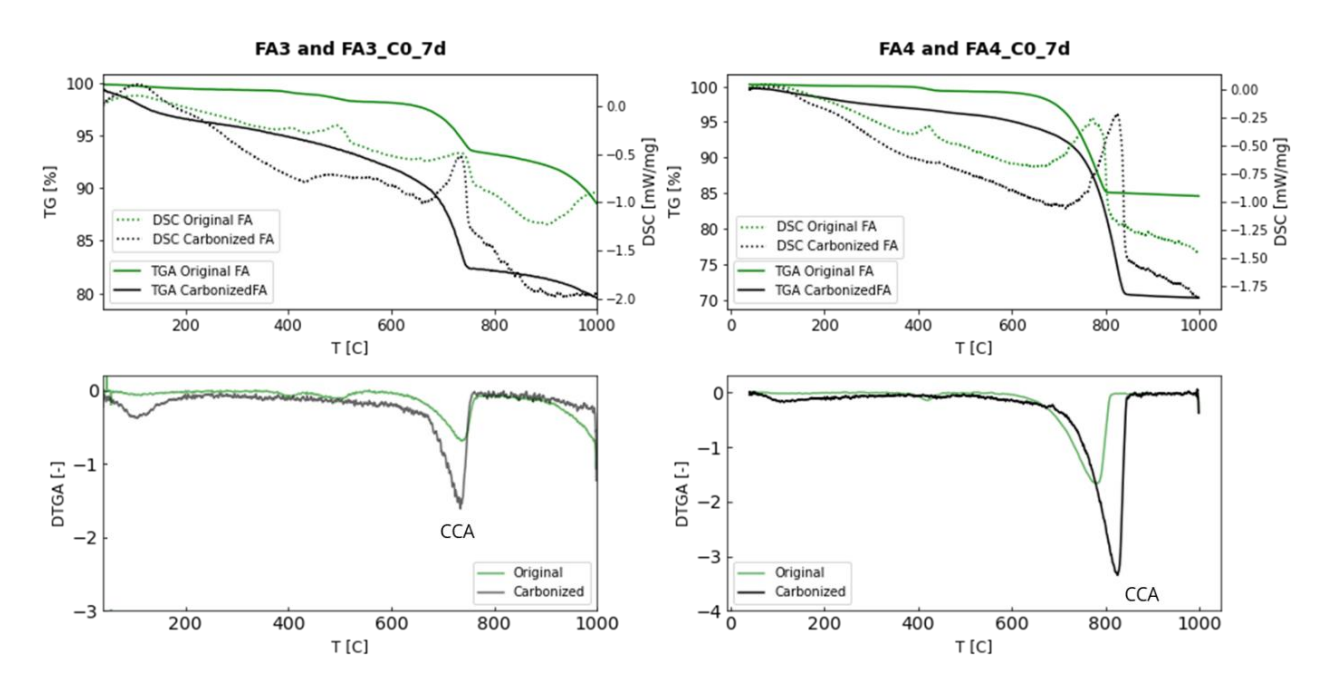


Figure 5.10: TG-DSC (top) and DTG (bottom curve of FA3 (left) and FA4 (right) pre- and post-carbonation.

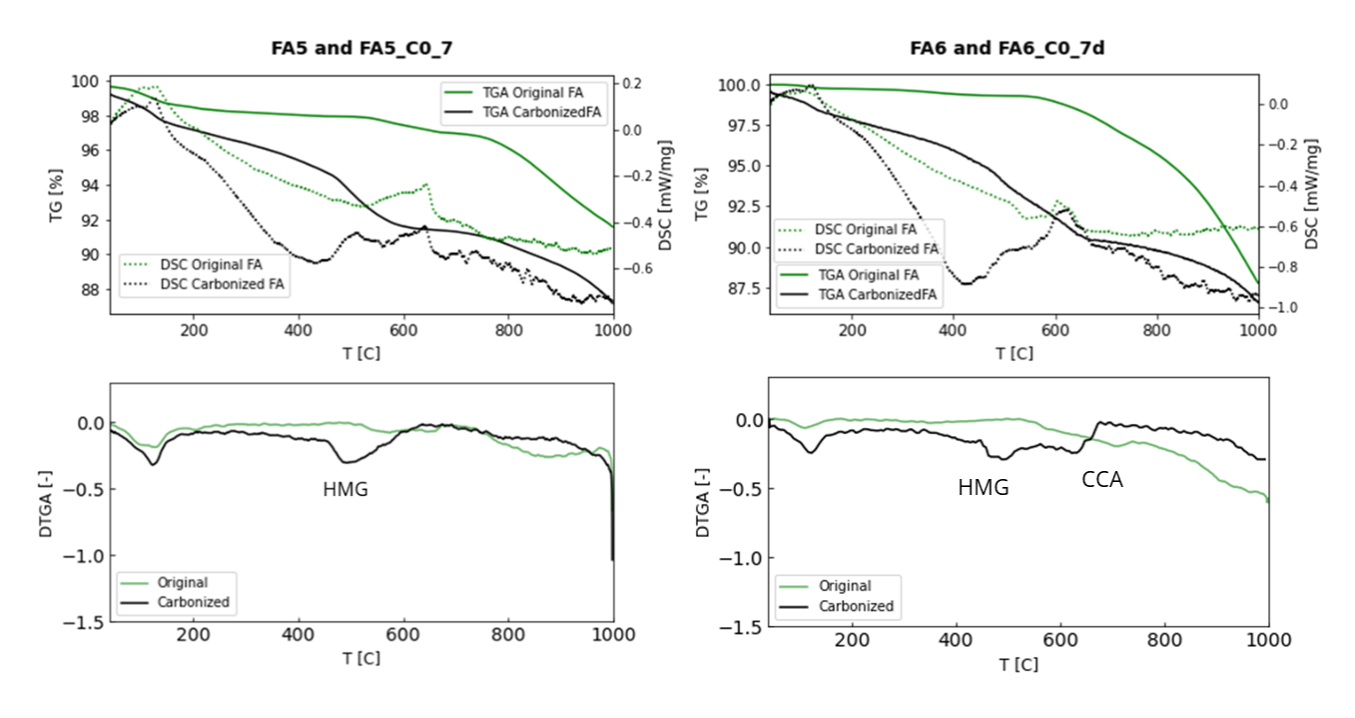


Figure 5.11: TG-DSC (top) and DTG (bottom curve of FA5 (left) and FA6 (right) pre- and post-carbonation.

Smaller peaks before 200°C were not investigates as they are associated with dehydration of gel phases (Nedeljković, 2019). Based on the TG-DTG curves, the peaks and drops corresponding on mineral carbonation are in between 500°C and 610°C for hydromagnesite, and between 670°C and 900°C for the degradation of calcite. The differences of the TG curves were used to estimate the total carbon-uptake of the materials. For FA2, FA3 and FA4 the mineral carbonation was determined only from the mass drop between 670°C and 900°C as only

calcite was formed. Differently from the QXRD results, degradation of magnesite did not show in the TG-curve, thus quantification of the mineralization degree only the other two degradations were considered.

The final effective mineralized carbon was calculated for each fly ashes as described in the methodology. The results are shown in Figure 5.12. Mineral carbonation was the highest in the binder having 12.2% of final mineralized carbon in the material. In FA2 7.26% of carbon was mineralized after carbonation, followed by FA3 that mineralized 4.7%, FA1 with 4.6% carbon taken, FA6 resulting in 4.27% and FA5 with 3.22% of carbon uptake.

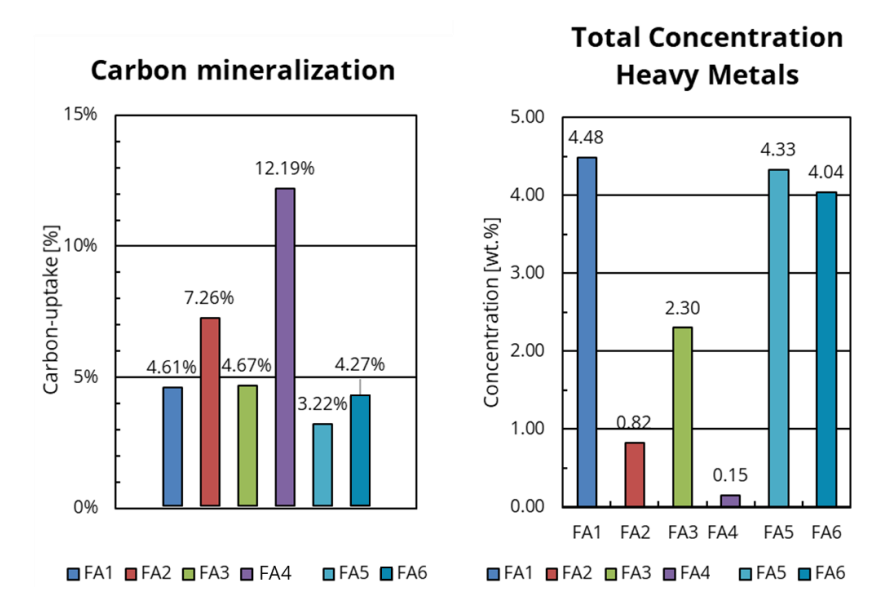


Figure 5.12: (Left) Carbon-uptake in wt.% of each material after 1 week of carbonation. (Right) summary of the relevant heavy metals' concentrations of each material.

5.2 Selection of fly ashes

Based on the analysis from the chemical composition of the material, the material with the highest amount of carbon uptake was FA2, the biomass fly ash. However, its heavy metals content was low compared to the other fly ashes, as summarized in Figure 5.12.

The results of the Weighted Sum Method are shown in Table 5.7. FA4 was not considered as it is the binder and thus not of interest to be immobilized in this research. Based on the results, the fly ash with the highest A-value was FA1. Even though the material did not have as high carbonation as FA2, the large quantity of heavy metals made the material scoring the highest. Based on this small analysis, FA1 was selected for the further immobilization process, given its high heavy metals concentrations and moderate carbonation capacity.

Considering the importance of ensuring that the material carbonizes, FA2 is chosen given its highest CO₂ binding capacity.

Table 5.7: Results of Weighted Sum Method to select the most feasible fly ash.

	FA1	FA2	FA3	FA5	FA6
Tot. heavy metals [%]	4.80%	0.82%	2.30%	4.33%	4.40%
m_{CO_2} [%]	4.61%	7.26%	4.67%	3.22%	4.27%
\overline{A}	4.71	3.72	3.37	3.83	4.34

6. Carbonation and immobilization

The following chapter presents and discusses the results from the preliminary carbonation experiment, highlighting the optimal carbonation conditions and the influence of water content and pressure on carbon uptake and reaction rate. In the second subchapter the preparation of the three mix designs is explained, describing the texture and physical appearance of the materials after carbonation, and curing. In the final section, the results of the compression and slake tests for each mix design are presented and compared to the reference sample.

6.1 Preliminary carbonation

6.1.1 Selection carbonation conditions (FA1_C1_1)

Figure 6.1 presents the TG-DSC curves of the original FA1, the FA carbonated for 1 day at low temperature, pressure and CO₂ concentrations (FA1_C01d), and the FA1 carbonated and higher temperature (FA1_C1_1). The TG-profile of the non-carbonated and carbonated material had a similar trend, showing a decomposition peak at 600°C. The carbonated curves deviated from the original material after 600°C following the same trend. This indicated that the final effective carbonation was similar under the two carbonation conditions.

The peak in the DSC curve of FA1_C1_1 was due to the evaporation of free water. The sample was not dried to ensure that no additional carbonation occurred after the test. The initial part of the TG curve was also normalised to the TG value of the original FA1 better visualize the mass drop caused by decarbonation rather than water evaporation.

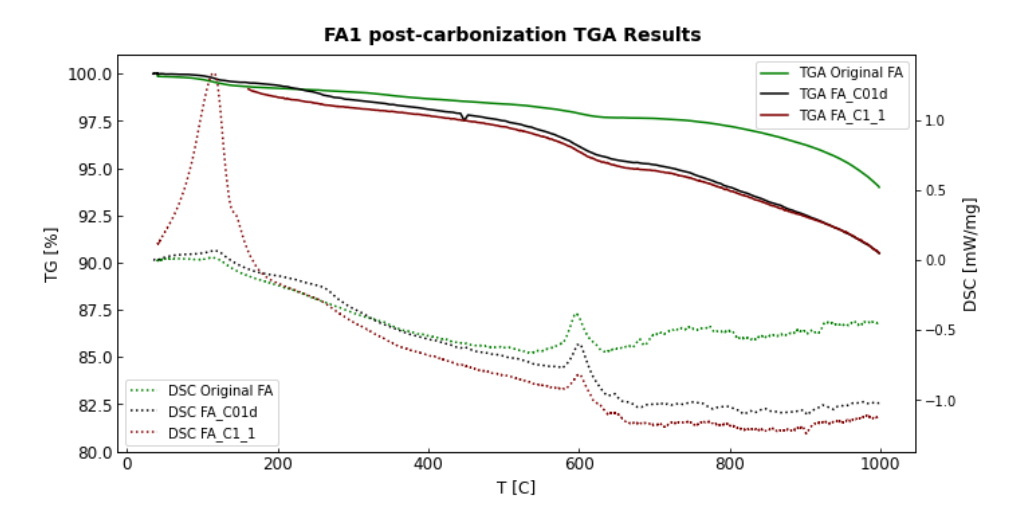


Figure 6.1: TG-DSC results of the original fly ash (FA1), the carbonated material at 1% CO₂ and 20°C for 1 day (FA1 C01d) and the carbonated FA1 at 40°C, 100% CO₂ for 2 h (FA1 C1 1).

The effective carbon dioxide mineralization at high temperature conditions was compared to the carbon-uptake after 1 day and 1 week in the carbonation chamber. The material carbonized at 40°C results in 2.66% effectively mineralized CO₂, close to the 2.59% carbon-uptake after 1 week of carbonation. Six days extra of carbonation resulted in 2% more carbonation, as shown in Table 6.1. By interpolating the values as explained in the Methodology, the optimal carbonation time for the Stevin I chamber was of 1 hour and 10 minutes.

Table 6.1: Carbon-uptake of fly ash after 1 and 7 days of carbonation at 20°C, 1 bar, 65% RH and 1% CO₂ and carbon-uptake of FA1 at 40°C, 2 bar, 100% CO₂.

•	FA1_C01d	FA1_C07d	FA1 _C1_1
Carbon-uptake	2.59%	4.61%	2.66%

6.1.2 Influence of water-content on carbon-uptake (FA4 C1 WC)

The binder was carbonized for two hours at 45°C, injecting 100% CO₂ at 15 bar. The material was initially carbonized without addition of water (FA4_C1_WC0) and then the experiment was repeat pre-mixing 10 g of FA with 3 g of demi-water. After carbonation, the materials were dried and tested with TGA. The results are presented in Figure 6.2.

The TG-DSC-DTA curves of the original material and the carbonated binder under dry condition overlap. At 400°C it seems that the lines deviate, but they end up overlapping from 800°C onwards. Another peak is detectable at 420°C in the original binder that remains after dry carbonation. The peak is associated in literature studies with dehydration of brucite or hydromagnesite (Winnefeld et al., 2019). However, FA_C07d contains 1% more of brucite and hydromagnesite but does not show the clear curve drop as in FA4. Dehydration of portlandite is another peak usually detected at a similar range, but it would not justify the results of the QXRD, showing that portlandite is still present in the sample even after wet carbonation, as shown in Figure 5.8.

The thermogravimetric curves of the material carbonated in wet conditions clearly diverge from the original sample, differently than the dry carbonation. The peak at 800°C in the DSC curve also increases, meaning that more heat was taken by the sample to decompose the mineralized carbon. The DTG peak is greatly pronounced in the wet carbonation, showing that more material carbonized.

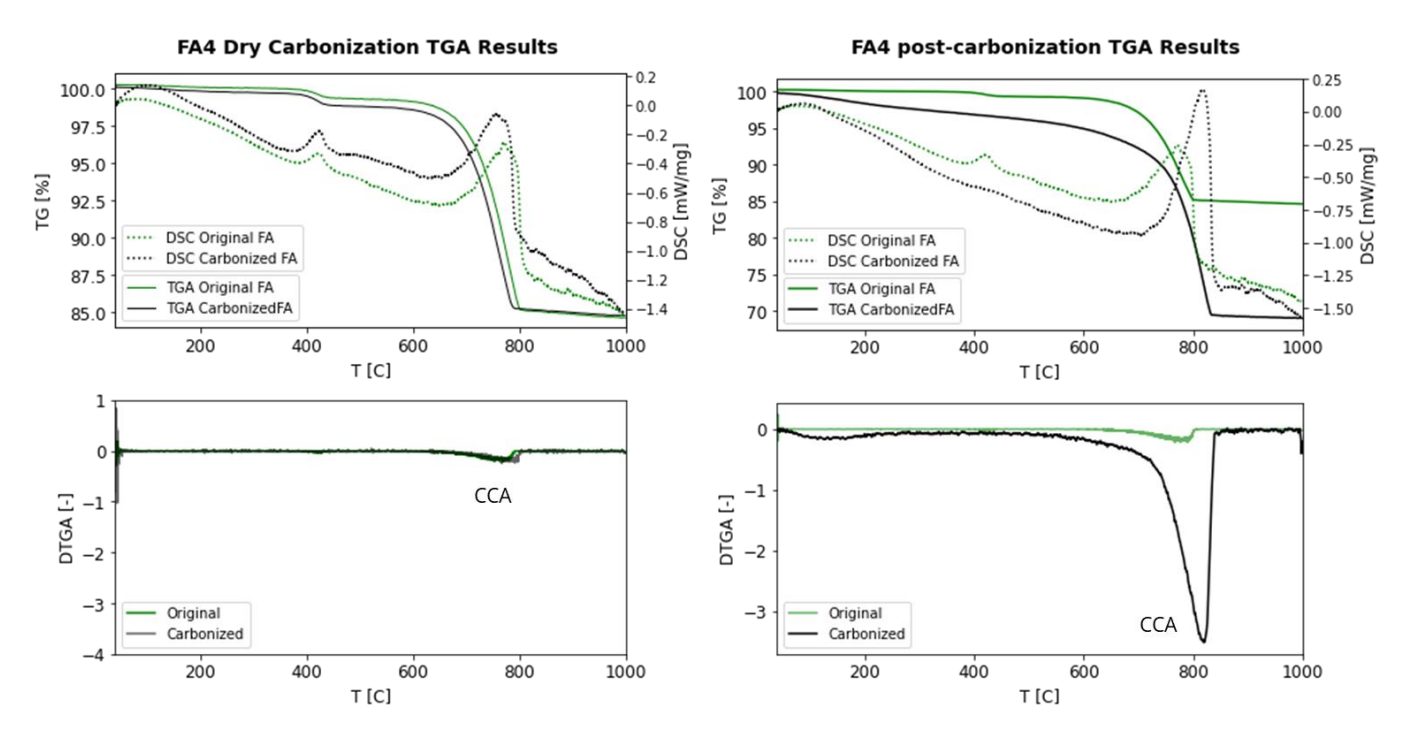


Figure 6.2: (Left) TG-DSC-DTG curve of original FA4 and FA4 carbonized in dry conditions and (right) with the addition of 3 ml of water in 10 g of solid material.

The effective carbonation of each material was determined and reported in Table 6.2 below. The difference of the FA4 and FA4_C1_WC0 curves shows that no carbonation occurred under dry carbonation. On the contrary of what found in the Literature Review, the direct reaction of gas and solid did not happen in the binder. The reason might be related to the fact that the reaction kinetics is much slower than in wet conditions. The reaction time might have not been sufficient for the given pressure and temperature conditions for the CO₂ to dissolve in the material. Additionally, the material in the research of Baciocchi et al. (2009) is not dried and contained 1.8% of residual water, facilitating the carbon-uptake.

The same carbonation but in wet conditions increased the carbonation to 13.6%. All available free lime was carbonated after only 2 h of carbonation. Not only the presence of water could speed the reaction kinetics, as found in Literature, but it was an important element to achieve effective carbonation, that otherwise would have not occurred in completely dry conditions.

Table 6.2: Effective carbon-uptake results from the carbonation of the binder FA4 under dry (FA4_C1_WC0) and wet conditions (FA4_C1_WC3).

	FA4_C1_WC0	FA4_C1_WC3
Carbon-uptake	0%	13.6%

6.1.3 Influence of pressure on reaction rate and carbon-uptake (FA1-B_C1_P)

In the third and last preliminary carbonation experiment a mixture of FA1, binder and water was prepared for the carbonation. This experiment was to assess the reaction rate and carbon uptake of the hazardous material already enriched with the binder to enhance carbonation reactions, as explained in the Methodology. Carbonation was conducted at 40° C, 100% CO₂ environment, with 0.3 ml/g of demi-water, at 1 bar and 2 bar of pressures.

The difference in concentration of CO₂ in the gaseous form at each moment of the carbonation reaction was determined by monitoring temperature and pressure variations. As the pressure gauge and the thermocouple record every 5 seconds values up to 0.01 bar and 0.01 °C, the minimum variations cause a high difference in the 2 h reaction time. An exponential fit function was used to average the data to a linear function, as shown in Figure 6.3. Carbon dioxide concentration inside the vessel drops rapidly in the first 6 minutes from the beginning of the reaction. The dissolution in the material slowly decreased until it reaches a constant ratio after 25 minutes.

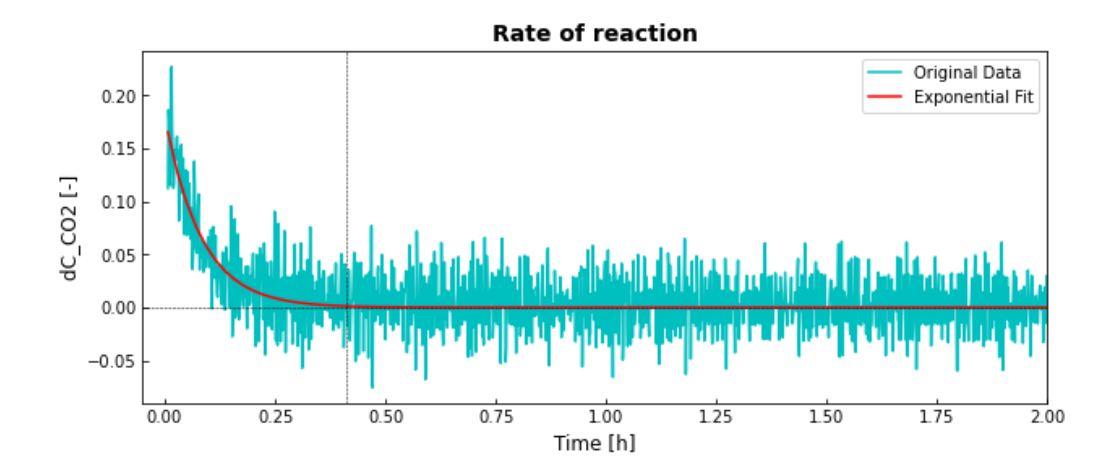


Figure 6.3: Rate of reaction throughout the carbonation experiment of the FA-binder mixture at 1 bar.

Figure 6.4 shows the rate of reaction of the material carbonized at 2 bar. Under the same carbonation temperature and water content, the dissolution on the water layer took only 12 minutes. Increasing the pressure halved the dissolution rate of the gas in the material.

It is to note that the real time for the dissolution of carbon dioxide was longer than indicated. The dissolution with atmospheric CO₂ began as soon as water was added to the system. Once reached the equilibrium with the atmospheric CO₂, the system was again perturbed as the material heated up inside the over prior switching on the CO₂ inlet gas. As some air was still present inside the vessel while the material was heated, more CO₂ was already dissolving and mineralizing inside the samples. The time from when water was added to the system until the gas was turned on, was not recorded, and differs for the two materials as it depended on the room temperature of the laboratory. Thus, this analysis was only an indication on the different reaction rates and the time should not be used as reference as effective carbonation dissolution time.

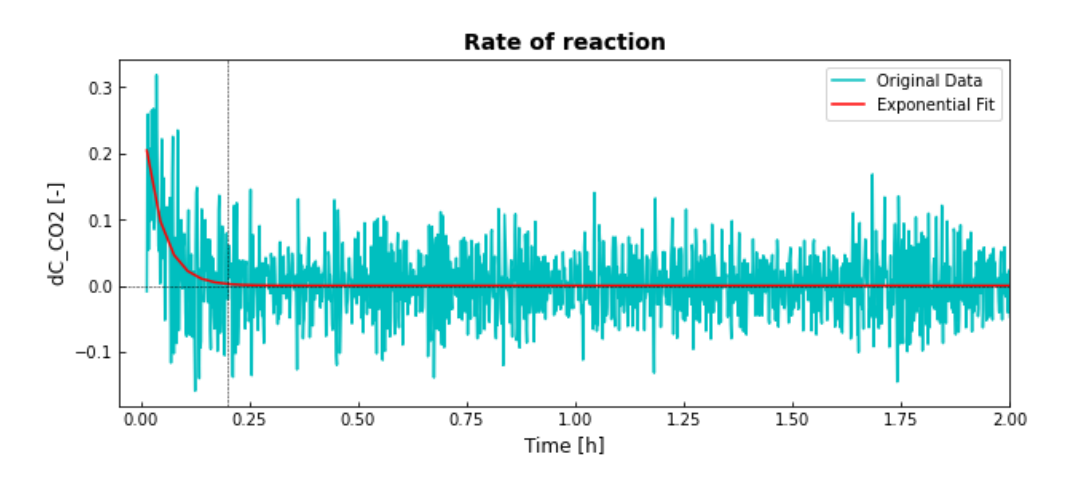


Figure 6.4: Evolution of reaction rate during the carbonation of FA1 and binder at 2 bar.

TGA was conducted on the materials and compared with the original FA1, results are shown in Figure 6.5. The TG curves of the carbonated fly ashes deviated significantly from the original fly ash, as also shown in the DTG curve by two large peaks at 620°C and 700°C. Based on the literature study and the phases formed post-carbonation on FA1 and FA4 (Figure 5.7 and Figure 5.8), the two peaks indicate the decarbonation of magnesite (MGC) and calcite (CCA). The peak of FA1-B_C1_P2bar from the degradation of calcite is more pronounced than the material

carbonized at 1 bar. Similarly, the TG-curve of the 2-bar material deviates from the other carbonized paste at 700°C.

The DSC curves of the carbonized materials show the same pattern but differ from the original fly ash. The peak in the DSC curve right before 600°C in the original sample has lowered and shifted to the right in the carbonized materials, as the hydromagnesite transformed to magnesite. At 700°C two peaks appear in the carbonated materials for the heat consumed for the degradation of newly carbonated calcite.

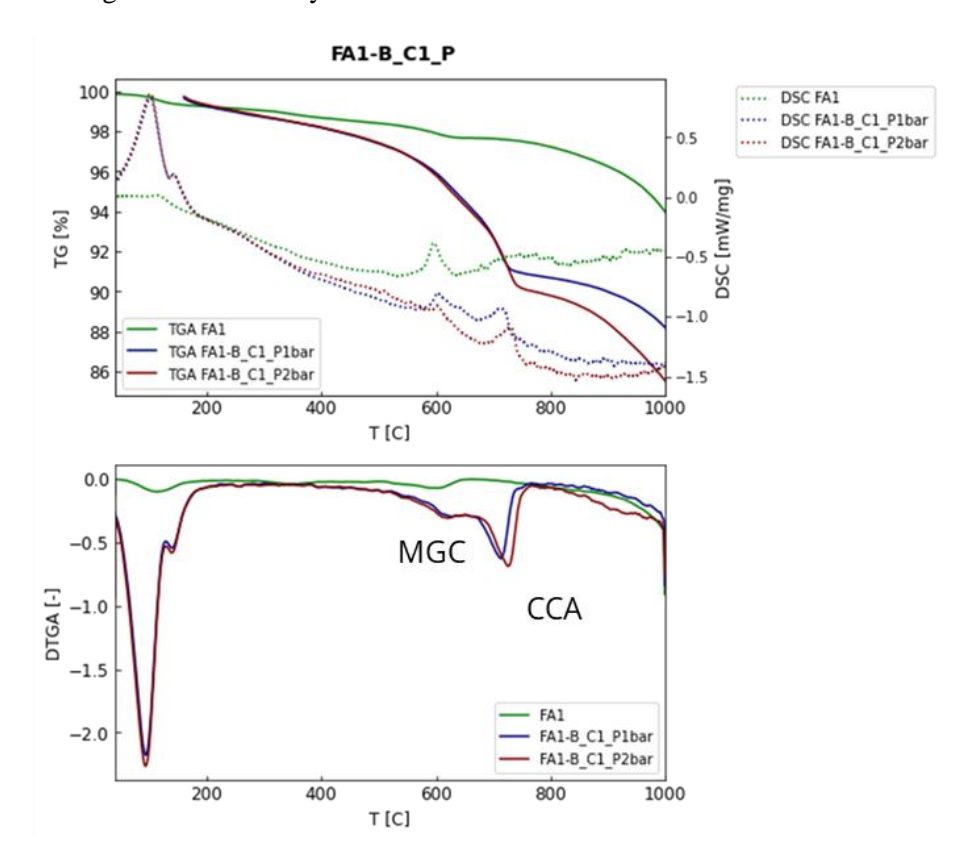


Figure 6.5: TG-DSC-DTG curves of the original FA1 and the carbonated FA1-B mixture at 1 bar and 2 bar.

To quantify the effective mineralized carbon, the mass differences were calculated and re-scaled for the initial carbonized material on an equivalent mixture with 77% FA1 and 23% binder. The final carbon-uptake from the carbonation reaction of the mixture at 1 bar was 7.2% of its total weight. Doubling the pressure resulted in a 9.9% of effective mineral carbonation.

Table 6.3: Effective carbon-uptake of carbonized FA1-binder mixtures at 1 bar and 2 bar.

	FA1-B_C1_P1bar	FA1-B_C1_P2bar
Carbon-uptake	7.22%	9.94%

6.2 Mixture designs

The hazardous FA1 was immobilized through 3 different routes. The material was initially pre-carbonized in the carbonation chamber for 1 day, at 1 bar, 20°C, 65% RH, 1% CO₂ and 0.3 ml/g of demi-water. The material was later mixed with the binder for casting and curing for 28 days (FA1_C2). The second immobilization route consisted of pre-carbonization of the mixture of FA1 and binder in the same carbonation conditions for 1 day. The material was then mixed again to add the remaining water and to cure the sample for 28 days (FA1-B_C2). The last carbonation route consisted of casting the material as the reference sample but instead of curing it in the curing chamber, it was left for 28 days in the carbonation chamber (FA1-B_C3). A reference sample (FA1-B_Ref) was also prepared to compare the results of the other immobilized materials.

6.2.1 Pre-carbonated FA (FA1_C2)

After one day in the carbonation chamber, a white layer or salts deposited on the surface of the material. The material had also hardened to a damp brittle crumble-like texture, as shown in Figure 6.6A. The water content retained in the material was estimated from the weight loss from the TGA analysis at 105°C, corresponding to 12% of the total mass. The equivalent dry content of FA1 was mixed with 30% of binder. The remaining 21.3% of demi-water, proportional to the dry FA1 content was added to the system during mixing and the material was casted in the polystyrene moulds. After 28 days, the material had hardened assuming the form of the mould, as shown in Figure 6.6B. The prisms after curing were still humid, although they were wrapped in plastic foil, and crumble on the edges.

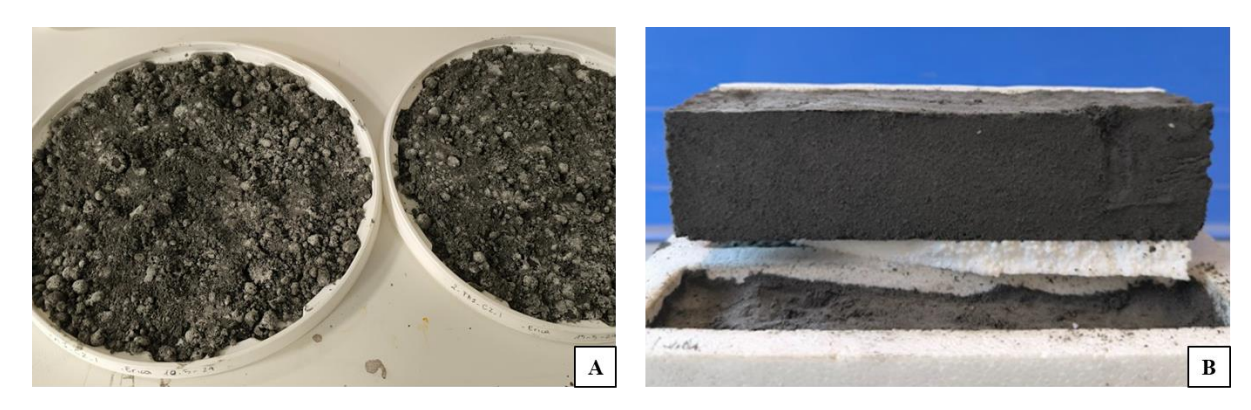


Figure 6.6: (A) FA1 after pre-carbonation and (B) immobilized FA1_C2 specimen after 28 days of curing.

The materials before casting and after casting were analysed through QXRD and TGA to determine the evolution of the carbonation and crystalline phases.

A summary of the results from the QXRD can be seen in Figure 6.7 and more in detail in

Table B.0.1 in Appendix B. Compared to the reference paste pre-curing, the pre-carbonate fly ash had much more anhydrite and calcite, but less magnesite and vaterite. As already seen previously, the anhydrite formed was probably a consequence of the crystallization of amorphous sulphites whereas the higher calcite was due to the pre-carbonation of FA1. Magnesite was lower in the carbonated fly ash but instead it was present in the higher proportion of merwinite, a magnesium-calcium silicate. The presence of vaterite in the non-carbonized reference sample might be the cause of carbonation of the material with atmospheric CO₂ or with the amorphous carbonates. Of the pure oxides more prone for carbonation, lime, periclase portlandite and C3S were present in higher quantities in the reference sample. The decrease in concentration was a consequence of the oxides already hydrated and carbonized in the pre-carbonated FA1. The pre-curing FA1_C2 had higher C2S as hydration product from

amorphous calcium and amorphous silica from the change in pH of the material due to mineral carbonation. Hydromagnesite was also present in FA1_C2, differently form the reference sample. Pre-carbonation and hydrations of the fly ash also generated large quantities of calcium aluminosilicate such as anorthite and ettringite.

During the 28 days of curing, the crystalline composition of the paste continued changing. The anhydrite composition decreased, with the sulphites going back to contribute to the amorphous phase. Lime, portlandite, C2S and C3S were almost fully consumed for the calcification of calcium carbonated and wollastonite (CaSiO₃). The formation of wollastonite was reported to occur from the reaction of silica and limestone at 400-450°C, thus it was not expected to be present in the material (Nair & Sairam, 2021). However, previous research also identified the evolution of the crystal after curing of hardened alkali activated cement paste with hazardous fly ash (Chen, 2023).

After 28 days, C-S-H gels decreased but C,N-A-S-H gels were formed. As the phases were only partially crystalline, their formation might be the cause of increase of the amorphous phase from 11% to 30% pre-curing and post-curing. When gels are present in larger quantities, previous researchers were also able to detect their presence in the XRD patterns combined with other methods (Qui et al., 2017).

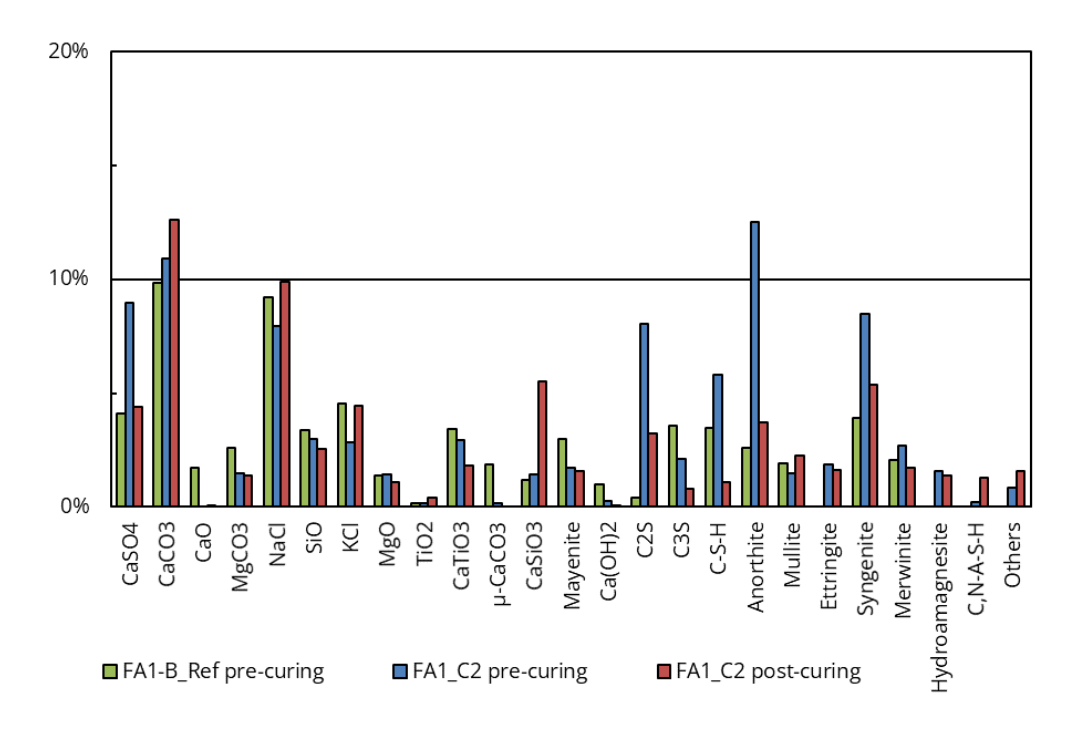


Figure 6.7: Results from Rietveld refinement of the QXRD patterns of the reference paste (FA1-B_Ref pre-curing), the pre-carbonated FA1 pre-curing (FA1_C2 pre-curing) and the paste with pre-carbonated FA1 after 28 curing (FA1_C2 post-curing).

To confirm the findings from the XRD analysis and to quantify the mineral carbonation, TGA was conducted on the materials pre- and post-curing. The DTG curves of FA1-B_Ref, FA1_C2 and FA1_C2 post-coring are plotted in Figure 6.8. The peak corresponding to the degradation of magnesite slowly disappears in the paste pre-curing and after curing, confirming the decrease in the crystalline magnesite. The calcite peak is higher already in the mixture with pre-carbonated FA compared to the reference, as more calcite was formed from the carbonation. The calcite peak in the material post-curing is slightly more pronounced than the pre-curing paste, as a result of the higher crystallization of calcium carbonates (Figure 6.7).

The peaks below 200°C are attributed to the decomposition of free water and hydrated gels such as C-A-S-H and N-A-S-H gels. Removed the peak for the free water evaporation, the peak of the gel phases is pronounced in the post-curing immobilized material, confirming the increase of amorphous phase in the material. The increase of gel phases can effectively immobilize the heavy metals present in the fly ash. Heavy metals can replace ions on the edges of the gel's chemical structure, can be physically encapsulated in between layers and substitute calcium ions in the structure, as shown previously in Figure 3.3. The peaks at 300°C are associated with the degradation of calcium-aluminium hydrates (Nedeljković, 2019; Sriwong et al., 2020; Zhang et al., 2021; Sun et al., 2024).

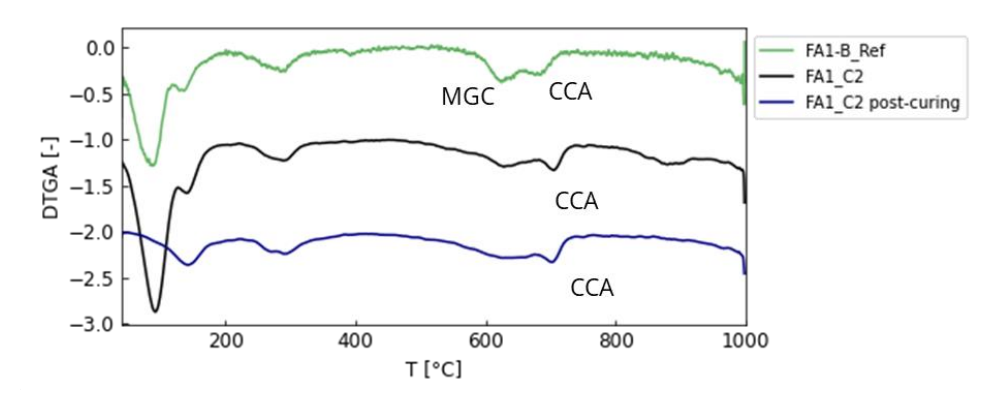


Figure 6.8: DTG curves of reference sample, pre-carbonized FA mixed with the binder and the hardened paste after 28 days.

The effective carbon uptake was determined from the TG-curves of the pre-curing and post-curing samples compared to the reference material. As shown in Table 6.4, the pre-carbonated fly ash mineralized 3.4% of its total FA-binder weight. The value was lower that the carbonation of only the FA (Table 6.1, Figure 5.12), but it was since the total weight was higher, as also the binder was present. Considering that 30 g of the binder were added every 100 g f fly ash, the expected carbonation should have been of only 1.92%, based on the previous results. However, the real carbon-uptake was of 2.2%, suggesting that some of the binder must have already started carbonating. The effective mineral carbonation after 28 days increased of 1.4%. The material during curing mineralized atmospheric CO₂ into new calcite while hardening the structure.

Table 6.4: Effective mineral carbonation of the FA1_C2 before and after curing.

	FA1_C2 pre-curing	FA1_C2 post-curing
Carbon-uptake	2.23%	3.67%

6.2.2 Carbonated mixture (FA1-B_C2)

A mixture of FA1, binder and water was prepared by maintaining constant the FA/binder ration of 100:30 and adding 0.3 ml/g of FA1. The material was carbonized for one day under the same carbonation conditions of FA1_C2. After 1 day, the material was removed from the carbonation chamber and analysed for the residual free water. The mass drop at 105°C was of 9.1%, corresponding to 11.9 ml of water for 100 g of FA. The material was mixed in a planetary mixer and adding 31.4 ml of demi-water for every 100 g of equivalent FA1. After carbonation, the material looked slightly drier compared to FA1_C2; it did not aggregate into crumbles and the layer of salts at the surface did not form, as shown in Figure 6.9A. After mixing with the remaining water, the material was dry compared to the previous case and barely castable, as shown in Figure 6.9B. After 28 days the hardened material, in Figure 6.9C, resulted in a weak structure, with a soil-like texture and still humid.



Figure 6.9: (A) Picture of FA1-B mixture after 1 day of carbonation. (B) Picture during mixing the carbonized material with the remaining water. (C) FA1-B_C2 specimen after 28 days of curing.

The crystalline phases identified are shown Figure 6.10 in below and in Table B.0.2 in Appendix B. Anhydrite and calcite concentrations were much higher in the pre-carbonated FA1-B compared to the reference sample. Anhydrites formed from the crystallization of the amorphous sulphites on the hazardous fly ash and calcite from the carbonation of lime in the FA and in the binder. After carbonation not all lime present in the paste was carbonized. C2S and C3S formed in the pre-carbonated mixture but their concentration decreased after curing, as well as for anhydrite. The structures crystallized into more stable calcite after 28 days of curing. The aluminium-silicates anorthite, mullite and ettringite formed after curing of the paste. The concentration of C-S-H gel also increased of almost 5% compared to the pre-cured material, but the total amorphous phase decreased from 10.6% to 5.2%.

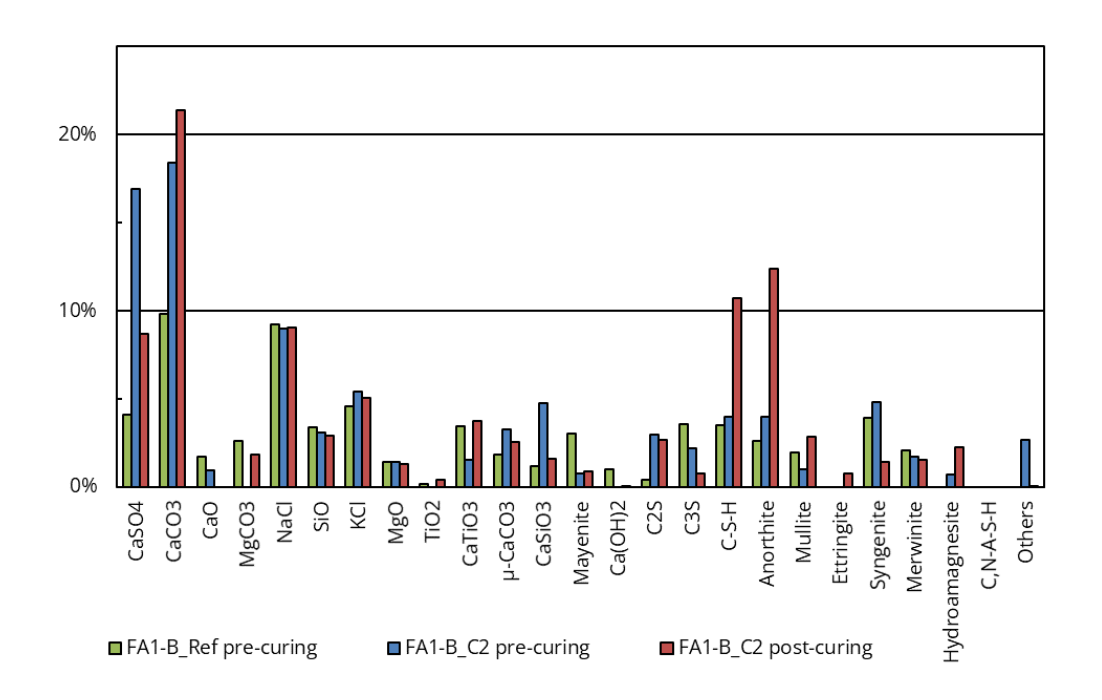


Figure 6.10: Results from Rietveld refinement of reference sample and the pre-carbonated paste of FA1 and binder before and after 28 days of curing.

The DTG curves confirmed the disappearance of magnesium carbonates in the pre-carbonated paste of FA1 and binder as shown in the QXRD patterns. During carbonation of the binder, magnesite reacted probably with calcium silicates to form hydromagnesite and calcite, causing the disappearance of the peak at 600°C. Differently from the TG profile of the raw FA1 in Figure 5.9, no clear peak for hydromagnesite was showed in the DTG curve. A small peak at 170°C appears in all the samples, probably from the decomposition of other hydrated phases and the C-S-H gel.

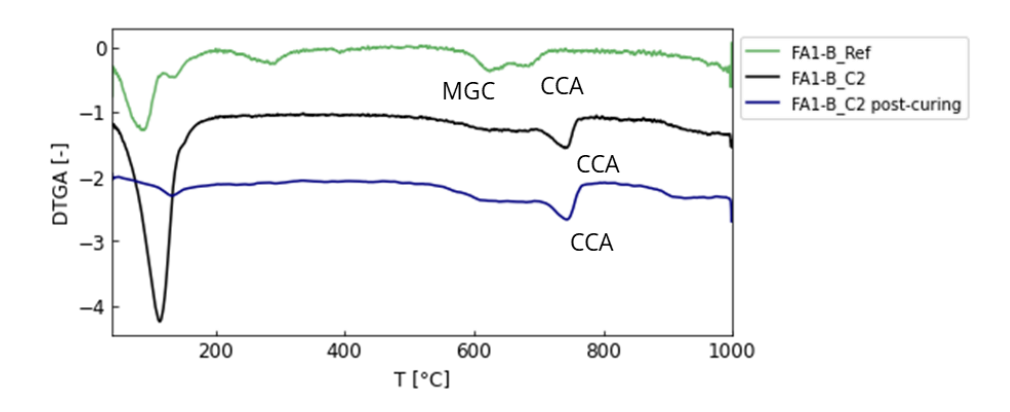


Figure 6.11: DTG curves of reference paste (FA1-B_Ref), carbonated FA1-binder paste before curing (FA1-B_C2) and after curing (FA1-B_C2 post-curing).

Table 6.5 shows the effective carbon-uptake after carbonation of the paste and after 28 days in the curing chamber. As can be seen in the table, the mineralized carbon reached 4.22% of total sample weight after carbonation. More

carbon dioxide was mineralized during the 28 days of curing as the remaining lime was fully consumed only at the end of the process. The final effective carbon-uptake of FA1-B_C2 after curing was of 6.2%.

Table 6.5: Effective mineral carbonation of the pre-carbonated paste FA1-B_C2 before and after curing.

	FA1-B_C2 pre-curing	FA1-B_C2 post-curing
Carbon-uptake	4.22%	6.20%

6.2.3 Carbonation after casting (FA1-B_C3)

The same paste as the reference sample was prepared with 1 kg of FA1, 300g of binder and 433 g of water. The materials were mixed as explained in the Methodology and casted in the polystyrene moulds, to be placed in the carbonation chamber at 20°C, 1 bar, 1% CO₂ and 65% RH. After three days in the carbonation chamber, the material had already mainly dried as shown in Figure 6.12A. At the 28th day the material was removed from the carbonation chamber. The specimens were hardened and compact, but a white crumbled surface formed on top of the sample, as can be seen in Figure 6.12B.

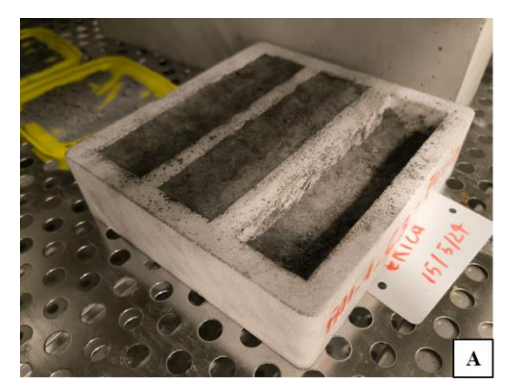




Figure 6.12: (A) FA1-B_C3 after 3 days in the carbonation chamber and (B) after 28 in the carbonation chamber.

The paste before curing in the carbonation chamber was the same as the reference sample, as they were prepared in the same way and with the same material. This can also be seen from the QXRD results shown in Figure 6.13, where all crystalline phases of the FA1-B_C3 paste match with the crystalline composition of the reference sample pre-curing. Anhydrite concentration in the reference sample was 4% lower than the FA1-B_C3 paste, resulting in 34.7% of amorphous phase in the reference sample and 28% of amorphousness paste that undergoes carbonation.

After 28 days of carbonation the calcite concentration had increased from 10% to 22.6% and all the lime present was consumed. Portlandite and C3S were not fully consumed for the carbonation, similarly to what observed after carbonation of the raw materials in Figure 5.7 and Figure 5.8. After carbonation and hydration of the paste, anorthite concentration increased, a calcium-alumina oxide, as well as for syngenite. Less than 1% of C,N-A-S-H gel formed after hardening of the paste, but the overall amorphous content of the material decreased form 28% to 3%, as the sulphites remained in the crystalline form. Differently from the previously immobilized materials FA1_C2 and FA1-B_C2, anhydrite did not recrystallize but instead it continued forming. In the Appendix B Table B.0.2 reports the detailed results from the Rietveld refinement of the QXRD patterns of FA1-B_C3 before and after curing.

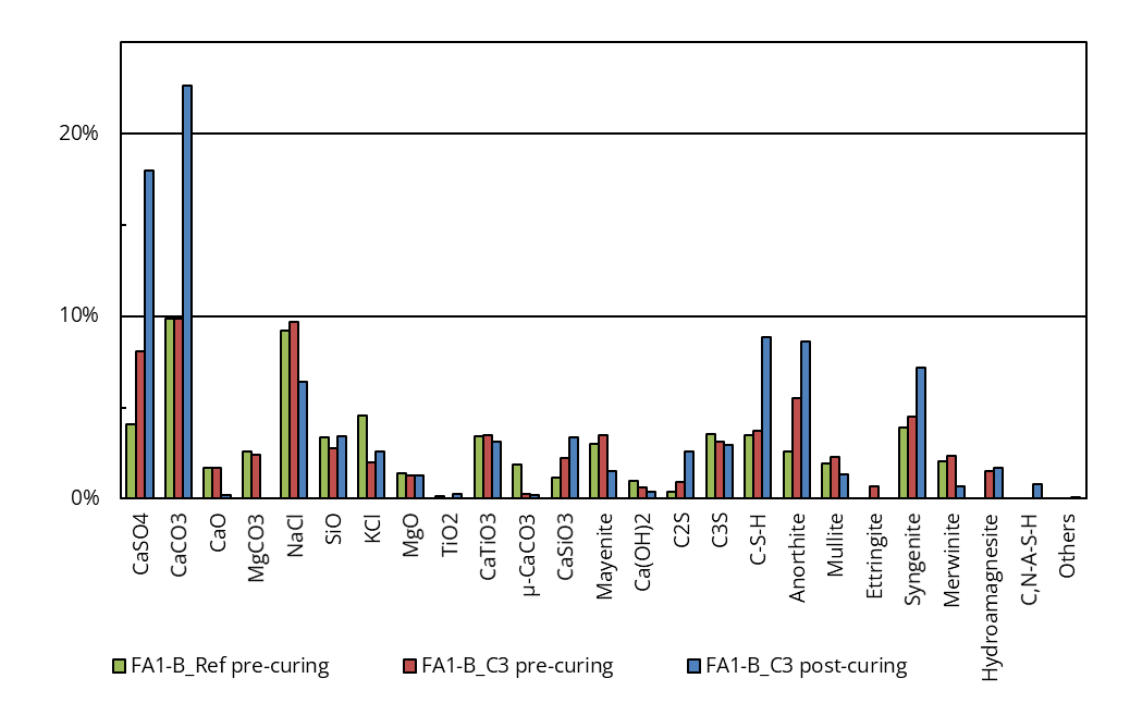


Figure 6.13: Results from quantification of XRD results of the reference sample and FA1-B_C3 before and after curing.

The increase of C-S-H in the XRD results can also be seen in Figure 6.14. The characteristic peaks of C-S-H are at 2Theta values of 14.7°, 29.6°, 31.7° and 49.3° (Siramanont et al., 2021). As the other peaks are near other larger peaks, only the smaller peak at 14.7° is plotted. The peak, being unique, clearly increased its magnitude after 28 days of curing, explaining the increase in concentration resulting from the QXRD analysis.

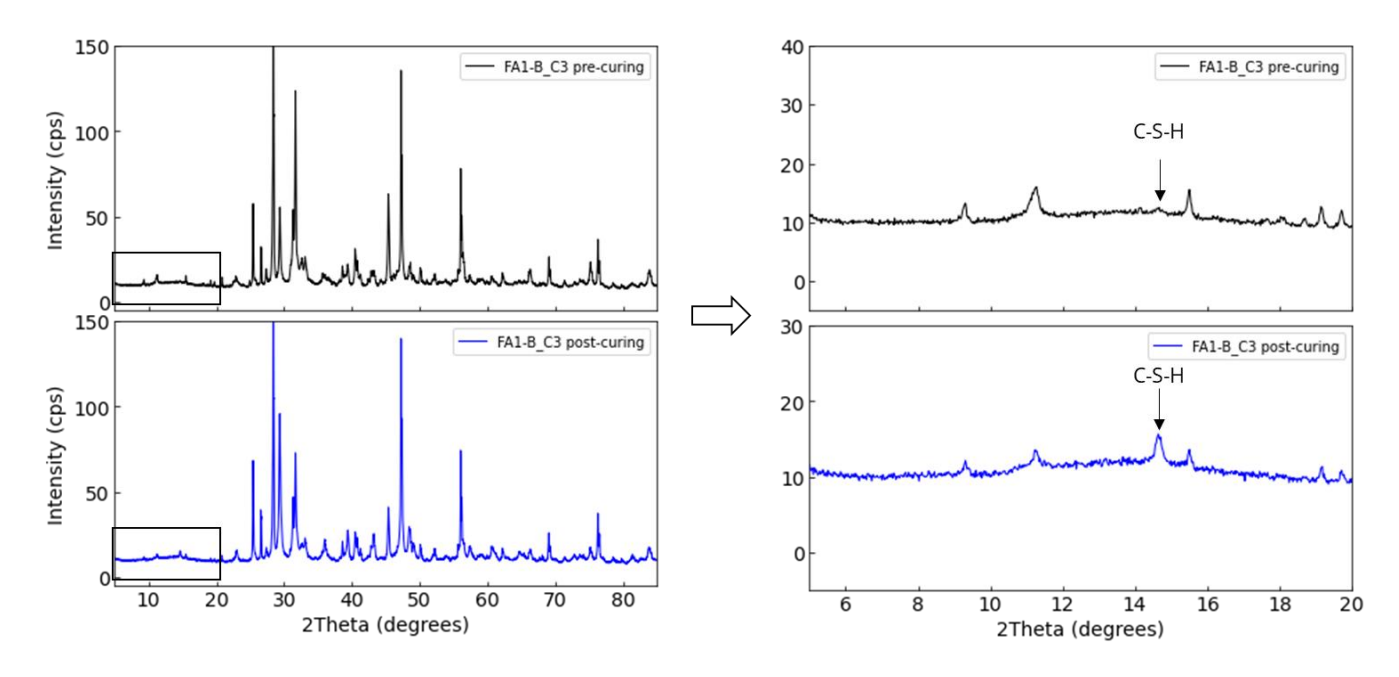


Figure 6.14: On the left are plotted the XRD profiles of FA1-B before and after curing, and on the right the parts of the spectrum between 5 and 20 2Theta degrees.

The DTG curves of the reference paste and the FA1-B_C3 before curing in Figure 6.15 show the exact same pattern, as they were prepared in the same way and originating from the same materials. After 28 of curing, the magnesite hump disappears and instead the calcite peak increases. This is also confirmed by the QXRD results showing an increase of calcite formation. The peak before 200°C is slightly more pronounced in the carbonated material, as the concentration of gels increased.

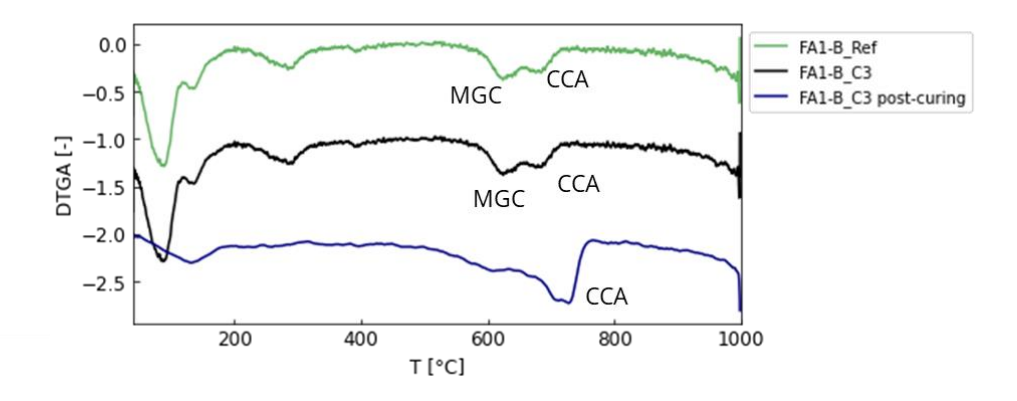


Figure 6.15: DTG curves of reference paste, FA1-B_C3 paste pre- and post-carbonation.

Even though the material has been in the carbonation chamber for 28 days, Table 6.6 shows the final effective carbon-uptake. The final uptake of 5.88% was lower than the effective carbonation post-curing of the precarbonated FA-binder paste. It is possible that, as carbonation occurred initially on the surface exposed to the gas, the rest of the conditions for the rest of the sample were not optimal for mineral carbonation. Even if all lime was carbonized, from the QXRD results the concentrations of portlandite and C3S did not decrease in the material after curing. On the contrary of the pre-carbonated paste, the prolonged exposure to carbonation did not result in higher

effective carbonation mineralization, as previously found in the research mentioned in the Literature Review (Saleh, 2021).

Table 6.6: Effective mineral carbonation of the FA-binder paste FA1-B_C3 before and after curing in the carbonation chamber.

	FA1-B_C3 pre-curing	FA1-B_C3 post-curing
Carbon-uptake	0%	5.88%

To ensure that the specimen was fully carbonized, the sample was rinsed with phenolphthalein. As can be seen from Figure 6.16A, the reference sample did not carbonize, turning to the characterising purple-pink colour of the pH indicator. This step was important to also determine whether the material was suitable for the pH-test, as it must be initially of pH higher than 10 for the test to be applicable. After curing, FA1-B_C3 was rinsed with phenolphthalein as shown in Figure 6.16B. The carbonized material barely changed colour if not for two small areas at bottom part of the sample. The regions, circled in Figure 6.16B, were covered by the casting mould, preventing the dissolution of CO₂ in the sample. Carbon dioxide penetrated most of the sample probably because of the high porosity of the material, as the empty voids between grains are visible by naked eye, as shown in the picture in Figure 6.16B.

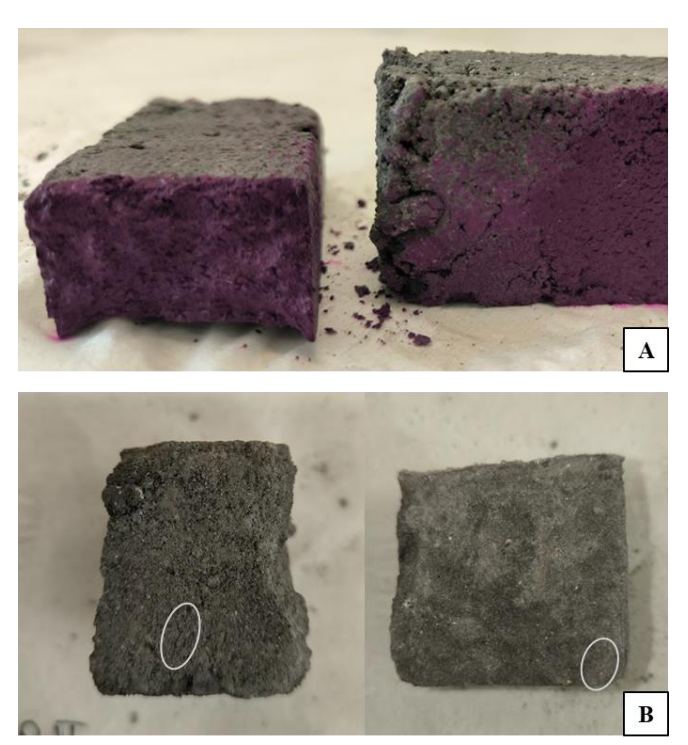


Figure 6.16: Pictures of the (A) reference material rinsed with phenolphthalein and (B) carbonized sample after 28 days of exposure. The circled parts indicate the areas where colour changed, but hardly visible in the picture.

6.3 Physical stability

At the 28th day of curing, all materials were tested their maximum flexural and compression strength. A block of each specimen was also tested for stability in water through the slake test.

6.3.1 Physical strength

The flexural strength test was performed starting from a minimum strength of 0.5 MPa. None of the samples complied with this minimum strength and broke before the end of the experiment.

The maximum compression strength of each immobilized material was determined through the compression strength test as described in the Methodology. Compressive strength results of the immobilized materials and the reference sample are shown in Figure 6.17. The average compression strength of the reference sample was almost touching the minimum strength required for the safe disposal of immobilized wate (Beschikking 2003/33/EG). This can be a consequence of the chose S/L ratio or of an improper compression of the paste to the mould. As can be seen from Figure 6.18A the breaking plane was relatively smooth, and no visible voids were present in the sample.

Compared to the reference samples, the materials pre-carbonated before casting showed a drastic decrease in strength. The strength after 28 days of curing of FA1_C1 was more than halved compared to the reference sample. As can be seen from Figure 6.18B, the material, still humid after curing, stays intact after compression. The breaking surface was discontinuous, resulting in weakened cohesion of the paste and lower compressive strength.

The pre-carbonated paste was not testable for compression as the material crumbles during demoulding. As can be seen from Figure 6.18C, the material had a humid soil-like texture and it disintegrates as soon as removed from the mould. Pre-carbonation of the binder activated the material that started hardening one day before it was mixed and casted. For this reason, the most of hardening reaction were already initiated and did not efficiently harden the paste once it was put in the mould.

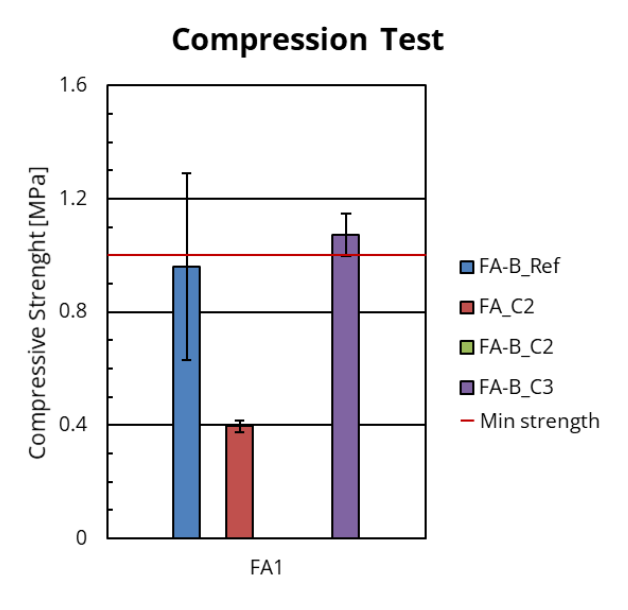


Figure 6.17: Compression tests results of the reference and the three different mix-designs with FA1. The maximum strength decreased for the pre-carbonated FA1_C2 and was non-detectable for FA1-B_C2. The average strength of FA1-B_C3 was higher than the reference sample.

Differently from the previous specimens, FA1-B_C3 resultd in a higher compressional strength. As can be seen from Figure 6.17, the average compressive strength of the material not only surpassed the strength of the reference, but also complied with the minimum strength required by the Dutch regulation Beschikking 2003/33/EG. After demoulding and compression test the specimen remained intact and broke along a more linear and structured plane,

as shown in Figure 6.18D. Still the fracture plane was not as smooth as a cement paste exposed to natural carbonation (Nedeljković, 2019), but the material performed much better than the paste made of pre-carbonated fly ash.

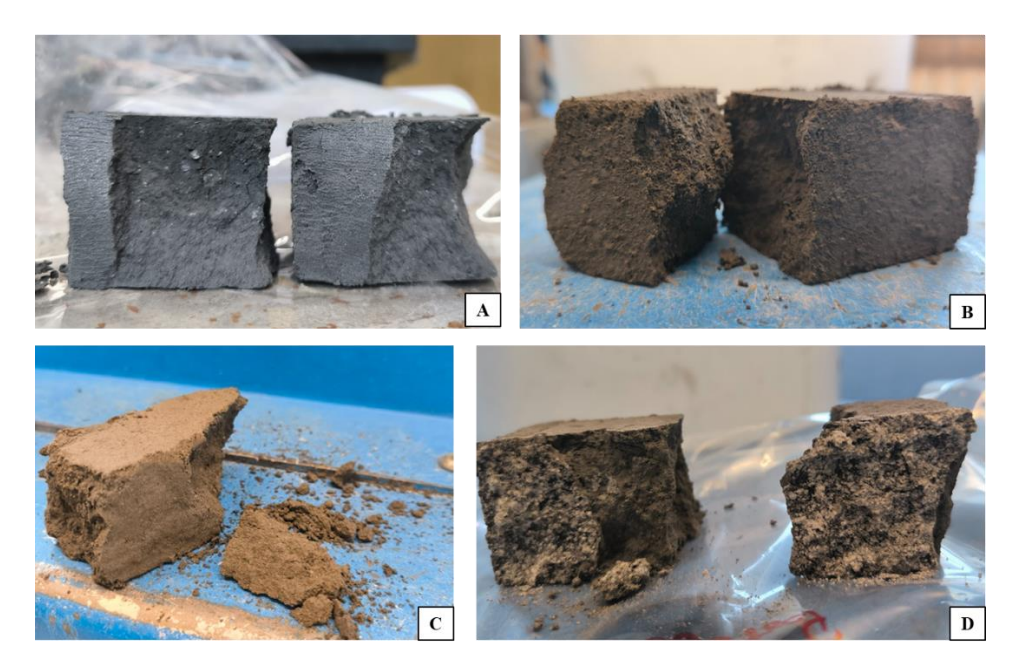


Figure 6.18: Pictures of (A) reference sample post-compression test, (B) FA1_C2 after compression test, (C) FA1-B_C2 after demoulding, (D) FA1-B_C3 after compression strength test.

6.3.2 Slake test

Slake test was performed on a cube of all materials and pictures of the slaking material are taken after 1 day, 3 days and 1 week. As can be seen from Figure 6.19, the water of all materials was limpid on the day they were immersed (day-0) and not much sediment was deposited. It is to note that the specimens used were the specimens after the compression strength test. Thus, the surface of the blocks crumbled, ending up at the bottom of the beakers. As soon as water was added, small air bubbles formed from the surface of the samples, indicating that water immediately penetrated the porous material. After one day, some extra material deposited at the bottom of all beakers. At this stage, the reference sample, FA1_C2, and FA1-B_C3 were still holding their structure, and not much more material deposited. On the contrary, FA1-B_C2 was already completely scattered in the water, and a large amount of paste deposited at the bottom.

After 3 days immersed in water, all carbonized samples had adsorbed enough water to be partially exposed to air, so additional water was slowly poured into all beakers. After the addition of water, FA1_C2 also started disintegrating and behaved like FA1-B_C2 after one day. Part of the immobilized block broke apart, and more material settled at the bottom of the beaker. The reference sample and FA1-B_C3 were also rinsed with water, but not as much as the other samples, and they maintained their structure. After 7 days, only the reference sample remained intact. FA1_C2 continued slaking, as could be seen from the increased deposition of material. The remaining material of FA1-B_C3 also sank to the bottom of the beaker, behaving like clay. FA1-B_C3, fully rinsed with water, started slowly slaking, and more material deposited at the bottom of the glass. The reference sample remained intact even after being fully immersed in water for seven days.

A score from 1 to 4 was assigned in Figure 6.19 to the materials, indicating the resistance to slaking. The reference sample resulted in the more stable material, followed by FA1-B_C3, FA1_C2 and FA1-B_C2, being the less stable in water.

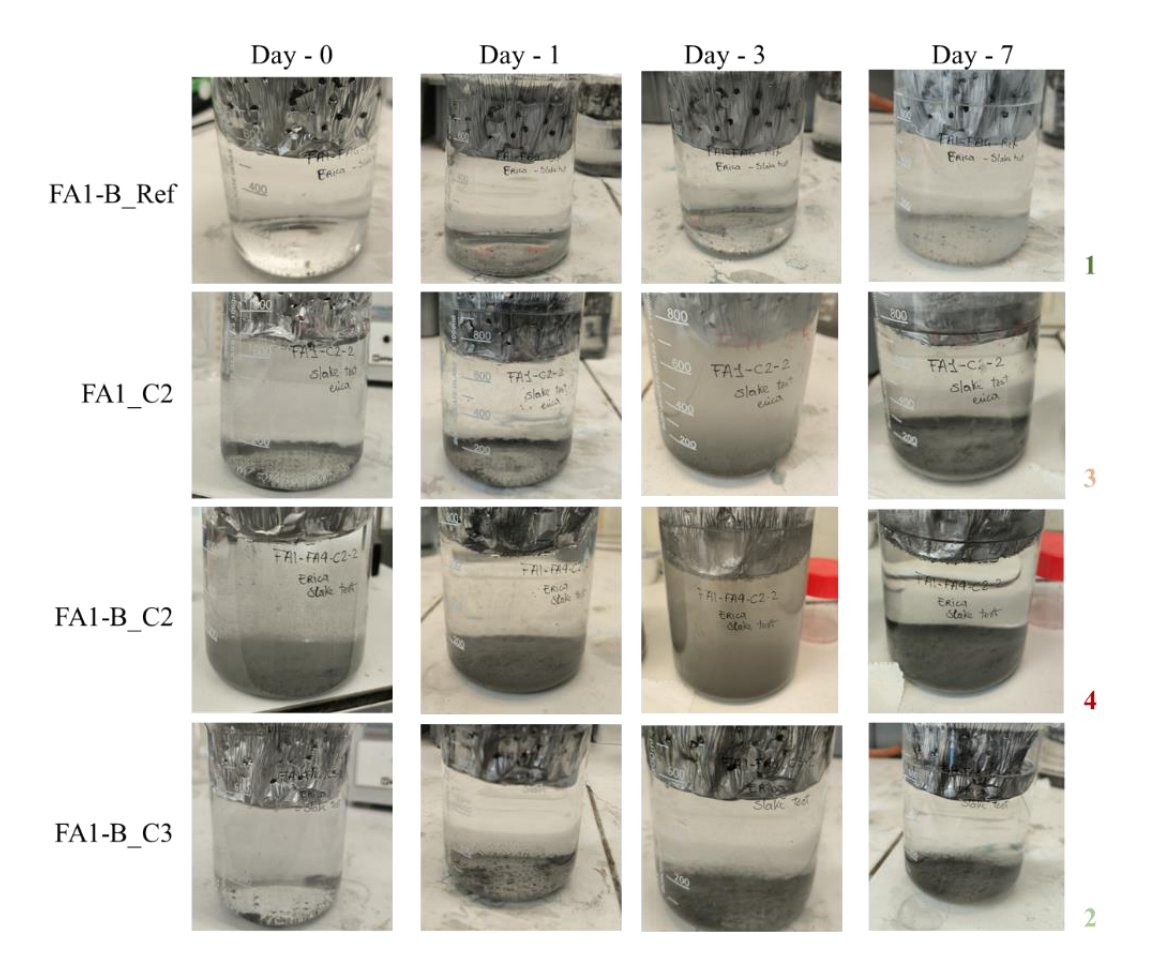


Figure 6.19: Slake behaviour of reference paste and immobilized materials at day-0, day-1, day-3 and day-7. Each material was scored to a number from 1 to 4, where 1 is the material that resulted in less slaking and 4 is the material with the least stable specimen in water.

7. Leachability of heavy metals

The moisture content of each specimen was determined to estimate the appropriate leaching materials, including the wet mass of the sample and the amount of liquid used for the test. After a one-day shaking test, the materials were separated as described in the chapter of Materials and Methods. The extracted filtrate was immediately tested for electrical conductivity, pH, and temperature. Whereas later characterization tests were conducted to analyse its cation and anion content and to determine the amount of leached heavy metals.

7.1 Leaching material

At the end of the curing process, all specimens exhibited a stable structure. Even if some parts crumbled, the overall grain size of the materials exceeded the 10 mm required for the test. Therefore, all pastes were hammered

to crush the material until 95% of the specimen reached the desired grain size. After removing the samples from the curing chamber, the specimen FA1-B_C2 was weak and crumbled during handling, as previously shown in Figure 6.18C. However, to ensure that all materials were treated equally, this specimen was also hammered to ensure all material passed through the sieve. Despite the humidity at the touch of FA1-B_C2, hammering allowed the material to crush and separate without needing to dry it at 40°C.

7.1.1 Moisture content samples

A portion of each immobilized material was dried at 105°C, and the weight variation was recorded to determine the dry matter content (DM) and moisture content (MC), as shown in Table 7.1. The DM and MC are inversely proportional; as one increases, the other decreases. FA1-B_C3 shows the lowest MC of 10.64% and the highest DM proportion of 90.38%, followed by the reference paste with 16.76% MC and 85.64% DM. Unlike the external wetness and stability of the material, FA1-B_C2 resulted the second to the most wet material with 81.0% DM and 23.44% MC, whereas FA_C2 resulted in the lowest DM of 77% and highest MC of 29.86%.

Table 7.1: Results of dry content matter and moisture content on the different mix designs of FA1.

	Dry Matter	Moisture Content	
FA1-B_Ref	85.64%	16.76%	
FA1_C2	77.00%	29.86%	
FA1-B_C2	81.01%	23.44%	
FA1-B_C3	90.38%	10.64%	

7.1.2 Amount of leachate

Based on the MC of each material, the equivalent wet mass targeted (m_w -target) is shown in Table 7.2. Three different batches (a, b, c) were prepared for each material in the range of the targeted wet mass. Based on the effective dry mass m_d , the amount of demi-water necessary for leaching was determined following the procedure in the Methodology.

Table 7.2: Target m_w for each material for leaching test, real m_w for each leaching test, equivalent m_d and leachate (L) for each bottle.

		m _w -target [g]	m _w [g]	m _d [g]	L [ml]
FA1_FA4_Ref_2		105.1±5.8			
	a		105.3	90.2	902
	b		105.1	90.0	900
	c		105.0	89.9	899
FA1_C2_2		116.9±6.5			
	a		116.9	90.0	900
	b		114.9	88.5	885
	c		114.7	88.3	883
FA1_FA4_C2_2		111.1±6.2			
	a		110.7	89.7	897
	b		111.4	90.2	902
	c		110.9	89.8	898
FA1_FA4_C3_2		99.6±5.5			
	a		99.6	90.0	900
	b		98.7	89.2	892
	c		95.8	86.6	866

Each batch was placed inside a 1-litre glass bottle, and the corresponding amount of leachate was poured inside. Pictures of the bottles before the shaking leaching test are presented in Figure 7.1. Similarly to the results from the slake test, the reference test and FA1-B_C3 remained compact as pebbles at the bottom of the bottle, whereas suspended solids increased the turbidity of the leachate in the pre-carbonated samples. After water was added to the bottles, bubbles began to form and slowly released, indicating the initiation of a chemical reaction or the infiltration of water into the empty voids of the material. After a few seconds, the bubbling decreased; excessive gas release could have potentially caused the bottle to explode during the 24-hour test. Therefore, after a few hours, one bottle was checked to ensure that the material was not pressurized. Only a small amount of additional gas was produced once the bottle was opened, allowing the experiment to resume.

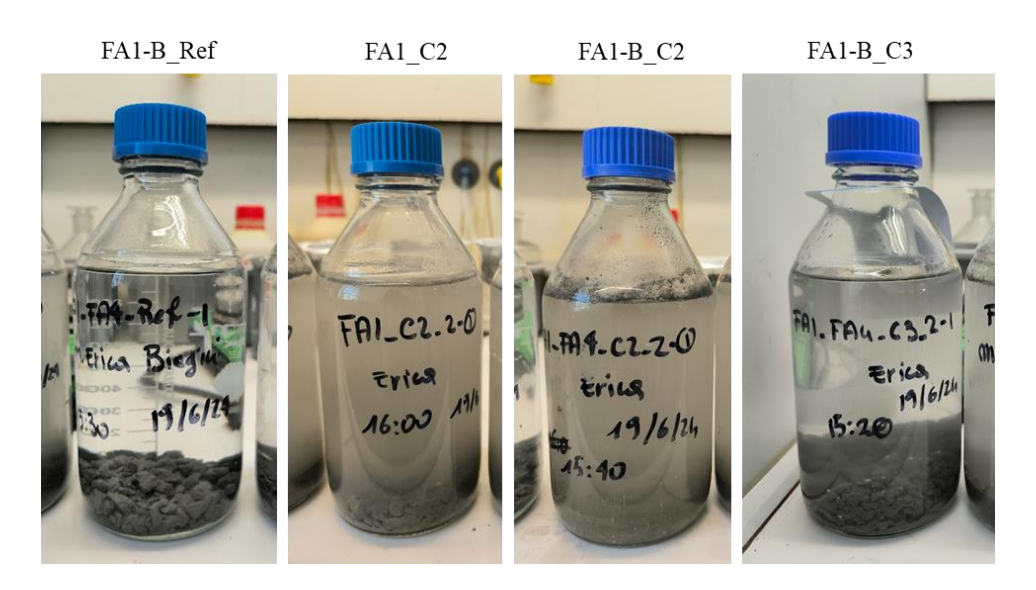


Figure 7.1: Leaching bottles before shake test. From left to right, reference sample, FA1_C2, FA1-B_C2 and FA1-B_C3.

7.2 Leaching procedure and extraction of leachate

At the end of one day of mixing in the end-over-end tumbler, all material was homogeneously mixed with the water, as shown in Figure 7.2. The sieved aggregate was fully crushed and only few agglomerations of immobilized material remained at the bottom of the bottles after the shaking test.

The sediment settled for 15 minutes before the extraction of the leachate began. The bottles were opened under the fume hood, releasing a small amount of gas with a faint scent of sulphur. The separation of the liquid took approximately half an hour for the reference material and FA1-B_C3, as most of the solids settled at the bottom of the bottle. Large amounts of suspended materials remained in FA1_C2 and FA1-B_C2 after 15 minutes, making the separation of the liquid from the solids much slower. Almost 10 ml of water was retained in the filter cakes of these pre-carbonated materials. The separation process for these two sample batches took one hour, and four different filter papers were used for each bottle to efficiently separate all the leachate.



Figure 7.2: Leaching bottles in the end-over-end tumbler after one day of shaking.

7.3 Analysis on the Leachate

7.3.1 Electrical conductivity, pH and temperature

The percolated water was immediately tested after separation from the solid suspended materials. The temperature of the liquids was the same as the ambient temperature: 18°C, 20°C, and 19°C, corresponding to the different temperatures on the five days of testing.

The results of the electrical conductivity and the pH of the percolated liquid are shown in Figure 7.3. The electrical conductivity of the pure FA1 and the reference paste was plotted together with the results of the carbonized materials. It is to notice that the device used to measure the electrical conductivity was old, and the maximum value detectable was 20 mS/m. The electrical conductivity of the percolate from the pure FA1 resulted in electrical conductivity higher than 20 mS/m, suggesting that many ions were freely dissolved in the water. The reference paste FA1-B_Ref had 9.75 mS/m of electrical conductivity, much lower compared to the pure fly ash. The conductivity of the pre-carbonated fly ash FA1_C2 was 10.26 mS/m, slightly higher than the reference sample, whereas in the pre-carbonated mixture and the sample carbonated while curing, the final conductivity decreased. The conductivity of the percolate from FA1-B_C2 resulted in the lowest value, being 8.61 mS/m, and for FA1-B_C3, it was 9.53 mS/m. The electrical conductivity was dependent on the ions, thus not only on the heavy metals but also on the salts dissolved in water. The analysis alone did not give indications of the effective heavy metals' leachability.

The pH of the liquids was also analysed while stirring the solutions. The pH of the pure FA1 was 11.41, highly basic but slightly more acidic than the reference sample. The production of portlandite and alkali during the hardening of the FA-binder paste resulted in a final material with a pH of 12.26. All carbonized materials resulted in a pH reduction in the final leachate, as shown in Figure 7.3. The pH of the percolates of FA1_C2, FA1-B_C2, and FA1-B_C3 decreased to 11.40, 10.71, and 10.01, respectively. At high pH, the solubility of heavy metals in water could increase or decrease, as reported in the Literature Review. Following previous research (Gasser et al., 2021; De Repentigny et al., 2018), the leachability of lead, zinc, nickel, and copper was expected to decrease to 10 and 100 mg/l or less when the pH decreased from 12 to 10. On the contrary, the solubility of silver, cadmium, and manganese was expected to increase at similar values.

It is to note that the error bars from the analyses were due to the reaction of the fluids with air. The longer the materials were exposed to the atmosphere, the more reactions occurred, causing variations in the pH and electrical conductivity of the liquids. In particular, the electrical conductivity fluctuated up to 2 mS/m after 20 seconds. The numbers reported for the conductivity were recorded after the first few seconds once the probe was immersed in the solution.

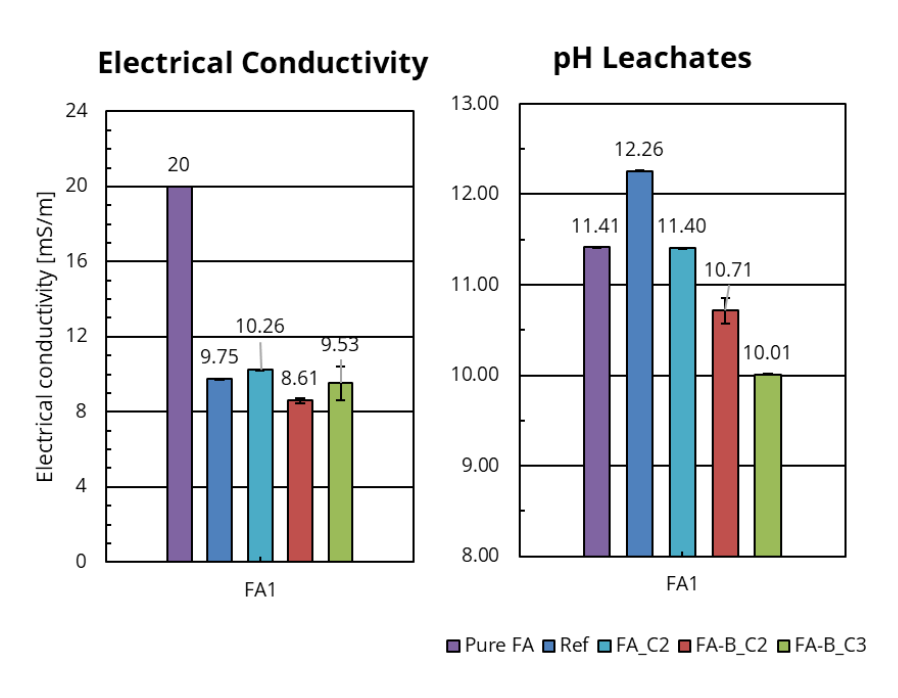


Figure 7.3: (Left) Results of electrical conductivity and pH measurements of the leachates. From left to right of each graph are displayed the values of pure FA1, the reference paste, FA1 C2, FA1-B C2 and FA1-B C3.

7.3.2 Heavy metals content and leaching species

The results from the analysis of the cationic composition of the samples are presented in Figure 7.4 below and in Table B.0.5 of the Appendix. The leachability of copper, lead, and zinc decreased for all the carbonized materials compared to the reference sample, as anticipated from the pH results. The leachability of lead in the reference sample was 44 mg/kg DM, much higher than that of the pure fly ash at 0.32 mg/kg DM, which was more similar to the leachability of the pre-carbonized fly ash FA1_C2 at 0.20 mg/kg DM. As previously explained, the leachability of all heavy metals highly depended on the pH of the environment. The pH of the leachates from the two experiments was almost the same, suggesting similar leachability of lead but not of the other elements. The leachability of barium decreased compared to the reference sample and pure fly ash only for FA1-B_C3, whereas the leachability of chromium and molybdenum increased. The concentrations of cadmium, antimony, selenium, and vanadium showed a slight increase compared to the reference sample, but they were all close to the minimum detectable levels and were present in much lower concentrations compared to the other elements. The concentrations of arsenic, nickel, and cobalt were lower than the detectable limit, thus not represented in the graph.

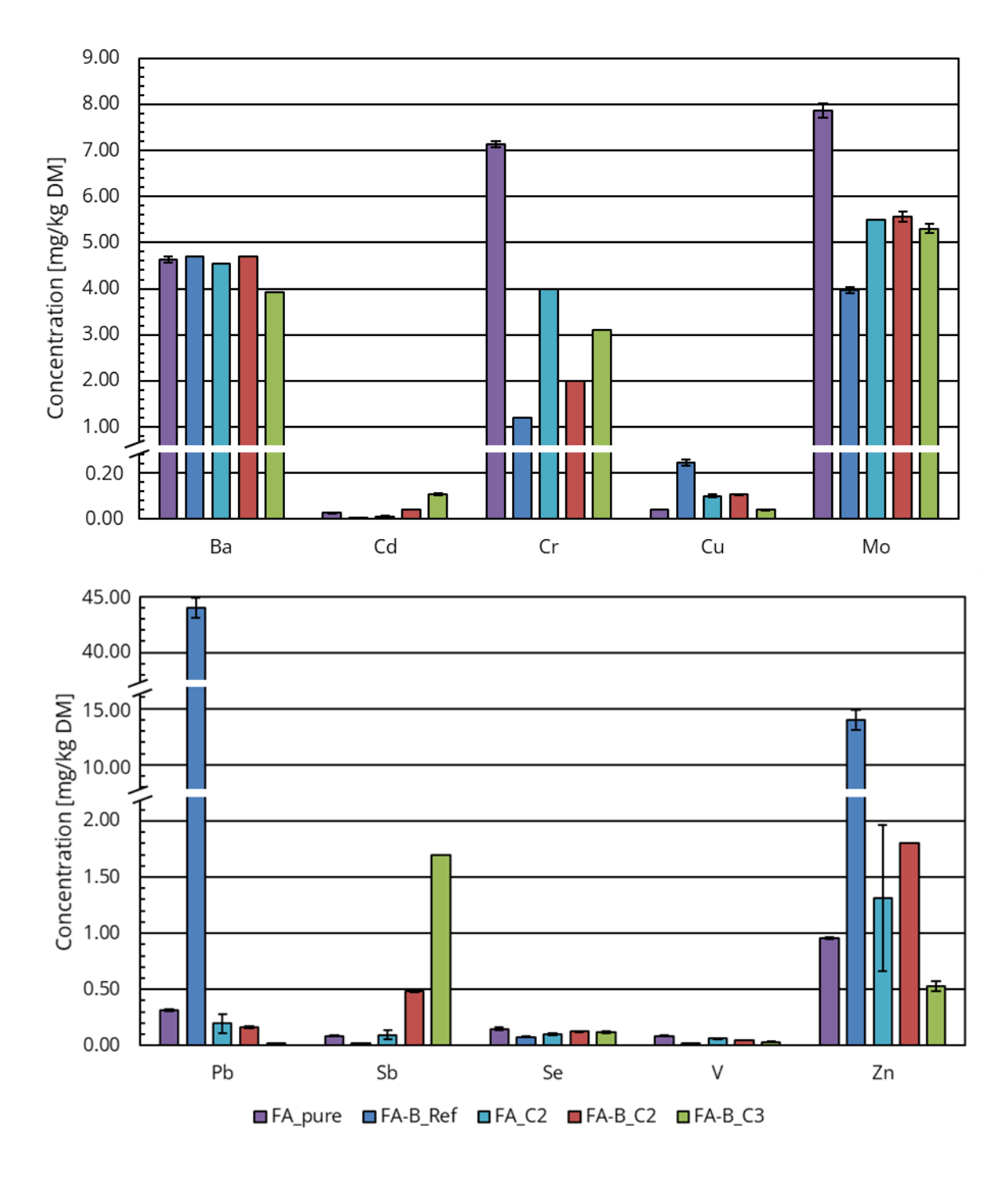


Figure 7.4: Leaching test results of the pure FA1, the reference sample and the carbonized samples. In the top graph are displayed, from left to right, the concentrations of bromide, cadmium, chromium, copper, and molybdenum. In the bottom graph are shown the concentrations in mg/kg of dry matter (DM) of lead, antimony, selenium, vanadium and zinc.

The anionic ions detected in the materials are shown in Figure 7.5. In all materials the solubility of the anionic species was reduced compared to the raw fly ash, but they all leach more compared to the reference sample. The

concentrations of the leached anionic compounds were two to three order of magnitude higher than the cations but none of them was a heavy metal.

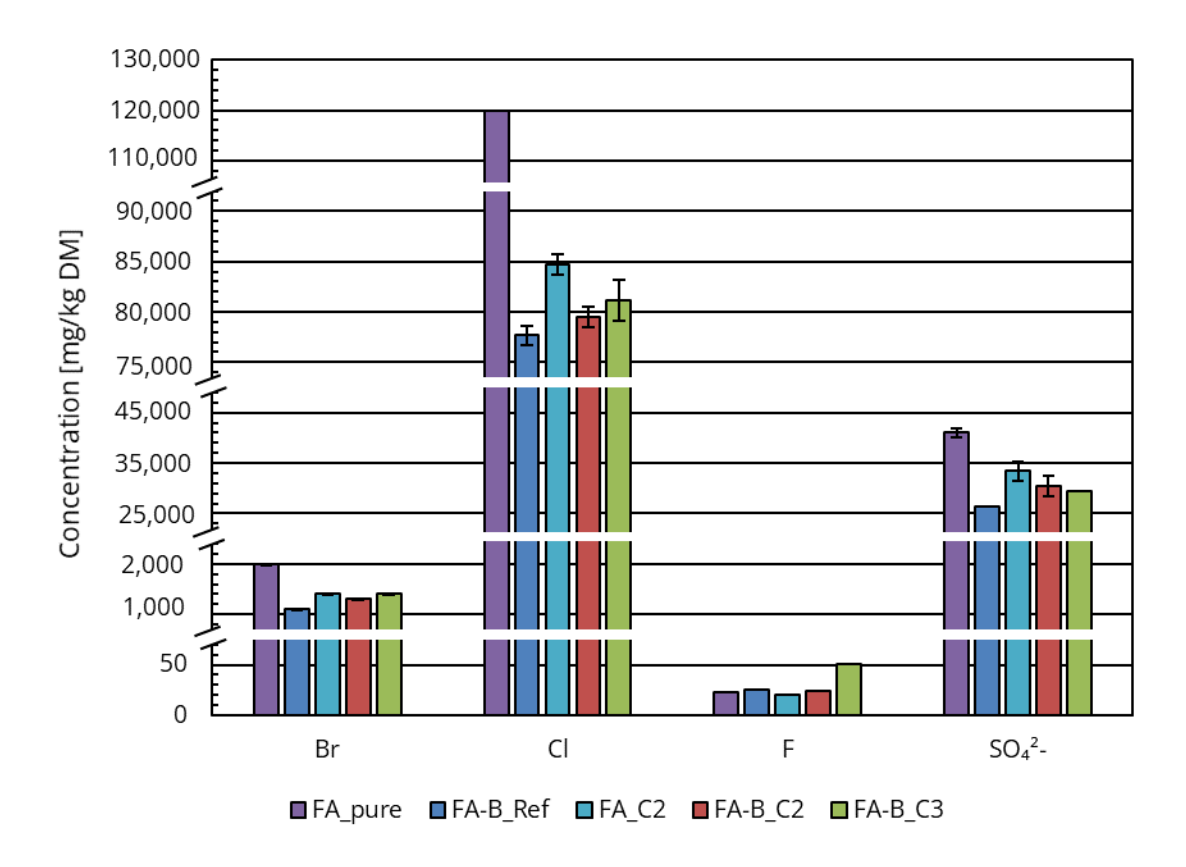


Figure 7.5: Leaching test results anionic compounds present in the pure FA1, the reference sample and the carbonized samples. From left to right are shown the concentrations in mg/kg DM of bromide, chloride, fluoride and sulphate.

The immobilization factors of each fly ashes are shown in Table 7.3, together with the final A. As shown in the table, the only material that performed closest to the reference sample was the pre-carbonated mixture of fly ash and binder FA1-B_C2, whereas FA1_C2 and FA1-B_C3 resulted in the same final score. Even considering the high decrease in the solubility of lead, copper, and zinc observed in FA1-B_C3, the increased leachability of the other ions resulted in a similar behavior compared to the pre-carbonated fly ash FA1_C2.

The final concentrations of the heavy metals were lower than in the reference sample, and most of the ions leached in concentrations lower than the maximum allowed by the Soil Quality Regulation, as shown previously in Table 3.2 (Ministerie van Infrastructuur en Waterstaat, 2022). The concentrations of arsenic, barium, cobalt, copper, nickel, selenium, tin, and vanadium were all below the limit for both the reference sample and all the other materials. Lead and zinc in the reference sample leached more than the limits of 42 mg/kg DM and 9.5 mg/kg DM, respectively, but all carbonized materials resulted in leaching concentrations more than 2 mg/kg DM below the limit. Chromium and molybdenum were the only heavy metals exceeding the concentrations in the regulation for all samples. In contrast, all other ions that were not heavy metals were present in concentrations far above the regulation. Fluoride concentrations were within the limit only for FA1_C2, but for all the other samples, they exceeded the limit by up to 30 mg/kg DM. Bromide, fluoride, chloride, and sulphates leached in concentrations more than 1000 mg/kg DM above the limits. The leaching of bromide and sulphates increased after carbonation.

Table 7.3: Immobilization I_i factor for every ion in all immobilized materials and the pure FA1, along with the final score A of the immobilization methods.

	Ba	Cd	Cr	Cu	Pb	Mo	Sb	Se	V	Zn	A
Pure FA1	6.7E-2	2.1E-5	5.6E-3	3.2E-5	2.5E-4	6.2E-3	6.8E-5	1.2E-4	6.9E-5	7.6E-4	0.31
FA1_C2	6.8E-2	9.0E-6	3.2E-3	7.9E-5	1.6E-4	4.4E-3	7.7E-5	8.1E-5	5.0E-5	1.0E-3	0.23
FA1-B_C2	6.6E-2	3.2E-5	1.6E-3	8.4E-5	1.3E-4	4.4E-3	3.8E-4	1.0E-4	4.0E-5	1.4E-3	0.22
FA1-B_C3	6.8E-2	8.4E-5	2.5E-3	3.2E-5	1.6E-5	4.2E-3	1.3E-3	9.5E-5	2.6E-5	4.2E-4	0.22

7.4 Discussion

The carbonation led to a higher immobilization efficiency of the overall MSWI fly ash. All materials undergoing the immobilization processes performed better than the reference sample. It was important to note that the carbonation did not decrease the leachability of all heavy metals: while the solubility decreased for highly environmentally damaging metals such as lead, other ions became more soluble. By comparing the results with the Dutch Soil Quality Regulation, there were only a few heavy metals that were not sufficiently immobilized in either the reference sample or the carbonized material. However, their magnitude was not much higher compared to the reference, suggesting that through a further column leaching test, their solubility would also be similar to the reference.

Even though solubility was linked to the pH of the solution, it also depended on the speciation of the material. As reported by other research (Larson et al., 2007), the solubility behaviour of lead sulphates was different compared to lead hydroxides, carbonates, and phosphates. To properly predict the behaviour of heavy metals' leachability based on the pH of the leaching solution, it was necessary to determine the species that formed bound to the heavy metals.

Finally, the variability of the waste heap was also an important factor. Even though the waste heap was constantly mixed and homogenized, small variations in the chemical composition might have resulted in significantly different results. For example, to verify that lead was effectively immobilized through carbonation, further investigations were necessary on materials with a fixed amount of lead. The high decrease in solubility of lead through carbonation had the potential to open the doors for mineral carbonation for lead-rich waste streams.

The ideal immobilization process for the MSWI FA1 was the pre-carbonation of the FA-binder mixture FA1-B_C2, which ensured that a severe reduction in pH did not significantly increase the solubility of other heavy metals. The A factor was the same for the material carbonated while curing FA1-B_C3 and slightly higher in the pre-carbonated fly ash FA1_C2. However, the leaching values for heavy metals were within the limits of the Soil Quality Regulation only in FA1_C2. The other immobilization processes slightly exceeded the limit, with FA1-B_C3 exceeding it more than the others, which was why FA1-B_C2 was the process that overall performed the best.

These results and evaluations were only an initial estimation; a column leaching test was necessary to determine whether the physical stability achieved with FA1-B_C3 also resulted in higher immobilization. The shake leaching test simulated only the worst-case scenario but did not represent the real conditions at which the material was stored in landfills.

8. Extra experiments

For a better comprehension and comparison of the immobilization process, the same mix designs used for FA1 were prepared by replacing the hazardous material with FA2. As previously shown in the Material Characterization results, FA2 was the material with the highest carbonation mineralization potential given the high lime content. The same carbonation conditions were used for the material, as well as the same FA/binder ration of 100:30 and FA/water ratio of 100:43.3. Even if the S/L ratio might not result optimal for this mix design, it was still chosen for comparability with the previous material.

This chapter presents the results from the TGA and the physical strength tests on the immobilized pastes. After curing, all materials are also subjected to the same leaching test as for FA1, and the results are presented at the end of the chapter.

8.1 Mixture designs

8.1.1 Pre-carbonated FA (FA2_C2)

The results from the TGA on the pre-carbonated FA2 are plotted in the DTG graph in Figure 8.1. A clear peak at 400°C in the reference sample slowly disappears in the pre-carbonated fly ash before and after curing, whereas the peak at 700 °C shifts to 750°C and increases its magnitude. The peak at 400°C is characteristic for portlandite (POR) which reacts during carbonation to form more calcite, resulting in the larger peak at the higher temperature.

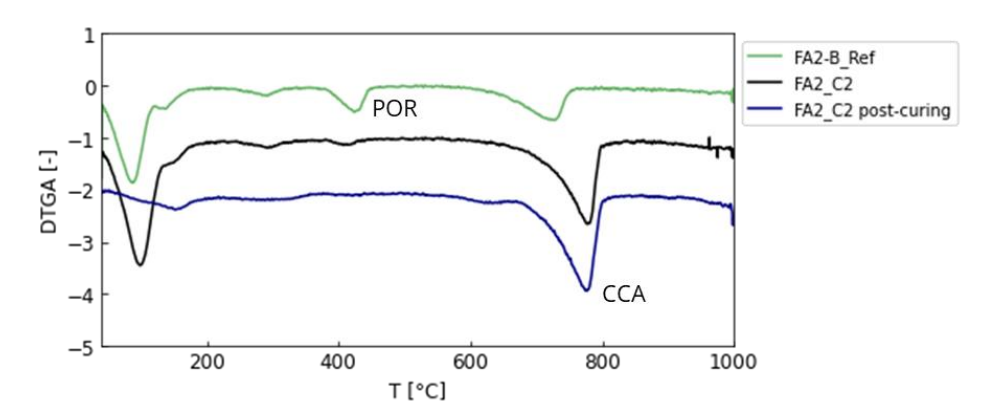


Figure 8.1: DTG profiles of the reference sample FA2-B_Ref, the pre-carbonated FA2_C2 and the pre-carbonated FA2 after 28 days of curing.

The effective mineral carbonation, also shown in Table 8.1, is of 7.1% after one day and continued increasing until reaching 9.8% after 28 days of curing. It is to note that the carbonation was determined in respect to the reference mixture of FA2 and binder, and it differed of less than 2% compared to the carbon uptake potential determined previously in the Carbon-uptake section.

Table 8.1: Effective mineral carbonation of the FA2_C2 before and after curing.

	FA2_C3 pre-curing	FA2_C3 post-curing
Carbon-uptake	7.10%	9.83%

8.1.2 Carbonated mixture (FA2-B_C2)

When FA2 was pre-mixed with the binder and some water, all portlandite present was fully consumed after one day in the carbonation chamber, as shown by the absence of the portlandite peak in the FA2-B_C2 curve in Figure 8.2. The calcite peak increases after one of carbonation but not much changed after 28 days of curing in the DTG curves.

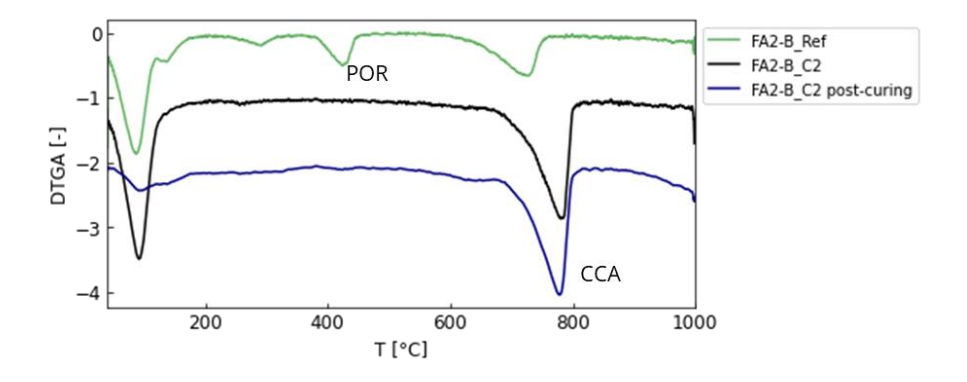


Figure 8.2: DTG curves of FA2-B_Ref, FA2-B_C2 and FA2-B_C2 after curing.

As no more portlandite was available in the system, after 28 day most of the available calcium had already reacted with carbon dioxide, as explained by the effective carbon-uptake in Table 8.2. After one day 9.8% of the total weight of the sample was newly formed calcite, whereas at the 28th day of curing less than 1% extra calcite formed.

Table 8.2: Effective mineral carbonation of the FA2-B C2 before and after curing.

	FA2-B_C2 pre-curing	FA2-B_C2 post-curing
Carbon-uptake	9.78%	10.71%

8.1.3 Carbonation after casting (FA2-B_C3)

The non-carbonized FA2-B_Ref sample turned of a bright pink colour after the phenolphthalein test, whereas FA2-B_C3 showed a clear separation in colour between the top and bottom part, as can be seen in Figure 8.3 A and B. Differently from the corresponding samples of FA1, this material was much less porous and it was possible that the gas did not penetrate homogeneously all sample, resulting in a net separation at 2.6 cm from the exposed surface. The bottom of the sample remained inside the mould for all 28 days as the previous case, preventing carbon dioxide to get in contact with the material. To avoid taking only the fully carbonized or non-carbonized part of the sample, a cross section of the material was grinded and used for the TGA further tests.

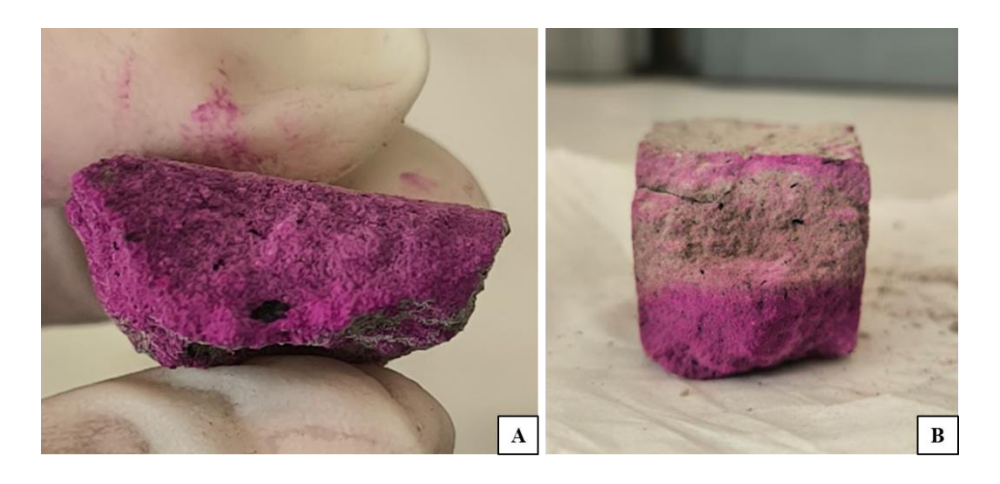


Figure 8.3: (A) Reference sample and (B) carbonized sample rinsed with phenolphthalein.

The DTG profile of FA2-B_C3 is almost the same as the reference sample, as the material was only carbonized by atmospheric conditions. However, as shown in Figure 8.4, after 28 days of curing in the carbonation chamber the profile DTG curve show the same pattern as the previous cases. The final effective carbon-uptake after 28 days is shown in Table 8.3 was of 10.8%.

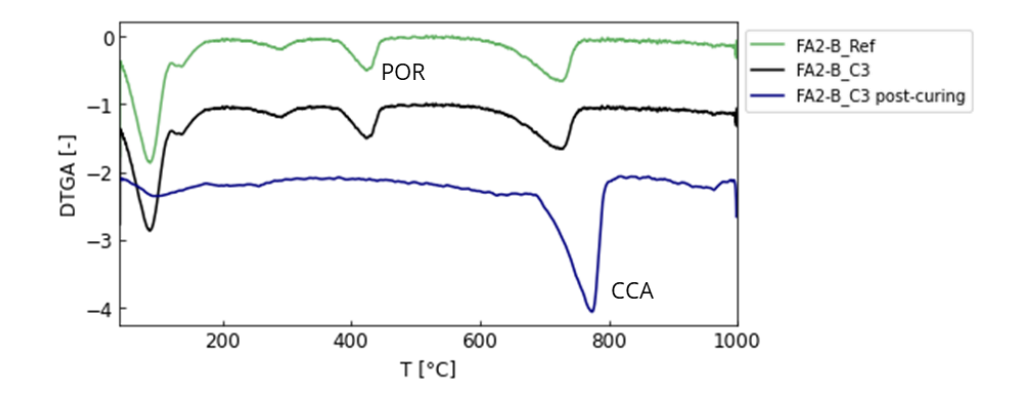


Figure 8.4: DTG curves of the reference sample, of FA2-B_C3 before and after curing in the carbonation chamber.

The effective carbon uptake of the three immobilized processes resulted in the highest for FA2-B_C3 but it also shows a difference of less than 1%, suggesting that all materials were equally carbonized.

Table 8.3:Effective mineral carbonation of the FA2-B_C3 before and after curing.

	FA2-B_C3 pre-curing	FA2-B_C3 post-curing
Carbon-uptake	0%	10.78%

8.2 Physical strength

After 28 days of casting, all specimens looked properly hardened and homogeneously distributed. As can be seen from Figure 8.5, there were almost no difference in between the reference samples and the carbonated FA2_C2 and FA2-B_C2. FA2-B_C3 showed a slightly lighter colour compared to the other samples, but the surface exposed to carbonation remained relatively smooth and of the same colour as the rest of the sample, differently from the equivalent FA1-B_C3.

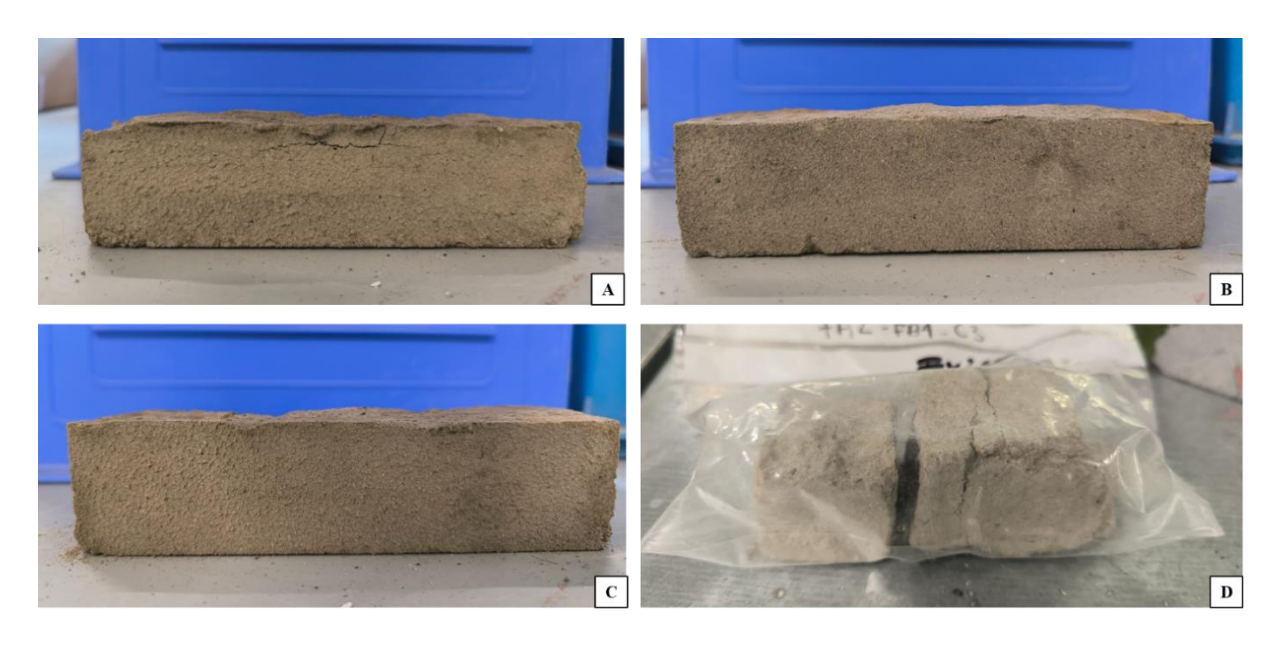


Figure 8.5: Pictures of (A) reference sample, (B) FA2_C2, (C) FA2-B_C2 and (D) FA1-B_C3 after demoulding.

The results of the compression strength test of the mix-designs with FA2 are shown in Figure 8.6. The pre-carbonated FA and the pre-carbonated binder resulted in much lower compressive strength compared to the reference sample, from 1.9 MPa to 0.65 MPa and 0.30 MPa. Carbonation of the casted paste during curing showed in increase in strength to 2.10 MPa.

Both the reference sample and FA2-B_C3 demonstrated compression strengths well above the 1 MPa threshold stipulated by the Dutch government regulations. Whereas the other two samples with pre-carbonated materials did not comply with the required strength criteria.

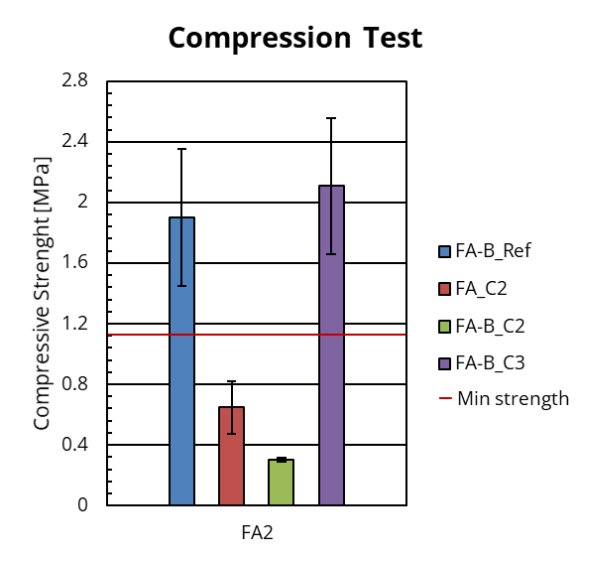


Figure 8.6: Compression test results of FA2. From left to right are represented the maximum strength of the reference sample, FA2_C2, FA2-B_C2 and FA2-B_C3.

8.3 Leachability of heavy metals

The immobilized materials were tested for DM and MC, in the same way as for FA1. The results are represented in Table 8.4. The MC was the lowest in FA2-B_C3, followed by FA2-B_C2 and FA2_C2, with the reference sample having the highest water content. The moisture contents were of respectively 10.64%, 16.76%, 23.44% and 29.86%.

The amount of equivalent wet mass and leachate were determined for each sub-sample based on their MC, and the materials were prepared following the same procedure as for FA1. The immobilized materials after 28 days of curing had a strong and stable structure, necessitating the use of a hammer on all samples to meet the maximum particle size requirements specified by the leaching standard.

Table 8.4: Results of dry content matter and moisture content on the different mix designs of FA2.

	Dry Matter	Moisture Content
FA2-B_Ref	75.41%	32.61%
FA2_C2_2	81.09%	23.32%
FA2-B_C2_2	83.58%	19.65%
FA2-B_C3_2	90.65%	10.32%

At the end of the 24 hours of the shaking test, the solids were separated from the liquid, and the percolate was analyzed for its electrical conductivity, pH, temperature, and anion and cation content. As shown in Figure 8.7, the electrical conductivity of the reference sample was much higher than all the carbonized materials. The electrical conductivity of the reference, which was 13.16 mS/m, decreased to 9.55 mS/m in FA2_C2 and 7.17 mS/m in FA2_B_C2. Of the carbonized materials, FA2-B_C3 had the highest electrical conductivity at 10.67 mS/m. The final pH of the percolate slightly decreased for all materials, going from 12.77 for the reference to 12.74, 12.44, and 11.92 respectively for FA2_C2, FA2-B_C2, and FA2-B_C3. This decrease was minimal compared to the mix designs of FA1. The temperature of the liquids recorded the same as the laboratory room temperature of 20°C and 19°C.

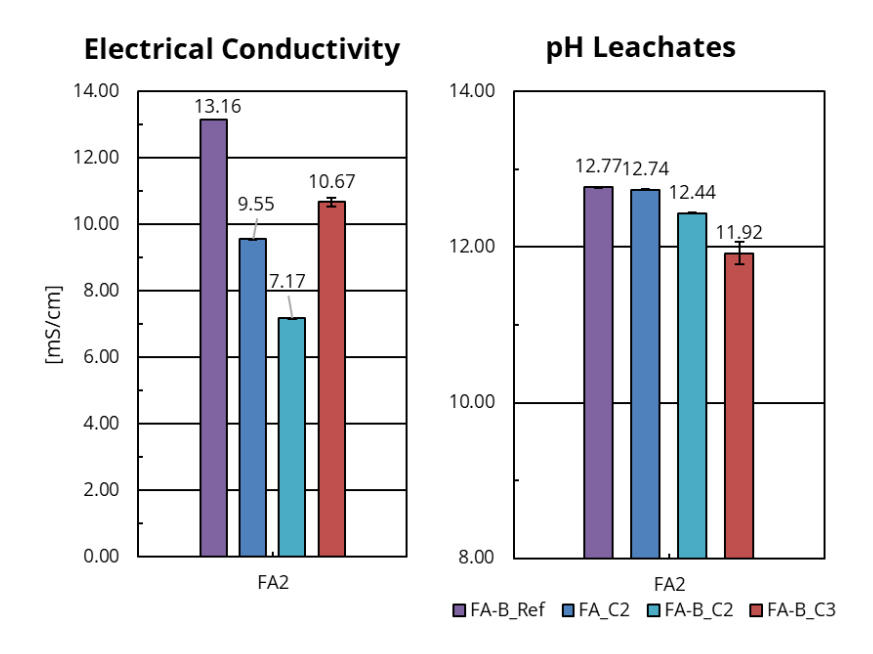


Figure 8.7: (Left) Results of electrical conductivity and pH measurements of the leachates. From left to right of each graph are displayed the values of the reference paste FA2-B_Ref, FA2_C2, FA2-B_C2 and FA2-B_C3.

The cationic composition of each immobilized mixture is shown in Figure 8.8 below. In this case, barium, lead, and zinc were in much lower concentrations in the leachate compared to the reference sample, but the leachability of chromium increased by more than 5 mg/kg DM in FA2-B_C3, and by a few milligrams in vanadium. The concentrations of molybdenum and selenium were similar for all samples, whereas the concentrations of cadmium, copper, and tin were almost at the minimum detectable.

The concentrations of the anions can be found in Table B.0.10. Similarly to FA1, the anions were present in much larger concentrations, exceeding 1000 mg/kg DM for chloride and sulfate, around 55 mg/kg DM for bromide, and 5 mg/kg DM for fluorine. Only fluorine ions were in lower concentrations in the carbonized materials; the rest were present in larger concentrations in all the other immobilized materials compared to the reference sample.

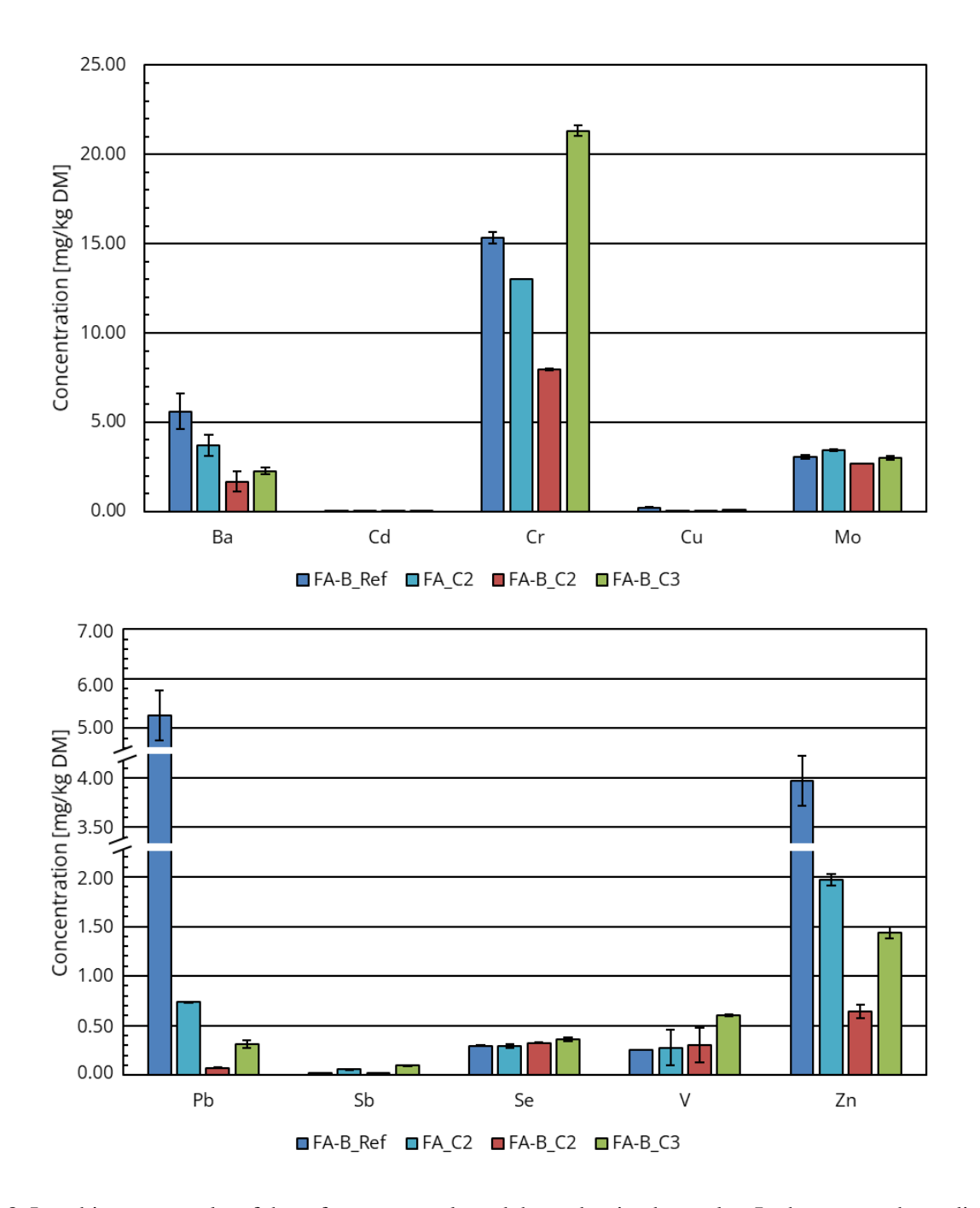


Figure 8.8: Leaching test results of the reference sample and the carbonized samples. In the top graph are displayed, from left to right, the concentrations of bromide, cadmium, chromium, copper, and molybdenum. In the bottom graph are shown the concentrations in mg/kg of dry matter of lead, antimony, selenium, vanadium and zinc.

As shown in Table 8.5, normalizing the increase of each ion, showed that both the pre-carbonation of the mixture FA2-B (FA2-B_C2) and the carbonation during curing (FA2-B_C3) resulted in a better immobilization performance compared to the reference sample. The leachability of lead and zinc was highly decreased through carbonation (Figure 8.8), compensating for the increased leachability of chromium and the other ions present in smaller quantities.

Chromium, molybdenum and selenium were, also for this fly ash, the only heavy metals that exceeded the limit from the past Soil Quality Regulation (Ministerie van Infrastructuur en Waterstaat, 2022). The concentration of lead, exceeding the limit in the reference sample, was significantly decreased from 3 mg/kg DM over the limit to 2 mg/kg DM below. For FA2, the fluoride and bromide concentrations were also below the maximum allowed, leaving only chloride and sulphates concentration as environmental concern.

Table 8.5: Immobilization I_i factor for every ion in all immobilized materials and the pure FA1, along with the final score A of the immobilization methods.

	Ba	Cd	Cr	Cu	Pb	Mo	Sb	Se	V	Zn	A
FA2_C2	1.1E-1	5.8E-5	3.8E-1	1.0E-1	2.2E-2	1.0E-1	5.8E-4	8.7E-3	5.8E-4	1.2E-1	1.1
FA2-B_C2	4.9E-2	5.8E-5	2.3E-1	7.9E-2	2.1E-3	7.9E-2	1.8E-3	8.6E-3	5.8E-4	5.7E-2	0.8
FA2-B_C3	6.6E-2	8.8E-5	6.2E-1	8.8E-2	9.2E-3	8.8E-2	5.8E-4	9.4E-3	8.8E-3	1.9E-2	0.5

8.4 Discussion

The mix designs prepared with BM FA (FA) resulted in much stronger and more stable structures compared to those made with FA1. The higher availability of free lime in FA2 increased both carbonation and hydration, contributing to the increased strength of the material. However, even though the overall strength was higher than that of MSWI FA, only the reference sample and the material carbonated during curing complied with the minimum strength imposed by Dutch regulation (Beschikking 2003/33/EG). The final strength of the reference sample and FA2-B_C3 outperformed the equivalent mixtures with FA1 by 1 MPa each.

From the analyses of the separated leaching solution, the electrical conductivity of the leachate from BM FA was similar to the conductivity of the mix designs prepared with FA1. Despite FA2 having a lower salt content than FA1, the electrical conductivity values were similar. Additionally, considering the higher carbonation capacity of FA2, the final pH of the leachate resulted in being higher than the pH from FA1. The high amount of alkali did not result in an effective decrease in the pH of the material, despite the higher mineral carbonation. As the leachability of heavy metals was highly influenced by the pH, the high pH values of the final immobilized material posed a risk to the effective immobilization of hazardous components.

The original concentrations of hazardous components in FA2 were much lower than in FA1, resulting in most of the components present in the material being within the maximum leachability allowed by the Soil Quality Regulation (Ministerie van Infrastructuur en Waterstaat, 2022). However, the similar positive decrease in lead leachability observed in FA1 after carbonation occurred also in FA2, as well as the persistence of chromium, molybdenum, and selenium in higher concentrations in the leachate. The immobilization process that performed the best was carbonation during curing (FA2-B_C3), followed by pre-carbonation of the mixture of fly ash and binder, differing from what was observed in FA1. Overall, carbonation effectively immobilized more heavy metals compared to the reference sample, suggesting that a higher carbonation potential of the fly ash also led to more efficient immobilization.

III. Closure

9. Discussion

The chemical composition of the material served as an important starting point for the research. Although, the general composition of the fly ashes was identified and already known from previous researchers, it was important to characterize fly ashes from the same source. The MSWI fly ashes resulted with the highest heavy metals contaminations, while the BM fly ashes contain the highest amounts of free lime and other compounds with high reactivity to carbon dioxide. Differently from other researcher's directions, carbonizing all fly ashes under optimal wet conditions helped in identifying the actual behaviour of each fly ash. Surprisingly, the amorphous phase and other oxides present in the MSWI-FA ended up carbonizing in materials where carbonation is not expected. This discovery ended up being a crucial step for the research as it opened the door to the potential of carbonising materials that have been previously discarded for their low free lime content. The evolution of the crystalline phases is also underlined in this study.

Materials with high salts and sulphites in the amorphous content crystallize large amounts of anhydrite after hydration and carbonation. Differently from what expected, anhydrite does not transform in calcite after the first seven days of carbonation. In contrast, materials with lower sulphites in the amorphous phase and higher free lime show less reduction in amorphous content, with calcium being hydrated and carbonated into calcite and vaterite.

Regarding the carbonation reactions, the preliminary carbonations at high temperature and pressure gave a nice indication on the rate of reaction and effective carbonation based on water content and pressure. The experimental setup makes it challenging to accurately predict the extent of carbonation. The reaction starts already outside the carbonation chamber and while the material is heated up, resulting in an over estimation of the efficiently mineralized CO₂. The experimental equipment at controlled temperature and pressure is efficiently used for estimating the ideal carbonation times under fixed conditions of the bigger carbonation chamber available at the university.

After 28 days of curing, the pre-carbonated mixture of FA and binder results in the highest carbonation. This is attributed to the material's high exposure surface for carbonation. However, during the analysis of the materials through QXRD and TGA, the results do not match. The amount of crystalline calcite is higher than the total mineralized CO₂ that includes amorphous, non-amorphous and other carbonations. Even though the QXRD does not present magnesium carbonates, the results from the TGA are more reliable than the Rietveld refinement. Therefore, the results from the QXRD are used only as a general indication of the phases and their presence, but the effective mineral carbonation if determined through TGA.

The results from the immobilization of the hazardous fly ashes FA1 and FA2 reveal some potential applicability of the materials in real-life scenarios. The structural stability required by the Dutch law is met by the reference sample and by the material carbonated during curing for 28 days. Two main reasons can be the cause of the instability of the other materials. Firstly, the mix design for the pre-carbonated fly ash is not optimal for castability. Secondly, in the pre-carbonated mixture FA-B_C2, the binder already activates during curing, resulting in insufficient reactivity to harden and compact the final material. The physical stability is also strictly related to the stability in water. Of the materials, only the reference sample and the FA-B_C3 resulted in a stable structure after one week in water. The carbonized material still started slaking after one week, thus further investigations at longer times are required.

The physical strength is however, not directly related with the carbonation efficiency, as the highest carbon-mineralization is reached by the pre-carbonated mixture FA-B_C2 with the lowest strength. The pre-carbonated mixture also results in the highest reduction of electrical conductivity of the leachate, suggesting that the liquid contains the lowest amounts of free ions and possible heavy metals. However, the pH is decreased significantly only in the long-carbonated material.

The ideal immobilization process was found to be dependent on the type of original material. As for the MSWI FA with low carbonation potential, the highest immobilization is reached by pre-carbonation of the sample with the highly reactive binder (FA1-B_C2). Differently, for the BM FA the highest immobilization is reached at the prolonged exposure of the material in the carbonation chamber. The mix design FA-B_C3 results however in the most promising immobilization method for further experiment. The sample is the only material that shows both structural strength and effective decrease of pH. While pH does not directly indicate higher immobilization, the physical encapsulation of heavy metals through carbonation cannot be tested through shake test but only with column test. Physically trapping the metals is one of the major factors of carbonation, thus it is important for further research to investigate such behaviour of a material that already immobilize more efficiently lead.

9.1 Limitations

Several limitations arose during this experimental study, dependent both on the experimental setup available, as well as the time restrictions of the research.

Firstly, a full understanding of the chemical reactions in the system is challenging, as only a portion of the material could be identified. The QXRD results indicates there are more than 25 different crystalline phases forming, without considering the undetected heavy metals and over 30% of the amorphous phase in each fly ash. This indicates that more analyses are necessary to better understand the chemical reactions and evolution of the material during carbonation and hydration.

It is also important to validate the experimental results. The carbonation percentages estimated in the study are relative to one experiment each. More experiments are necessary to quantify the carbonation potential of the materials and the relevant statistical information to better predict the behaviour of the waste heaps.

Another aspect that is not optimal is the choice of the internal standard for the QXRD analysis. As all materials present a multitude of peaks, the internal standard overlaps some of the smaller peaks, resulting in a higher error in the final interpretation, as also previously investigated by other researchers (Zhao et al., 2018). The refinement is also limited by the extensive COD database used, where some peaks are not precisely matched. The average GOF generated is of 2.7, relatively high for crystalline materials but low for the high amount of diverse crystalline phases in the wate-fly ashes.

The setup used for the preliminary carbonation experiments is not representative for a future industrial application. The main reasons are that only a maximum 10 g of materials can be added, that the fly ashes are not stirred during the process and that the real temperature of the solid material is unknow. In industrial applications, larger batches must be reacted, sometimes not matching the results of the lab-scale experiment. Additionally, stirring helps the reactivity of the material with the gas, but at the same time it might have the effect of speeding undesired reactions, as well as the temperature of the material.

The S/L ratio is not maintained constant throughout the experiment. During carbonation the ration is maintained constant to the amount of fly ash, but when carbonation is done with adding the binder the effective L/S used lowers. Similarly, during casting the amount of free water in the pre-carbonated pastes is considered and deducted from the casting water as some materials were still humid. However, not all the free water might have been reactive water, causing the material to not be in the same casting conditions as the reference material.

Another important aspect that was not considered in the research is the stability of the material in the surrounding environment. The landfill where the material is safely immobilized is exposed to air and atmospheric changes, causing the material to change properties compared to the freshly formed conditions. The leaching tests recommended previously in this research and based on the Dutch regulations do not mimic this change in the environment. Rainwater itself has a variable pH that depends on the pollution and other environmental factors (Charlson & Rodhe, 1982). Previous research has examined the limitations of standardized leaching methods and proposed further experiments to determine the behaviour of heavy metals under changes in environments (Dijkstra, 2007; van der Sloot et al., 2007; Kosson et al., 2004).

9.2 Recommendations

To better understand the reaction processes and the effectiveness of the immobilization, several recommendations are proposed.

- Utilizing Scanning Electron Microscopy (SEM) can help providing information into the immobilization
 process and the locations of heavy metals in the structures. CT scanning can also offer a clearer picture of
 mineralization and crystallization resulting from carbonation within the sample. The FT-IR spectra of
 carbonated pastes should be analysed as previous research to identify the carbonate bands and detect
 exactly where the carbon bonds.
- Further development on the carbonation equipment are necessary to investigate the industrial applicability of the methodology. An example is to increase the carbonation batch size and incorporating a stirrer, while maintaining controlled temperature and pressure, to better predict the behaviour of larger batches of materials.
- New mix designs should also be tested combining BM FA and MSWI FA to increase carbonation and strength of the materials. Additionally, casting in the carbonation chamber for longer periods can help with assessing the long-term effects of carbonation. The pre-carbonated FA and FA-binder mixture should also be re-prepared by drying the samples after carbonation at 40°C and adding a constant S/L proportions as used in the reference sample.
- Further column tests on the carbon-cured fly ashes are recommended to test the leachability in a real-life scenario on a landfill and to determine the performance based on the requirements from the applied Dutch regulation (Beschikking 2003/33/EG).
- Ph-static leaching test should also be conducted to determine the effective influence of pH on the leachability of the heavy metals (Stichting Koninklijk Nederlands Normalisatie Instituut, 2015). The material is exposed to 8 solutions at different pH for 48h and the final eluate is filtered and analysed. This test has the objective of identifying the change in leachability of each hazardous component that, as well known from the literature, varies for each element based on the pH and other species present (Dijkstra, 2007; van der Sloot et al., 2007; Kosson et al., 2004). Previous papers investigated the behaviour of singular heavy metal dissolution at different pH but, from other research, this process is much more complicated and harder to model or predict when other heavy metals and chemical complexes are present in the sample. For example, at pH between 8 and 10, the dissolution of Molybdenum increases whereas the leachability of Cadmium decreases (Dijkstra, 2007). This will also ensure that the percolated water would not affect the surrounding immobilized material as the pH is basic and not neutral as the leachate used in the leaching tests.

10. Conclusion

This study investigates the potential for enhancing the immobilization of heavy metals in hazardous fly ashes through mineral carbonation. Initially, the research examines five different fly ashes to determine their chemical composition and carbonation potential. Results indicate that fly ashes with the highest lime content exhibit the greatest carbonation potential; however, even those with very limited free lime content show some degree of carbonation. The MSWI FA1 sample is selected for further experimentation due to its amorphous phase and other oxides, which efficiently mineralize carbon dioxide.

Water results being the main driving factor of carbonation, without the material cannot mineralize CO₂. Similarly, at only 2 bar higher pressure the time of carbon uptake halved compared to the experiment at 1 bar, and the effective mineral carbonation increases of 2.5%.

Pre-carbonizing the fly ash or pre-carbonation of the fly ash-binder mixture results in lowering the final physical strength of the immobilized material. on the contrary, carbonation during curing results in increased strength and stability of the material. The final strength of the equivalent BM FA is 1 MPa higher than the MSWI FA1, but both comply with the Dutch requirements on the safe disposal of immobilized wastes. The highest carbonation is reached for the pre-carbonated fly-ash mixture, followed by the sample cured in the carbonation chamber.

The immobilization route resulting in the highest reduction of pH of the leachate and the highest strength is the material cured in the carbonation chamber for 28 days. Carbonation of both MSWI FA and BM FA results in a high decrease of lead leachability but the effective immobilization compared to the reference sample is reached in FA2-B_C3. All carbonized MSWI FA perform better than the reference accordingly to the shake test, even though the change in pH decreases the solubility of some heavy metals and increases the leachability of others.

These results show that the immobilization processes outperform the reference samples, as well as the comparison of the leaching materials with the soil decree used in the past by the Dutch government reveals promising results. The carbonized materials meet most of the requirements necessary for construction materials, expected to be higher than for a landfill. Additionally, the materials are tested for a worst-case-possible scenario. Performing already better than the reference samples and decreasing the leachability of lead, carbonation of hazardous fly ash has the prospective to open the doors to a future with less carbon emissions and a cleaner environment.

10.1 Future research

A promising aspect for the research would be to mix different fly ashes to increase the effective carbonation without adding more binder. The immobilization is strictly related to the final pH of the material and the physical stability of the immobilized material. Thus, further research could investigate the substitution of part of the fraction of FA1 with FA2 to determine whether the carbonation increases and, with that, the physical stability of the material. The overall heavy metals concentration will also decrease, but the BM FA is also a by-product that instead of being separately immobilized could be used to enhance the carbonation and final physical strength of MSWI FA that have much lower concentrations of free lime and portlandite. It is recommended to try to replace the MSWI FA initially by 10% up to 70%. Higher quantities would correspond to just immobilizing the BM FA with the binder.

Bibliography

Ali, M. M., Hossain, D., Al-Imran, A., Khan, M. S., Begum, M., & Osman, M. H. (2021). Environmental pollution with heavy metals: A public health concern. *Heavy metals-their environmental impacts and mitigation*, 771-783.

Altree-Williams, A., Pring, A., Ngothai, Y., & Brugger, J. (2017). The carbonatation of anhydrite: kinetics and reaction pathways. *ACS Earth and Space Chemistry*, *1*(2), 89-100.

Azam, M., Setoodeh Jahromy, S., Raza, W., Wesenauer, F., Schwendtner, K., & Winter, F. (2019). Comparison of the characteristics of fly ash generated from bio and municipal waste: fluidized bed incinerators. *Materials*, 12(17), 2664.

Baciocchi, R., Costa, G., Di Bartolomeo, E., Polettini, A., & Pomi, R. (2009). The effects of accelerated carbonation on CO₂ uptake and metal release from incineration APC residues. *Waste Management*, 29(12), 2994-3003.

Bernardo, E., Scarinci, G., & Colombo, P. (2012). Vitrification of waste and reuse of waste-derived glass. In *Encyclopedia of Sustainability Science and Technology* (pp. 11581-11613). Springer.

Bertos, M. F., Simons, S. J. R., Hills, C. D., & Carey, P. J. (2004). A review of accelerated carbonation technology in the treatment of cement-based materials and sequestration of CO2. *Journal of hazardous materials*, *112*(3), 193-205.

Beschikking 2003/33/EG. Council Decision of 19 December 2002 establishing criteria and procedures for the acceptance of waste at landfills pursuant to Article 16 of and Annex II to Directive 1999/31/EC. https://eurlex.europa.eu/LexUriServ/LexUriServ.do?uri=OJ:L:2003:011:0027:0049:NL:PDF

Chen, B. (2023). Utilization of mswi bottom ash as a mineral resource for low-carbon construction materials: Quality-upgrade treatments, mix design method, and microstructure analysis.

Cengel, Y. A., Boles, M. A., & Kanoğlu, M. (2005). *Thermodynamics: an engineering approach* (5th edition). New York: McGraw-hill.

Chester, J. (2016). Waste to energy. Retrieved from https://www.theflipflopi.com/blog/2016/12/09/2016128waste-to-energy

De Leeuw, M., & Koelemeijer, R. (2022). Decarbonisation options for the dutch waste incineration industry. *Netherlands Environmental Assessment Agency: Bilthoven, The Netherlands*.

De Repentigny, C., Courcelles, B., & Zagury, G. J. (2018). Spent MgO-carbon refractory bricks as a material for permeable reactive barriers to treat a nickel-and cobalt-contaminated groundwater. *Environmental Science and Pollution Research*, 25, 23205-23214.

Dijkstra, J. J. (2007). Development of a consistent geochemical modelling approach for leaching and reactive transport prosesses in contaminated materials. Wageningen University and Research.

El-Hassan, H. (2020). Accelerated Carbonation Curing as a Means of Reducing Carbon Dioxide Emissions. In *Cement Industry-Optimization, Characterization and Sustainable Application*. IntechOpen.

Eurofins. (n.d.). Is-NE-007-V2 uitloogonderzoek. Retrieved from https://cdnmedia.eurofins.com/european-west/media/55533/is-ne-007-v2-uitloogonderzoek.pdf

European Court of Auditors. (2023). *EU actions to address the increasing amount of hazardous waste*. https://www.eca.europa.eu/lists/ecadocuments/rw23_02/rw_hazardous_waste_en.pdf

European Environmental Agency. (2023). Heavy Metal Emissions in Europe. Retrieved from https://www.eea.europa.eu/en/analysis/indicators/heavy-metal-emissions-in-europe

Eurostat. (2023). *Waste statistics*. Statistics Explained. https://ec.europa.eu/eurostat/statistics-explained/index.php?title=Waste_statistics#Waste_generation_excluding_major_mineral_waste

Feng, L., Yi, S., Zhao, S., Zhong, Q., Ren, F., Liu, C., Zhang, Y., Wang, W., Xie, N., Li, Z., & Cui, N. (2024). Recycling of Aluminosilicate-Based Solid Wastes through Alkali-Activation: Preparation, Characterization, and Challenges. *Buildings*, *14*(1), 226.

Franklin, J. A., & Chandra, R. (1972, May). The slake-durability test. In *International Journal of Rock Mechanics and Mining Sciences & Geomechanics Abstracts* (Vol. 9, No. 3, pp. 325-328). Pergamon.

Frost, R. L., Bahfenne, S., Graham, J., & Martens, W. N. (2008). Thermal stability of artinite, dypingite and brugnatellite—Implications for the geosequestration of green house gases. *Thermochimica Acta*, 475(1-2), 39-43.

Gabrovšek, R., Vuk, T., & Kaučič, V. (2006). Evaluation of the hydration of Portland cement containing various carbonates by means of thermal analysis. *Acta Chim. Slov*, 53(2), 159-165.

Gao, Q., Bao, L., Zhu, P., Jiang, X., Zheng, H., & Shen, F. (2022). Mathematical Simulation of Iron Ore Fines Sintering Process with Solid Fuel Segregation Distribution and Corresponding Heat Pattern Study. *Metals*, *12*(12), 2126.

Gasser, M., OST, R. B., & OST, A. G. (2021). Treating MSWI Bottom Ash with Sodium Carbonate.

Global Carbon Project. (December 5, 2023). Carbon dioxide emissions from the manufacture of cement worldwide from 1960 to 2022 (in million metric tons) [Graph]. In *Statista*. Retrieved January 17, 2024, from https://www.statista.com/statistics/1299532/carbon-dioxide-emissions-worldwide-cement-manufacturing/

Government of the Netherlands. (2024). Environmental Management Act (Wet milieubeheer). Retrieved June 14, 2024, from https://wetten.overheid.nl/BWBR0003245/2024-03-30

Guang, Y. (2024). Portland Cement. Lecture CIEM1000: Science of Construction Materials. TU Delft: TU Delft.

Guo, B., Liu, B., Yang, J., & Zhang, S. (2017). The mechanisms of heavy metal immobilization by cementitious material treatments and thermal treatments: A review. *Journal of environmental management*, 193, 410-422.

Hartono, E., Wardani, S. P. R., & Muntohar, A. S. (2019). Slake durability of the compacted-siltstone fragment with cement stabilization. *GEOMATE Journal*, *17*(64), 123-130.

Hollingbery, L. A., & Hull, T. R. (2010). The thermal decomposition of huntite and hydromagnesite—a review. *Thermochimica Acta*, 509(1-2), 1-11.

Hopkinson, L., Kristova, P., Rutt, K., & Cressey, G. (2012). Phase transitions in the system MgO–CO2–H2O during CO2 degassing of Mg-bearing solutions. *Geochimica et Cosmochimica Acta*, 76, 1-13.

- Huber, F., Blasenbauer, D., Mallow, O., Lederer, J., Winter, F., & Fellner, J. (2016). Thermal co-treatment of combustible hazardous waste and waste incineration fly ash in a rotary kiln. *Waste management*, 58, 181-190.
- Ji, L., & Yu, H. (2018). Carbon dioxide sequestration by direct mineralization of fly ash. *Carbon dioxide* sequestration in cementitious construction materials (pp. 13-37). Woodhead Publishing.
- Jianguo, J., Maozhe, C., Yan, Z., & Xin, X. (2009). Pb stabilization in fresh fly ash from municipal solid waste incinerator using accelerated carbonation technology. *Journal of Hazardous Materials*, 161(2-3), 1046-1051.
- Kolios, A., Mytilinou, V., Lozano-Minguez, E., & Salonitis, K. (2016). A comparative study of multiple-criteria decision-making methods under stochastic inputs. *Energies*, 9(7), 566.
- Król, A., Mizerna, K., & Bożym, M. (2020). An assessment of pH-dependent release and mobility of heavy metals from metallurgical slag. *Journal of hazardous materials*, *384*, 121502.
- Krutul, D., Zielenkiewicz, T., Zawadzki, J., Radomski, A., Antczak, A., & Drozdzek, M. (2014). Influence of urban environment originated heavy metal pollution on the extractives and mineral substances content in bark and wood of oak (Quercus robur L.). *Wood Res*, 59(1), 177-190.
- Larson, S. L., Malone, P. G., Weiss, C. A., Martin, W. A., Trest, C., Fabian, G., ... & Wright, J. (2007). Treatment and Management of Closedor Inactive Small Arms Firing Ranges. *US Army Corps of Engineer Research and Development Center*.
- Lecomte, T., Ferreria de La Fuente, J. F., Neuwahl, F., Canova, M., Pinasseau, A., Jankov, I., ... & Delgado Sancho, L. (2017). Best available techniques (BAT) reference document for large combustion plants. Industrial emissions directive 2010/75/EU (Integrated pollution prevention and control) (No. JRC107769). Joint Research Centre (Seville site).
- Li, X., Bertos, M. F., Hills, C. D., Carey, P. J., & Simon, S. (2007). Accelerated carbonation of municipal solid waste incineration fly ashes. *Waste management*, 27(9), 1200-1206.
- Li, Z. S., Fang, F., Tang, X. Y., & Cai, N. S. (2012). Effect of temperature on the carbonation reaction of CaO with CO2. *Energy & Fuels*, 26(4), 2473-2482.
- Li, B., Giordano, R., Tulliani, J. M., & Meng, Q. (2024). Effect of sea salt on carbonation and CO2 uptake in cement mortar. *Construction and Building Materials*, 438, 137212.
- Li, B., Zhang, S., Li, Q., Li, N., Yuan, B., Chen, W., ... & Yu, Q. (2019). Uptake of heavy metal ions in layered double hydroxides and applications in cementitious materials: Experimental evidence and first-principle study. *Construction and Building Materials*, 222, 96-107.
- Liu, L., Li, W., Song, W., & Guo, M. (2018). Remediation techniques for heavy metal-contaminated soils: Principles and applicability. *Science of the total environment*, *633*, 206-219.
- Lo, Y., & Lee, H. M. (2002). Curing effects on carbonation of concrete using a phenolphthalein indicator and Fourier-transform infrared spectroscopy. *Building and environment*, *37*(5), 507-514.
- Mazzella, A., Errico, M., & Spiga, D. (2016). CO2 uptake capacity of coal fly ash: Influence of pressure and temperature on direct gas-solid carbonation. *Journal of Environmental Chemical Engineering*, 4(4), 4120-4128.

McIlvried, H. G., & Massoth, F. E. (1973). Effect of particle size distribution on gas-solid reaction kinetics for spherical particles. *Industrial & Engineering Chemistry Fundamentals*, 12(2), 225-229.

 $\label{eq:mida} \begin{tabular}{lll} Mida, & R. & (2009). & Fact & sheet: & Biomass & incineration. & Retrieved & from & https://zerowasteoz.org.au/wp-content/uploads/2017/12/factsheet-biomass.pdf & Retrieved & from & Retrieved & from & Retrieved & from & Retrie$

Mineralz. (n.d. a). *Products*. https://www.mineralz.com/producten-en-diensten/deponie/afvalstoffen-maasvlakte

Mineralz. (n.d. b). Deponie. Retrieved from https://www.mineralz.com/producten-en-diensten/deponie

Ministerie van Infrastructuur en Waterstaat. (2022) IENW/BSK-2022/203483, houdende vaststelling van de Regeling bodemkwaliteit 2022. Retrieved from https://wetten.overheid.nl/BWBR0023085/2023-12-21

Mitchell, M. J., Jensen, O. E., Cliffe, K. A., & Maroto-Valer, M. M. (2010). A model of carbon dioxide dissolution and mineral carbonation kinetics. *Proceedings of the Royal Society A: Mathematical, Physical and Engineering Sciences*, 466(2117), 1265-1290.

Nair, N. A., & Sairam, V. (2021). Research initiatives on the influence of wollastonite in cement-based construction material-A review. *Journal of Cleaner Production*, 283, 124665.

Nakai, I. (2017). X-ray fluorescence analysis. Encyclopedia of Earth Sciences Series, 1-5.

Nathanson, J. A. (2020). Treatment, storage, and disposal. Retrieved from https://www.britannica.com/technology/hazardous-waste-management/Treatment-storage-and-disposal

Nedeljković, M. (2019). Carbonation mechanism of alkali-activated fly ash and slag materials: In view of long-term performance predictions.

Ni, P., Xiong, Z., Tian, C., Li, H., Zhao, Y., Zhang, J., & Zheng, C. (2017). Influence of carbonation under oxyfuel combustion flue gas on the leachability of heavy metals in MSWI fly ash. *Waste Management*, 67, 171-180.

Park, Y. J., & Heo, J. (2002). Conversion to glass-ceramics from glasses made by MSW incinerator fly ash for recycling. *Ceramics International*, 28(6), 689-694.

Qiu, J., Zhao, Y., Xing, J., & Sun, X. (2017). Fly ash-based geopolymer as a potential adsorbent for Cr (VI) removal. *Desalin. Water Treat*, 70, 201-209.

Qin, J., Zhang, Y., Yi, Y., & Fang, M. (2022). Carbonation of municipal solid waste gasification fly ash: effects of pre-washing and treatment period on carbon capture and heavy metal immobilization. *Environmental Pollution*, 308, 119662.

Ram, L. C., Srivastava, N. K., Tripathi, R. C., Thakur, S. K., Sinha, A. K., Jha, S. K., ... & Mitra, S. (2007). Leaching behavior of lignite fly ash with shake and column tests. *Environmental Geology*, *51*(7), 1119-1132.

Rijkswaterstaat. (2021). Afvalverwerking in Nederland, gegevens 2019. Retrieved from https://open.rijkswaterstaat.nl/publish/pages/137413/afvalverwerking_in_nederland_gegevens_2019.pdf

Ren, P., Ling, T. C., & Mo, K. H. (2022). CO2 pretreatment of municipal solid waste incineration fly ash and its feasible use as supplementary cementitious material. *Journal of hazardous materials*, 424, 127457.

Robertson, S. (2011). Direct estimation of organic matter by loss on ignition: methods. *SFU Soil Science Lab*, 1-11.

Saleh, H. (Ed.). (2021). Cement Industry: Optimization, Characterization and Sustainable Application. BoD–Books on Demand.

Segni, R., Vieille, L., Leroux, F., & Taviot-Guého, C. (2006). Hydrocalumite-type materials: 1. Interest in hazardous waste immobilization. *Journal of Physics and Chemistry of Solids*, 67(5-6), 1037-1042.

Setoodeh Jahromy, S., Jordan, C., Azam, M., Werner, A., Harasek, M., & Winter, F. (2019). Fly ash from municipal solid waste incineration as a potential thermochemical energy storage material. *Energy & fuels*, 33(7), 5810-5819.

Singh, R., & Budarayavalasa, S. (2021). Solidification and stabilization of hazardous wastes using geopolymers as sustainable binders. *Journal of Material Cycles and Waste Management*, 23, 1699-1725.

Siramanont, J., Walder, B. J., Emsley, L., & Bowen, P. (2021). Iron incorporation in synthetic precipitated calcium silicate hydrates. *Cement and Concrete Research*, *142*, 106365.

Shi, H. S., & Kan, L. L. (2009). Leaching behavior of heavy metals from municipal solid wastes incineration (MSWI) fly ash used in concrete. *Journal of hazardous materials*, 164(2-3), 750-754.

Sriwong, C., Phrompet, C., Tuichai, W., Karaphun, A., Kurosaki, K., & Ruttanapun, C. (2020). Synthesis, microstructure, multifunctional properties of mayenite Ca12Al14O33 (C12A7) cement and graphene oxide (GO) composites. *Scientific Reports*, 10(1), 11077.

Statista. (2024). Topic: Bioenergy in Europe. Retrieved from https://www.statista.com/topics/5219/bioenergy-industry-in-europe/#topicOverview

Stichting Koninklijk Nederlands Normalisatie Instituut. (2002). Characterization of waste - Leaching - Abbreviated leaching test of granular wastes and sludge - Part 1: One-stage batch inspection at a liquid to solid ratio of 2 l/kg for materials with a high solids content and with particle size below 4 mm (without or with size reduction) (NEN-EN 12457-1:2002 en). Retrieved from https://connect.nen.nl/Standard/Detail/82492?compId=10037&collectionId=0

Stichting Koninklijk Nederlands Normalisatie Instituut. (2004). Leaching characteristics - Determination of the leaching of inorganic components from moulded or monolitic materials with a diffusion test - Solid earthy and stony materials (NEN 7375)

Stichting Koninklijk Nederlands Normalisatie Instituut. (2009). Water - Determination of dissolved anions by liquid ion chromatography - Part 1: Determination of bromide, chloride, fluoride, nitrate, nitrite, phosphate and sulphate (NEN-EN-ISO 10304-1)

Stichting Koninklijk Nederlands Normalisatie Instituut. (2013). Method of testing cement - Part 2: Chemical analysis of cement (NEN-EN 196-2:2013). Retrieved from https://connect.nen.nl/Standard/PopUpStandard?RNR=184482&search=&Native=0&token=ec43e05c-0f24-42fa-952e-5dd0d44ae457

Stichting Koninklijk Nederlands Normalisatie Instituut. (2016). Methods of testing cement - Part 1: Determination of strength (NEN-EN 196-1:2016). Retrieved from https://connect.nen.nl/Standard/Detail/219352?compId=10037&collectionId=0

Stichting Koninklijk Nederlands Normalisatie Instituut. (2019). Testing hardened concrete - Part 3: Compressive strength of test specimens (NEN-EN 12390-3). Retrieved from https://connect.nen.nl/standard/openpdf/?artfile=3614358&RNR=3614358&token=0645427b-3651-43ff-8ea6-8cde479deeeb&type=pdf#pagemode=bookmarks

Stichting Koninklijk Nederlands Normalisatie Instituut. (2023). Water - Applications of inductively coupled plasma mass spectrometry - Part 2: Determination of selected elements including uranium isotopes (NEN-EN-ISO 17294-2)

Stichting LAP3. (n.d.). *Afvalbeheer*. LAP3. https://lap3.nl/sectorplannen/afval/

Sun, Y., Chen, B., Zhang, S., Blom, K., Luković, M., & Ye, G. (2024). Characterization, pre-treatment, and potential applications of fine MSWI bottom ash as a supplementary cementitious material. *Construction and Building Materials*, 421, 135769.

Tang, P., Chen, W., Xuan, D., Cheng, H., Poon, C. S., & Tsang, D. C. (2020). Immobilization of hazardous municipal solid waste incineration fly ash by novel alternative binders derived from cementitious waste. *Journal of hazardous materials*, 393, 122386.

Tchounwou, P. B., Yedjou, C. G., Patlolla, A. K., & Sutton, D. J. (2012). Heavy metal toxicity and the environment. *Molecular, clinical and environmental toxicology: volume 3: environmental toxicology*, 133-164.

Tominc, S., & Ducman, V. (2023). Methodology for evaluating the CO2 sequestration capacity of waste ashes. *Materials*, *16*(15), 5284. https://doi.org/10.3390/ma16155284

Vermilyea, D. A. (1969). The dissolution of MgO and Mg (OH) 2 in aqueous solutions. *Journal of the Electrochemical Society*, 116(9), 1179.

Vespa, M., Dähn, R., & Wieland, E. (2014). Competition behaviour of metal uptake in cementitious systems: An XRD and EXAFS investigation of Nd-and Zn-loaded 11 Å tobermorite. *Physics and Chemistry of the Earth, Parts A/B/C*, 70, 32-38.

Vu, T. H., & Gowripalan, N. (2018). Mechanisms of heavy metal immobilisation using geopolymerisation techniques—A review. *Journal of Advanced Concrete Technology*, 16(3), 124-135.

Wagh, A. S. (2016). Chemically bonded phosphate ceramics: twenty-first century materials with diverse applications. Elsevier.

Wahlström, M., Fällman, A. M., Hjelmar, O., Karstensen, K. H., Sveinsdottir, E. L., & Song, X. M. (1998). Development of a quick leaching test for monolithic materials by using factorial design. *Talanta*, 46(3), 365–374. https://doi.org/10.1016/s0039-9140(97)00407-4

Wan, X., Zhao, T., & Wittmann, F. H. (2012). Influence of carbonation on the chloride concentration in the pore solution of concrete. *epair*, *R*.

Wang, Y., Qi, T., Chu, J., & Zhao, W. (2010). Production of TiO 2 from CaTiO 3 by alkaline roasting method. *Rare metals*, 29, 162-167.

Wang, T., Yi, Z., Guo, R., Huang, H., Garcia, S., & Maroto-Valer, M. M. (2021). Particle carbonation kinetics models and activation methods under mild environment: the case of calcium silicate. *Chemical Engineering Journal*, 423, 130157.

Werner, M., Hariharan, S. B., Bortolan, A. V., Zingaretti, D., Baciocchi, R., & Mazzotti, M. (2013). Carbonation of activated serpentine for direct flue gas mineralization. *Energy Procedia*, *37*, 5929-5937.

Wet milieubeheer. (2024). Retrieved from https://wetten.overheid.nl/BWBR0003245/2024-03-30

Winnefeld, F., Epifania, E., Montagnaro, F., & Gartner, E. M. (2019). Further studies of the hydration of MgO-hydromagnesite blends. *Cement and Concrete Research*, 126, 105912.

Xu, X., Liu, W., Chu, G., Zhang, G., Luo, D., Yue, H., ... & Li, C. (2019). Energy-efficient mineral carbonation of CaSO4 derived from wollastonite via a roasting-leaching route. *Hydrometallurgy*, 184, 151-161.

Yuan, Q., Yang, G., Zhang, Y., Wang, T., Wang, J., & Romero, C. E. (2022a). Supercritical CO2 coupled with mechanical force to enhance carbonation of fly ash and Heavy Metal Solidification. *Fuel*, *315*, 123154. https://doi.org/10.1016/j.fuel.2022.123154

Yuan, Q., Zhang, Y., Wang, T., Wang, J., & Romero, C. E. (2022b). Mineralization characteristics of coal fly ash in the transition from non-supercritical CO2 to supercritical CO2. *Fuel*, *318*, 123636.

Yuan, Q., Zhang, Y., Wang, T., & Wang, J. (2023). Characterization of heavy metals in fly Ash Stabilized by carbonation with Supercritical CO2 Coupling Mechanical Force. *Journal of CO2 Utilization*, 67, 102308. https://doi.org/10.1016/j.jcou.2022.102308

Zajac, M., Skocek, J., Ben Haha, M., & Deja, J. (2022). CO2 mineralization methods in cement and concrete industry. *Energies*, 15(10), 3597.

Zhang, Y., Ma, Z., Fang, Z., Qian, Y., Zhong, P., & Yan, J. (2020). Review of harmless treatment of municipal solid waste incineration fly ash. *Waste Disposal & Sustainable Energy*, 2, 1-25.

Zhang, J., Ke, G., & Liu, Y. (2021). Early hydration heat of calcium sulfoaluminate cement with influences of supplementary cementitious materials and water to binder ratio. *Materials*, 14(3), 642.

Zhao, H., Li, H., Bao, W., Wang, C., Li, S., & Lin, W. (2015). Experimental study of enhanced phosphogypsum carbonation with ammonia under increased CO2 pressure. *Journal of CO2 Utilization*, 11, 10-19.

Zhao, P., Lu, L., Liu, X., De la Torre, A. G., & Cheng, X. (2018). Error analysis and correction for quantitative phase analysis based on rietveld-internal standard method: whether the minor phases can be ignored?. *Crystals*, 8(3), 110.

Appendices

A. Literature review

Parameter	Emissiewaarden in mg/m ²
As	50
Ва	1500
Cd	5
Со	60
Cr	500
Cu	500
Hg	1
Мо	900
Ni	400
РЬ	5000
Sb	50
Se	60
Sn	50
V	1500
W	250
Zn	800
Br	5000
CI	250000
CN-com	220
CN-vrij	20
F	2500
504	250000

Figure A.0.1: Limit leachability values per chemical component (Beschikking 2003/33/EG).

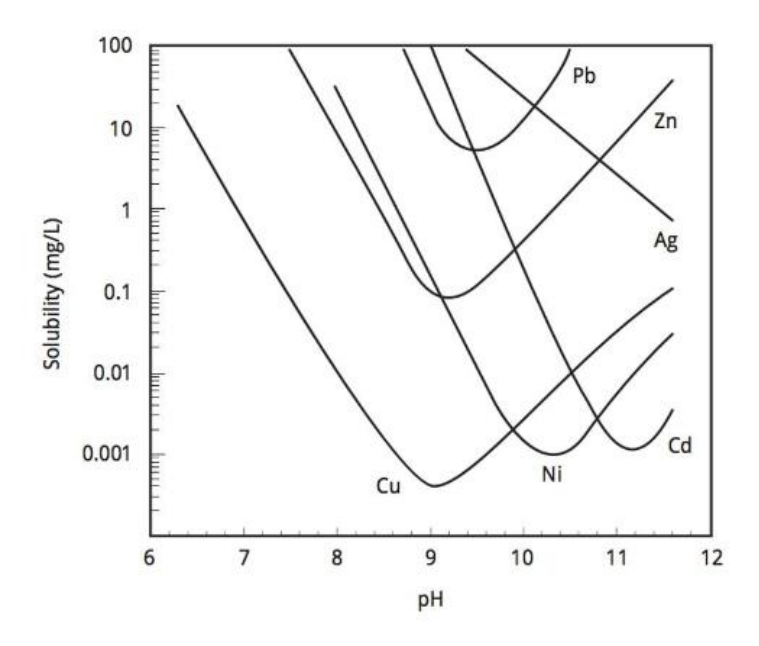


Figure A.O.2: Solubility of heavy metal hydroxides based on pH (Gasser et al., 2021).

B. Experimental investigation

B.1 Methodology

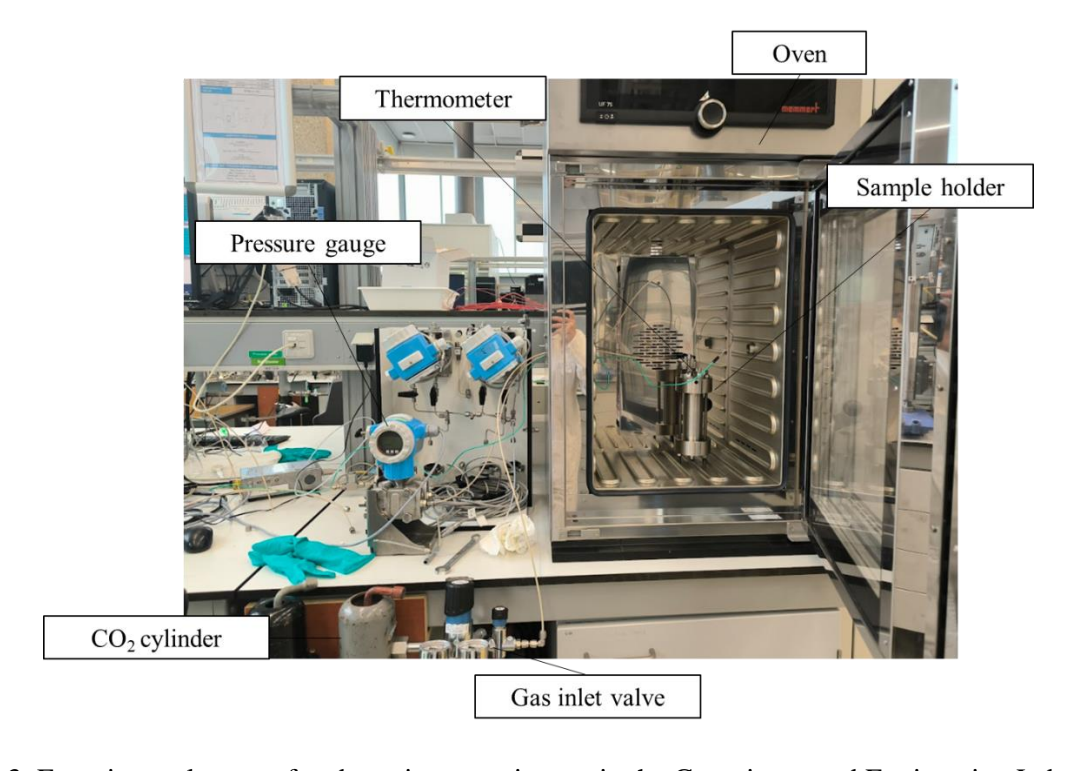


Figure B.0.3: Experimental setup of carbonation experiments in the Geoscience and Engineering Laboratory.

B.2 Characterization experiments

To estimate the carbonation performance of each fly ashes the theoretical CO₂ sequestration capacity ($Th_{m_{CO_2}}$) is calculated following previous research (Ji & Yu, 2018) and as shown in Eq. (B.1). The theoretical maximum carbon-uptake depends mainly on the initial lime (n_{CaO}), portlandite ($n_{Portlandite}$), brucite ($n_{Brucite}$) and periclase (n_{MgO}) content. Each carbonation reaction occurs at 1:1 mole ratio of reagents, thus all compounds appear in the equation simply from their number of moles that is calculated by multiplying the mass fraction m_x found from the QXRD with the molecular mass of each species M_x .

$$Th_{m_{CO_2}} = n_{CaO} + n_{MgO} + n_{Portlandite} + n_{Brucite}$$
 (B.1)

Following Ji & Yu (2018), the theoretical sequestration capacity and carbonation efficiency $\delta(\%)$ can be determined as shown in Eq. (B.2).

$$\delta(\%) = \frac{m_{CO_2}}{Th_{m_{CO_2}}} \times 100$$
 (B.2)

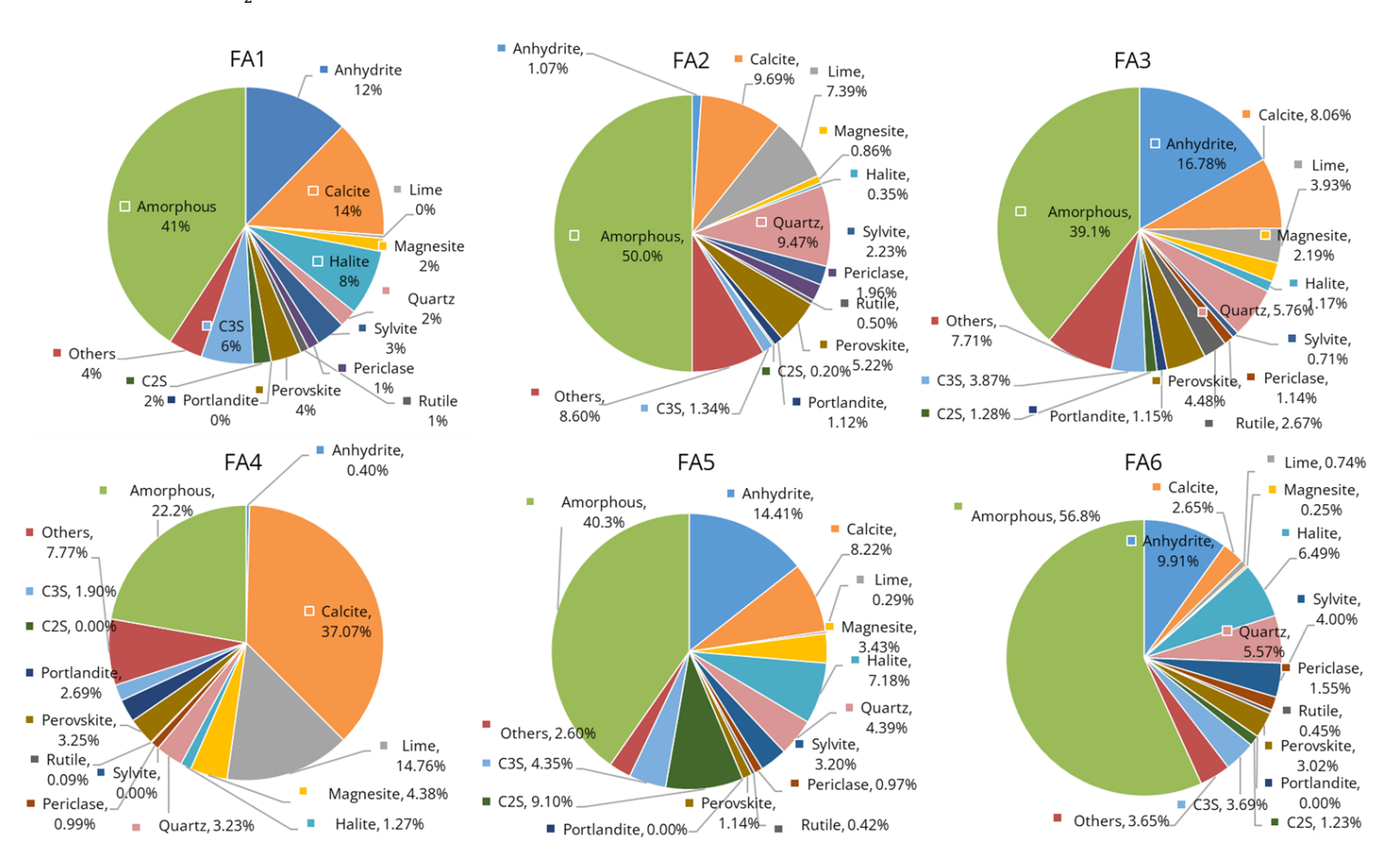


Figure B.0.4: Crystalline phases identified from QXRD analysis on the pure fly ashes.

B.2 Carbonation Experiments

Table B.0.1: Extended list of QXRD results of immobilized FA1 calculated through Rietveld refinement. In the table are shown the results of the reference paste and the paste with pre-carbonated fly ash before and after 28 days

of curing. Crystalline		FA1-B_Ref pre-	FA1_C2 pre-	FA1_C2 post-
phase	Formula	curing	curing	curing
Anhydrite	CaSO4	4.08%	8.96%	4.42%
Calcite	CaCO ₃	9.84%	10.9%	12.60%
Lime	CaO	1.71%	0.00%	0.07%
Magnesite	$MgCO_3$	2.59%	1.50%	1.40%
Halite	NaCl	9.24%	7.96%	9.90%
Quartz	SiO	3.36%	2.97%	2.53%
Sylvite	KCl	4.56%	2.85%	4.45%
Periclase	MgO	1.41%	1.42%	1.11%
Rutile	${ m TiO_2}$	0.16%	0.17%	0.41%
Perovskite	CaTiO ₃	3.44%	2.96%	1.81%
Vaterite	μ-CaCO₃	1.85%	0.15%	0.00%
Wollastonite	CaSiO ₃	1.18%	1.43%	5.50%
Mayenite	$Ca_{12}Al_{14}O_{32}$	3.00%	1.72%	1.58%
Portlandite	$Ca(OH)_2$	0.99%	0.25%	0.05%
C2S	(CaO) ₃ SiO ₂	0.41%	8.07%	3.22%
C3S	$(CaO)_2SiO_3$	3.56%	2.12%	0.81%
C-S-H	$\text{Ca}_{2.25}[ext{Si}_3 ext{O}_{7.5}(ext{OH})_{1.5}] \cdot 8 ext{H}_2 ext{O}$	3.48%	5.79%	1.11%
Anorthite	$CaAl_2Si_2O_8$	2.59%	12.53%	3.72%
Mullite	$3Al_2O_3 \cdot 2SiO_2$	1.93%	1.50%	2.26%
Ettringite	Ca ₆ Al ₂ (SO ₄) ₃ (OH) ₁₂ · 26H ₂ O	0.00%	1.88%	1.63%
Syngenite	$K_2Ca(SO_4)_2 \cdot H_2O$	3.92%	8.50%	5.35%
Merwinite	$Ca_3Mg(SiO4)_2$	2.05%	2.69%	1.71%
Hydromagnesi te	$(Mg_5(OH)_2(CO_3)_4(H_2O)_4)$		1.60%	1.40%
C,N-A-S-H			0.23%	1.27%
	Others	0.01%	0.84%	1.57%
	Amorphous	34.7%	11.0%	30%
	GOF	2.94	2.70	2.97

Table B.0.2: Extended list of QXRD results of immobilized FA1 calculated through Rietveld refinement. In the table are shown the results of the pre-carbonated paste of FA1 and binder before and after 28 days of curing, and

the results of the specimen cured in the carbonation chamber.

Crystalline	Formula	FA1-B_C2 pre-	FA1-B_C2	FA1-B_C3 pre-	FA1-B_C3
phase		curing	post-curing	curing	post-curing
Anhydrite	CaSO4	16.94%	8.71%	8.1%	18.00%
Calcite	$CaCO_3$	18.40%	21.40%	9.87%	22.61%
Lime	CaO	0.02%	0.00%	1.70%	0.18%
Magnesite	$MgCO_3$	0.00%	1.84%	2.42%	0.00%
Halite	NaCl	9.00%	9.07%	9.70%	6.38%
Quartz	SiO	3.09%	2.88%	2.75%	3.45%
Sylvite	KCl	5.40%	5.03%	2.01%	2.62%
Periclase	MgO	1.42%	1.32%	1.26%	1.28%
Rutile	TiO_2	0.00%	0.39%	0.00%	0.27%
Perovskite	CaTiO ₃	1.53%	3.74%	3.51%	3.10%
Vaterite	μ-CaCO ₃	3.25%	2.55%	0.27%	0.22%
Wollastonit e	CaSiO ₃	4.72%	1.61%	2.24%	3.34%
Mayenite	$Ca_{12}Al_{14}O_{32}$	0.75%	0.88%	3.50%	1.51%
Portlandite	$Ca(OH)_2$	0.00%	0.05%	0.65%	0.40%
C2S	$(CaO)_3SiO_2$	2.95%	2.65%	0.92%	2.61%
C3S	$(CaO)_2SiO_3$	2.21%	0.73%	3.10%	2.94%
C-S-H	$Ca_{2.25}[Si_3O_{7.5}(OH)_{1.5}] \cdot 8H_2O$	4.00%	10.73%	3.75%	8.84%
Anorthite	$CaAl_2Si_2O_8$	3.99%	12.40%	5.50%	8.62%
Mullite	$3Al_2O_3 \cdot 2SiO_2$	0.98%	2.87%	2.28%	1.32%
Ettringite	Ca ₆ Al ₂ (SO ₄) ₃ (OH) ₁₂ ·26H ₂ O	0.00%	0.73%	0.70%	0.00%
Syngenite	$K_2Ca(SO_4)_2 \cdot H_2O$	4.79%	1.42%	4.50%	7.20%
Merwinite	$Ca_3Mg(SiO4)_2$	1.68%	1.51%	2.33%	0.70%
Hydromag nesite	$(Mg_5(OH)_2(CO_3)_4(H_2 O)_4)$	0.68%	2.25%	1.50%	1.72%
C,N-A-S-H		0.00%	0.00%	0	0.78%
	Others	3.60%	0.06%	1.26%	0.01%
	Amorphous	10.6%	5.2%	28%	1.90%
	GOF	3.00	2.92	2.86	2.63

B.3 Leachability of Heavy Metals

Table B.0.3: Wet mass, equivalent dry mass and final volume of leachate for each FA1 mix design.

	$M_w[g]$	$M_d[g]$	Leachate [ml]
	a	105.3	90.2
FA1-B_Ref	b	105.1	90.0
	c	105	89.9
	a	116.9	90.0
FA1_C2	b	114.9	88.5
	c	114.7	88.3
	a	110.7	89.7
FA1-B_C2	b	111.4	90.2
	С	110.9	89.8
	a	99.6	90.0
FA1-B_C3	b	98.7	89.2
	c	95.8	86.6

Table B.0.4: Wet mass, equivalent dry mass and final volume of leachate for each FA2 mix design.

	-	M _w [g]	M _d [g]	Leachate [ml]
	a	105.3	90.2	902
FA2-B_Ref	b	105.1	90.0	900
	c	105.0	89.9	899
	a	116.9	90.0	900
FA2_C2	b	114.9	88.5	885
	c	114.7	88.3	883
	a	117.7	90.6	906
FA2-B_C2	b	110.7	89.7	897
	c	111.4	90.2	902
	a	110.9	89.8	898
FA2-B_C3	b	99.6	90.0	900
	c	98.7	89.2	892

Table B.0.5: Pure FA1, reference sample and immobilized samples' leachates heavy metals composition. From left to right are displayed the concentrations in mg/kg of dry matter of arsenic, bromide, cadmium, chromium, cobalt, copper and lead.

		As	Br	Cd	Cr	Co	Cu	Pb
	a	0.06	2000	0.02	7.2	< 0.02	0.04	0.31
FA1_pure	b	0.06	2000	0.03	7.1	< 0.02	0.04	0.32
	c	0.06	2000	0.03	7.1	< 0.02	0.04	0.32
	a	< 0.01	1200	< 0.002	1.2	< 0.02	0.26	45
FA1-B_Ref	b	< 0.01	1200	< 0.002	1.2	< 0.02	0.17	43
	c	< 0.01	1200	0.004	1.2	< 0.02	0.3	46
	a	< 0.01	1400	0.01	4	< 0.02	0.12	0.25
FA1_C2	b	< 0.01	1400	0.004	4	< 0.02	0.06	0.1
	c	< 0.01	1400	0.02	4	< 0.02	0.12	0.24
	a	< 0.01	1300	0.04	2	< 0.02	0.11	0.17
FA1-B_C2	b	< 0.01	1300	0.04	2	< 0.02	0.11	0.16
	c	< 0.01	1300	0.04	2	< 0.02	0.1	0.16
	a	< 0.01	1400	0.1	3.1	< 0.02	< 0.02	< 0.02
FA1-B_C3	b	< 0.01	1400	0.09	3.1	< 0.02	< 0.02	< 0.02
	c	< 0.01	1400	0.13	3.1	< 0.02	0.04	0.02

Table B.0.6: Pure FA1, reference sample and immobilized samples' leachates heavy metals composition. From left to right are displayed the concentrations in mg/kg of dry matter of molybdenum, nickel, antimony, selenium, tin, vanadium and zinc.

		Mo	Ni	Sb	Se	Sn	V	Zn
	a	7.9	< 0.03	0.086	0.16	< 0.02	0.08	0.96
FA1_pure	b	8	< 0.03	0.084	0.15	< 0.02	0.09	0.95
	c	7.7	< 0.03	0.089	0.14	< 0.02	0.09	0.97
	a	4	< 0.03	< 0.02	0.07	< 0.02	< 0.02	15
FA1-B_Ref	b	3.9	< 0.03	< 0.02	0.087	< 0.02	< 0.02	12
	c	4	< 0.03	0.022	0.082	< 0.02	< 0.02	15
	a	5.5	< 0.03	0.088	0.11	< 0.02	0.07	2.2
FA1_C2	b	5.5	< 0.03	0.063	0.1	< 0.02	0.06	0.55
	c	5.5	< 0.03	0.14	0.099	0.03	0.06	1.2
	a	5.7	< 0.03	0.48	0.13	< 0.02	0.05	1.8
FA1-B_C2	b	5.5	< 0.03	0.49	0.12	< 0.02	0.05	1.8
	c	5.5	< 0.03	0.48	0.13	< 0.02	0.05	1.8
	a	5.4	< 0.03	1.7	0.13	< 0.02	0.03	0.53
FA1-B_C3	b	5.2	< 0.03	1.7	0.11	< 0.02	0.03	0.48
	c	5.3	< 0.03	1.7	0.12	< 0.02	0.04	0.57

Table B.0.7: Pure FA1, reference sample and immobilized samples' leachates heavy metals composition. From left to right are displayed the concentrations in mg/kg of dry matter of barium, chlorine, fluorine and sulphate.

8	1 7	Ba	Cl	F	SO ₄ ² -
	a	4.6	120000	<20	41000
FA1_pure	b	4.6	120000	25	42000
•	c	4.7	120000	24	41000
	a	4.6	75000	29	28000
FA1-B_Ref	b	5.1	76000	24	28000
	c	4.4	75000	23	28000
	a	4.8	90000	< 20	33000
FA1_C2	b	4.6	88000	< 20	32000
	c	4.2	90000	< 20	33000
	a	4.8	78000	25	30000
FA1-B_C2	b	4.7	79000	21	31000
	c	4.6	80000	25	31000
	a	3.9	82000	48	30000
FA1-B_C3	b	3.9	82000	44	30000
	c	4	83000	61	30000

Table B.0.8: Pure FA2, reference sample and immobilized samples' leachates heavy metals composition. From left to right are displayed the concentrations in mg/kg of dry matter of arsenic, bromide, cadmium, chromium, cobalt, copper and lead.

		As	Br	Cd	Cr	Co	Cu	Pb
	a	< 0.01	52	< 0.002	16	< 0.02	0.22	5.9
FA2-B_Ref	b	< 0.01	54	< 0.002	15	< 0.02	0.23	5.6
	c	< 0.01	56	< 0.002	15	< 0.02	0.17	5.4
	a	< 0.01	55	< 0.002	13	< 0.02	0.06	0.73
FA2_C2	b	0.01	56	< 0.002	13	< 0.02	0.06	0.74
	c	< 0.01	56	< 0.002	13	< 0.02	0.05	0.74
	a	< 0.01	59	< 0.002	7.9	< 0.02	0.03	0.07
FA2-B_C2	b	< 0.01	60	< 0.002	7.9	< 0.02	0.03	0.07
	c	0.01	60	< 0.002	8	< 0.02	0.04	0.08
	a	0.03	63	0.003	21	< 0.02	0.08	0.36
FA2-B_C3	b	0.03	70	< 0.002	21	< 0.02	0.06	0.3
	c	0.03	64	< 0.002	22	< 0.02	0.06	0.28

Table B.0.9: Pure FA2, reference sample and immobilized samples' leachates heavy metals composition. From left to right are displayed the concentrations in mg/kg of dry matter of molybdenum, nickel, antimony, selenium, tin, vanadium and zinc.

		Mo	Ni	Sb	Se	Sn	V	Zn
	a	3	< 0.03	< 0.02	0.29	< 0.02	< 0.02	4.2
FA2-B_Ref	b	3.2	< 0.03	< 0.02	0.3	< 0.02	< 0.02	4
	c	3	< 0.03	< 0.02	0.3	< 0.02	< 0.02	3.7
	a	3.5	< 0.03	0.062	0.3	< 0.02	0.23	2
FA2_C2	b	3.4	< 0.03	0.064	0.27	< 0.02	0.22	2
	c	3.4	< 0.03	0.063	0.31	< 0.02	0.23	1.9
	a	2.7	< 0.03	< 0.02	0.33	< 0.02	0.3	0.68
FA2-B_C2	b	2.7	< 0.03	< 0.02	0.32	< 0.02	0.3	0.56
	c	2.7	< 0.03	< 0.02	0.32	< 0.02	0.3	0.68
	a	2.9	< 0.03	0.1	0.37	< 0.02	0.61	1.5
FA2-B_C3	b	3.1	< 0.03	0.096	0.37	< 0.02	0.59	1.4
	c	3	< 0.03	0.1	0.34	< 0.02	0.61	1.4

Table B.0.10: Pure FA2, reference sample and immobilized samples' leachates heavy metals composition. From left to right are displayed the concentrations in mg/kg of dry matter of barium, chlorine, fluorine and sulphate.

	P-my - m - m			,	
		Ba	C1	F	SO_4^2 -
	a	6	10000	<20	4200
FA2-B_Ref	b	5.4	10000	< 20	4100
	c	5.4	10000	< 20	4100
	a	3.7	11000	5.1	3500
FA2_C2	b	3.7	11000	4	3500
	c	3.7	11000	6.3	3500
	a	1.7	12000	2.1	18000
FA2-B_C2	b	1.6	12000	< 2.0	18000
	c	1.7	12000	< 2.0	18000
	a	2.3	13000	4.1	14000
FA2-B_C3	b	2.3	13000	6.9	14000
	c	2.2	13000	4.5	14000